Department of Bioproducts and Biosystems

Hybrid Architectures at the Nanoscale: Constructing Materials through Electrostatic Interactions

Ahmed Shaukat

Aalto University

DOCTORAL THESES

Aalto University publication series
DOCTORAL THESES 186/2023

Hybrid Architectures at the Nanoscale: Constructing Materials through Electrostatic Interactions

Ahmed Shaukat

A doctoral thesis completed for the degree of Doctor of Science (Technology) to be defended, with the permission of the Aalto University School of Chemical Engineering, at a public examination held at the lecture hall KE2 of the school on 10 November 2023 at 13:00.

Aalto University
School of Chemical Engineering
Department of Bioproducts and Biosystems
Biohybdrid Materials

Supervising professors
Professor Mauri A. Kostiainen
Aalto University, Finland

Thesis advisors
Dr. Eduardo Anaya-Plaza
Aalto University, Finland

Preliminary examiners
Dr. Thomas G. W. Edwardson
ETH Zürich, Switzerland

Professor Amy Szuchmacher Blum
McGill University, Canada

Opponents
Professor Tobias Beck
University of Hamburg, Germany

Aalto University publication series
DOCTORAL THESES 186/2023

ISBN 978-952-64-1511-6 (printed)
ISBN 978-952-64-1512-3 (pdf)
ISSN 1799-4934 (printed)
ISSN 1799-4942 (pdf)
http://urn.fi/URN:ISBN:978-952-64-1512-3

Images: Cover image: Fluorescent protein crystal with Aalto logo photobleached on it. Credits: Prof. Jaakko Timonen

Unigrafia Oy
Helsinki 2023

Finland

NORDIC SWAN ECOLABEL
Printed matter
4041-0619

Author
Ahmed Shaukat

Name of the doctoral thesis
Hybrid Architectures at the Nanoscale: Constructing Materials through Electrostatic Interactions

Publisher School of Chemical Engineering

Unit Department of Bioproducts and Biosystems

Series Aalto University publication series DOCTORAL THESES 186/2023

Field of research Chemical Engineering

Manuscript submitted 21 September 2023 **Date of the defence** 10 November 2023

Permission for public defence granted (date) 5 October 2023 **Language** English

☐ **Monograph** ☒ **Article thesis** ☐ **Essay thesis**

Abstract

Nature's intricate biomolecular assemblies inspire crafting nano- and microscale functional materials. Comprising nucleotides, amino acids, and saccharides, these structures orchestrate cellular functions with precision. Replicating this complexity artificially is challenging, but nanoscale techniques, especially nature-mimicking self-assembly, offer atomic-level precision through non-covalent interactions. Electrostatic self-assembly stands out for versatility, enabling diverse functional materials. This reversible process facilitates the exact arrangement of charged components. Moreover, the utilization of biomolecule-based materials as building blocks in nanomaterials presents a promising avenue, leading to the development of highly biocompatible functional systems. This convergence of principles is exemplified in this thesis, which demonstrates how functional and self-assembling biohybrid materials can be constructed precisely by synergistically combining DNA origami and protein cages with molecular glues.

Thus, Publication I opens the study by designing hybrid bundles, uniting cationic dyes like zinc phthalocyanine with negatively charged DNA origami. This synergy enhances optical properties and stability, effectively showcasing the potential of electrostatic self-assembly in customizing material traits.

Publication II extends the study by introducing Janus-type phthalocyanines with two different DNA origami structures, resulting in optically active biohybrids resistant to aggregation. This underscores the role of ionic strength in self-assembly and disassembly processes, deepening the insights into biohybrid material formation.

Publication III delves into crystalline assemblies, harnessing electrostatic self-assembly of pillar[5]arene with apoferritin, unveiling promising prospects for water remediation. This endeavor highlights the versatile capabilities of biomolecular self-assembly in addressing pressing environmental challenges.

Publication IV demonstrates the formation of protein-protein co-crystals involving cationic fluorescent protein and negatively charged apoferritin, thereby showcasing robust optical properties with potential applications in biological light-emitting diodes.

In summation, the collective body of work presented in this thesis underscores the potential of electrostatic self-assembly in crafting intricate biohybrid materials. These findings provide understanding of electrostatic self-assembly, establishing a path for preparing cutting-edge nanomaterials with applications in nanomedicine, optoelectronics, and water treatment. This research effectively links intricate biomolecular assemblies and synthetic constructs, potentially finding utility in novel solutions across multifarious sectors.

Keywords protein cages, DNA origami, electrostatic interaction, self-assembly

ISBN (printed) 978-952-64-1511-6 **ISBN (pdf)** 978-952-64-1512-3

ISSN (printed) 1799-4934 **ISSN (pdf)** 1799-4942

Location of publisher Helsinki **Location of printing** Helsinki **Year** 2023

Pages 180 **urn** http://urn.fi/URN:ISBN:978-952-64-1512-3

Acknowledgments

The research presented in this dissertation unfolded within the esteemed confines of the Biohybrid Materials Group at Aalto University, spanning the period from August 2019 to July 2023. I sincerely thank the Academy of Finland, the Magnus Ehrnrooth Foundation, and the European Research Council for their generous funding, which enabled my pursuit of a doctoral position. Additionally, I express my deep thanks to the Finnish Foundation for Technology Promotion for their crucial financial support, which has played an instrumental role in facilitating my research endeavors and the realization of this dissertation.

I wish to begin by extending my deepest gratitude to the esteemed Prof. Mauri Kostianen for graciously accepting me into the group. From the very outset, your unwavering support and guidance have been indispensable to my journey. Your profound expertise, extensive knowledge and unwavering commitment to academic excellence have profoundly influenced the trajectory and caliber of my research. Your invaluable insights and our stimulating discussions have consistently challenged me to expand my intellectual horizons and venture into unexplored territories of inquiry. Moreover, I would like to wholeheartedly express my deep appreciation for the invaluable contributions of Dr Eduardo Anaya-Plaza. Your exceptional guidance and insightful input have played a pivotal role in not only the successful completion of my dissertation but also my personal growth. Eduardo, you have been there for me like a supportive family member, providing unwavering belief in my potential, endless patience, and continuous encouragement. Your dedication and immeasurable contributions to my academic and professional growth are imprinted in my journey. I am forever indebted to you, and your impact will always be cherished.

I extend my heartfelt gratitude to Dr Thomas Edwardson and Prof. Amy Blum for their meticulous pre-examination of this dissertation and the invaluable comments they provided. Their thorough scrutiny and insightful feedback have undoubtedly enhanced the quality and rigor of my research. I am deeply appreciative of their commitment to scholarly excellence. Additionally, I am immensely grateful to Prof. Tobias Beck for graciously accepting the role of the opponent in the forthcoming defense. Your expertize and critical engagement will undoubtedly contribute to a robust examination of the research presented in this dissertation. I sincerely appreciate your willingness to participate in this important academic endeavor.

I extend my deep gratitude to all the co-authors, whose skills, insights, and consistent dedication during the projects have played a pivotal role in the exceptional research outcomes and publications we have successfully attained. Your invaluable contributions, dedication, and shared enthusiasm have greatly enriched the depth and quality of my research. Collaborating with each of you has been an enriching experience that has shaped my perspectives and expanded my knowledge. Thank you for your unwavering commitment and remarkable contributions to our collective success.

To my esteemed past and present colleagues at the Biohybrid Materials Group, I extend my heartfelt gratitude for your unwavering support, thought-provoking discussions, and remarkable spirit of collaboration. The knowledge you've brought, your invaluable input, and your strong sense of teamwork have been instrumental in influencing the direction and quality of my research. I appreciate the inspiring atmosphere we've cultivated, and I'll forever hold dear the instances of working together and sharing insights. To my ever-patient office buddies, Sofia and Iris, I can't thank you enough for putting up with my constant chatter, being there to lend a helping hand whenever I needed it, and sharing countless moments of laughter. We've experienced it all, from joyous triumphs to the occasional heartbreak of failed experiments. Our shared moments of misery have forged an unbreakable bond between us! Here's to navigating the twists and turns of science together, always finding humor along the way! Daniel and Alba, I'll miss our fun corridor and lab talks. They were stress-busting gems that brought immense joy to my days. Our laughter-filled exchanges were truly priceless, brightening even the dullest of moments. Thank you for infusing my journey with endless smiles and contagious laughter!

In my doctoral journey, learning about TEM, especially the mind-boggling Cryo-TEM technique, has been a thrilling rollercoaster ride. I owe a tremendous debt of gratitude to the incomparable Dr Jani Seitsonen, whose expertise and guidance were like a guiding light in the TEM labyrinth. But that's not all! I must also extend my heartfelt appreciation to Prof. Jaakko Timonen, who was my beacon of knowledge in the world of fluorescence microscopy. His patient mentorship and valuable insights have been instrumental in my understanding of this intricate technique. To both of these remarkable mentors, I am forever grateful for their unwavering dedication and immeasurable contributions to my scientific growth. Together, they have shaped my journey into an unforgettable adventure of scientific exploration.

To my incredible friends Hammad, Deepika, and Arun, I owe you a gratitude debt that could give even the most legendary Bollywood blockbusters a run for their money! Your unwavering support, understanding, and endless encouragement have been like the superhero cape that kept me soaring through this wild journey. You've provided me with emotional sustenance, laughter that could rival a comedy club, and the motivation to conquer any obstacle in my path. And during those challenging times, you've lent me your ears like a 24/7 helpline, proving that you're not just friends, but certified therapists in disguise. Thank you for being the comedic sidekicks to my doctoral adventures!

Lastly, and most importantly, I extend my heartfelt gratitude to my family. To my incredible parents, Shaukat Ali and Shahnaz, I am forever grateful for your unwavering love, support, and countless sacrifices. Your unwavering belief in my potential has been the driving force behind my accomplishments. You have nurtured my thirst for knowledge and provided me with every opportunity to chase my dreams. To my amazing siblings, Suneina, Daniya, and Sidra, thank you for your constant encouragement, understanding, and unwavering belief in me. Your presence in my life has been a constant source of strength and inspiration. And to my loving fiancé Anum, thank you for being my rock, my pillar of support, and my biggest cheerleader. Your unwavering belief in me and your unconditional love has fueled my determination and kept me going even during the most challenging times. I am incredibly grateful to have you by my side on this journey.

To all those mentioned and to those who have supported me in countless other ways, I am deeply grateful for your contributions to my personal and academic growth. Your belief in my abilities and your presence in my life has made this journey truly meaningful and rewarding. Thank you for being a part of my doctoral experience.

Espoo, 3 September 2023
Ahmed

Contents

List of Abbreviations and Symbols

0D	zero-dimensional
1D	one-dimensional
24HB	24-helix bundle
2D	two-dimensional
3D	three-dimensional
60HB	60-helix bundle
6HB	6-helix bundle
A	adenine
aFt	apoferritin
C	cytosine
CCMV	cowpea chlorotic mottle virus
d_{aFt}	diameter of apoferritin
D_h	hydrodynamic diameter
DLS	dynamic light scattering
DNA	deoxyribonucleic acid
DO	DNA origami
DPBF	1,3-diphenylisobenzofuran
DX	double-crossover
EMSA	electrophoretic mobility shift assay
EtBr	ethidium bromide
FBS	fetal bovine serum
FCC	face-centered cubic
FFT	fast Fourier transforms
FP	fluorescent protein
Ft	ferritin

G	guanine
GFP	green fluorescent protein
HOMO	highest occupied molecular orbitals
HSA	human serum albumin
ICP-OES	inductive coupled plasma-optical emission spectrometry
LED	light-emitting diode
LUMO	lowest unoccupied molecular orbitals
MO	methyl orange
NIR	near-infrared
nt	nucleotides
P10+	pillar[5]arene with 10 cationic charges
Pc	phthalocyanines
PDT	photodynamic therapy
PEG	polyethylene glycol
pI	isoelectric point
PS	photosensitizer
PX	paranemic crossover
ROS	reactive oxygen species
SA	self-assembly
SAXS	small-angle X-ray scattering
scmGL	supercharged green lantern protein
ssDNA	single-stranded DNA
T	thymine
TEM	transmission electron microscopy
Tris	tris(hydroxymethyl)aminomethane
UV-Vis	ultraviolet-visible
VLP	virus-like particle
wt	wild-type
ZnPc	zinc phthalocyanine
ε_0	vacuum electric permittivity constant
ε	relative permittivity of the medium

$^1O_2$	singlet oxygen
a	lattice constant
c_i	densities of the electrolyte ions
e	electronic charge
F	force
k	Debye-Hückel parameter
q	point charges
r	radius
z_i	valencies of the electrolyte ions
Z	surface charge of the particle

List of Publications

This doctoral dissertation consists of a summary of the following publications which are referred to in the text by their numerals.

I. Ahmed Shaukat, Eduardo Anaya-Plaza, Sofia Julin, Veikko Linko, Tomas Torres, Andrés de la Escosura and Mauri A. Kostiainen. *Phthalocyanine–DNA Origami Complexes with Enhanced Stability and Optical Properties*. Chemical Communications, **2020**, 56, 7341–7344, DOI: 10.1039/D0CC01916J

II. Asma Rahali,* **Ahmed Shaukat**,* Verónica Almeida-Marrero, Bassem Jamoussi, Andrés de la Escosura, Tomás Torres, Mauri A. Kostiainen, Eduardo Anaya-Plaza. *A Janus-Type Phthalocyanine for The Assembly of Photoactive DNA Origami Coatings*. Bioconjugate Chemistry, **2021**, 6, 1123–1129, DOI: 10.1021/acs.bioconjchem.1c00176. *Equal contribution

III. Ahmed Shaukat, Eduardo Anaya-Plaza, Ngong Kodiah Beyeh, Mauri A. Kostiainen. *Simultaneous Organic and Inorganic Host-Guest Chemistry within Pillararene-Protein Cage Frameworks*. Chemistry–A European Journal. **2022**, 19, e202104341, DOI: 10.1002/chem.202104341

IV. Marta Patrian,* **Ahmed Shaukat**,* Mattia Nieddu,* Jesús A. Banda-Vázquez, Jaakko V. I. Timonen, JP Fuenzalida-Werner, Eduardo Anaya-Plaza, Mauri A. Kostiainen, and Rubén D. Costa. *Supercharged Fluorescent Protein-Apoferritin Cocrystals for Lighting Applications*. **2023**, accepted in ACS Nano. *Equal contribution

Author's Contribution

Publication I: Phthalocyanine–DNA Origami Complexes with Enhanced Stability and Optical Properties

AS conducted all the self-assembly experiments, digestion experiments, and data analysis. EAP and SJ participated in photostability assay and TEM imaging, respectively. EAP synthesized the phthalocyanines and SJ folded the DNA origami for all the experiments. AS wrote the manuscript and made corrections according to the suggestions of co-authors and reviewers.

Publication II: A Janus-Type Phthalocyanine for The Assembly of Photoactive DNA Origami Coatings

AR synthesized and characterized the phthalocyanine. AS carried out all experiments and data analysis involving self-assembling phthalocyanine with DNA origami. AS wrote the manuscript involving DNA origami complexation and made corrections according to the suggestions of co-authors and reviewers.

Publication III: Simultaneous Organic and Inorganic Host-Guest Chemistry within Pillararene-Protein Cage Frameworks

AS conducted all the experiments and data analysis except the adsorption isotherms, which were carried out by MAK. The pillararenes synthesis and characterization were conducted by NKB and EAP. AS wrote the manuscript and made corrections according to the suggestions of co-authors and reviewers.

Publication IV: Supercharged Fluorescent Protein-Apoferritin Cocrystals for Lighting Applications

MP designed and expressed the green lantern protein. AS prepared and characterized the crystalline assemblies by DLS, spectrophotometry, optical microscopy, SAXS, and Cryo-TEM. JT carried out fluorescence microscopy. MN prepared and characterized the LED device. AS wrote the manuscript part involving crystalline assemblies and made corrections according to the suggestions of co-authors and reviewers.

1. Introduction

Nature provides exemplary templates for the formation of functional and complex materials, using biomolecule building blocks such as nucleotides, amino acids, and saccharides, with near-atomic precision. When arranged into nano- and microscale architectures, these structures perform intricate cellular functions, such as transferring and maintaining genetic information, storing energy, and transducing biological signals. The specific functionality and structural integrity of these hierarchical structures often depend on their spatial orientation. Although such biological structures are abundant and provide valuable insights, the task of artificially constructing materials with high precision and controlling their structural features at a small scale remains a formidable challenge. Despite this, advancements in nanoscale techniques inspired by biomolecular assemblies have spurred rapid growth in nanomaterial research.[1,2] Of the many techniques found in nature, bottom-up approaches like self-assembly (SA) have enabled the creation of highly organized objects with nanometer-scale precision, a feat that traditional top-down nanofabrication techniques struggle to achieve.[3,4]

SA is a vital area of bottom-up research in the increasingly miniaturized world of technology and nanotechnology. The fundamental engineering principle behind SA is the deliberate design of molecular building blocks that can spontaneously interact and assemble in a stepwise manner through the formation of multiple weak non-covalent chemical bonds. These interactions additionally confer reversibility to the system, enabling the assembled structures to be disassembled into their individual molecular components, much like the process of assembling and disassembling a Lego set. The behavior of materials at the nanoscale is significantly different from that at larger scales, and their constituents' organization plays a crucial role in determining their properties.

In biomolecules, SA is a fundamental process, where molecules spontaneously organize themselves into specific structures or complexes without external guidance. Biological materials, like deoxyribonucleic acid (DNA) forming a double helix, proteins creating intricate structures, lipids composing cellular membranes, viral capsids shielding genomes, and amyloid aggregates causing neurodegenerative diseases, exemplify the variety of interactions and functions of SA.

The utilization of biomolecules-based building blocks using SA, particularly supramolecular interactions can lead to the development of innovative and sustainable materials with applications in catalysis, biosensing, and drug delivery.[2,5] One paradigmatic example is the use of DNA molecules designed to self-

assemble into specific shapes using complementary base-pairing interactions. This approach, known as DNA nanotechnology, has been used to create a wide range of nanoscale structures *e.g.*, DNA origami, from simple shapes to more complicated structures such as robots and circuits.[6] Moreover, by leveraging the canonical properties of DNA, it is possible to create a range of functionalized materials through diverse strategies,[7] which includes the interaction of DNA-based nanostructures with proteins,[8] stimuli-responsive polymers,[9,10] or small molecules. Similarly, proteins are capable of remarkable SA, forming highly specific and intricate protein assemblies.[11] These assemblies have diverse biological functions such as the execution of complex biochemical processes and the creation of structural materials that shape the cell, and when these assemblies are formed artificially, these higher-order structures can be used as multifunctional material for biomedicine and drug delivery or as biomimetic systems to study biological processes.[12] Proteins with high symmetry, such as protein cages, are particularly well-suited for constructing extraordinary higher-order structures due to their exceptional modularity and stability. Due to such remarkable properties, both DNA and proteins have now been extensively used as construction materials and building blocks for creating intricate assemblies and higher-order materials offering several advantages in nanoscience and material science.[11,13–17] The materials formed by DNA and proteins provide high specificity and efficiency, robustness, multimodality, versatility, and ease of fabrication.

Self-assembling structures present different degrees of order: from amorphous aggregates where non-contacting molecules lack regular orientation, to crystal lattices characterized by consistent interparticle distance and orientation across the entire structure. Despite their differences, both types of structures can be considered assembled, and each has its advantages depending on the application. Arranged configurations can yield distinct characteristics, such as catalytic properties, whereas disordered materials often exhibit enhanced durability and greater ease of production.[4] The properties of biomolecules-based materials are often influenced by their composition and structure, and their distinctive characteristics hold potential not only for biomedical and healthcare applications but also for electronics, energy, environment, and food sectors.[18] To advance the development of these biomaterials based on SA, conducting experiments is imperative, as research delves into the impact of ionic strength, pH, temperature, and building unit properties on the SA process and the resulting structure. Additionally, comprehending the susceptibility of these structures in physiological environments, which include degrading agents like nucleases for nucleic acid-based biomaterials, is crucial. As these SA techniques continue to evolve, it is highly probable that the development of increasingly intricate and functional nanoscale biomolecules-based materials will emerge in the future.

Although the synthesis of nanoparticles with varying sizes and shapes has been significantly enhanced, the uneven distribution of synthetic nanoparticles poses challenges that can be surmounted by utilizing flawlessly consistent biological nanoparticles to guide the SA process. This approach enables researchers to examine the correlation between biological nanoparticle characteristics and assembly formation.

1.1 Objective and outline

This dissertation presents a study on the development of biohybrid materials through the electrostatic SA of DNA nanostructures and protein cages with various cationic molecular glues. Specifically, the DNA nanostructures are constructed by folding a long single-stranded DNA (ssDNA) scaffold into arbitrary shapes, commonly referred to as DNA origami (DO), while the protein cage under investigation is ferritin (Ft) or apoferritin (aFt) derived from horse spleen. As both DO and (a)Ft possess an overall negative charge at neutral pH in aqueous media, they were paired with different cationic moieties to form hybrid assemblies. This dissertation also provides insights into how the ionic strength of the media impacts the electrostatic SA of DO and protein cages with cationic moieties and thereby directs the SA of multicomponent hierarchical structures. These findings bear significance in diverse applications, including nanomedicine, optoelectronics, and water treatment.

A photosensitizer called zinc phthalocyanine (ZnPc) was employed to create bundles or complex assemblies with DO, while crystalline supramolecular assemblies were formed using Ft or aFt with the host-guest molecules such as pillararenes decorated with various numbers of cationic charges. Furthermore, the extension of this approach to protein-protein assemblies using supercharged green lantern protein (scmGL) with aFt showcases the potential of these building blocks in constructing diverse biohybrid materials. Although DO and protein cages are both robust biological nanoparticles that have been extensively studied individually, their usage as self-assembling building blocks has been limited. However, their symmetrical and robust nature makes them ideal for this purpose.

The theoretical background of how SA and subsequently, electrostatic SA can be exploited to form different biohybrid structures is provided in Chapter 2. This also includes selected examples of similar studies done using the biomolecules-based building blocks studied under this dissertation *i.e.*, DO and protein cages. A brief description of these biomolecules-based building blocks together with different cationic molecular glues utilized in this dissertation such as phthalocyanines, pillararenes, and fluorescent protein (FP) is also given in the same chapter (Figure 1). The materials and methods employed in this study, along with the corresponding characterization techniques, are thoroughly elucidated in Chapter 3. Building upon the aforementioned emphasis, Chapter 4 delves into a comprehensive analysis and discussion of the specific outcomes highlighted in each publication. Finally, Chapter 5 serves as the concluding section, presenting the overarching findings of the research, elucidating their implications, and providing a roadmap for future directions that warrant further exploration.

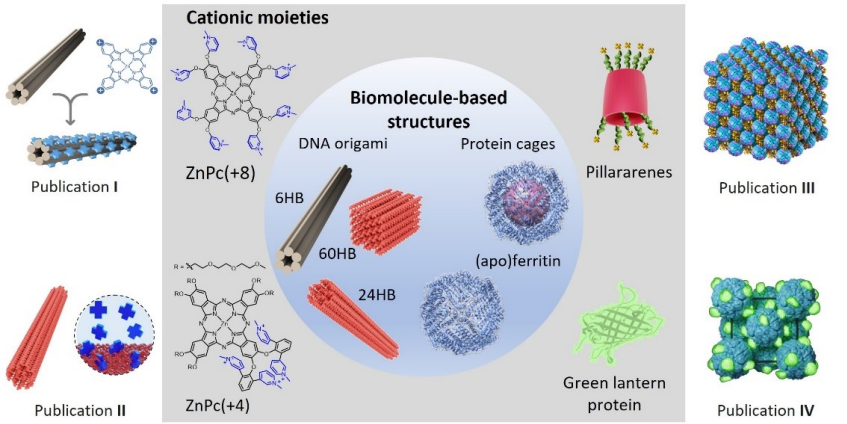

Figure 1: Schematic representations of the electrostatically self-assembling systems studied in this dissertation. Middle circle: DNA origami (6HB, 24HB, 60HB) and protein cages (Ft and aFt), the biomolecules-based building blocks used in the publications. Grey rectangle: cationic moieties in the dissertation such as ZnPc with 4 or 8 charges, pillararenes, and green lantern protein. Publication **I**. DO (6HB) SA with octa-cationic ZnPc. Publication **II**. DO (24HB and 60HB) SA with tetra-cationic ZnPc. Publication **III**. Co-crystals of protein cages (aFt and Ft) and deca-cationic pillararene. Publication **IV**. Co-crystals of aFt and cationic green lantern protein. The images were produced using UCSF Chimera and blender.

In Publication **I**, exploiting the negatively charged phosphate backbone of the 6-helix bundle (6HB) DO, hybrid bundles are formed with octa-cationic zinc phthalocyanine. The resultant assemblies show deaggregation of ZnPc which is translated into improved optical properties. Coating the 6HB with ZnPc also increased the stability of 6HB against endonucleases, a property highly demanded to increase the circulation time of DO inside the biological environment.

Publication **II** demonstrates a Janus-type phthalocyanine containing four cationic charges on one side and polyethylene glycol chains on the other side, bound with two different types of DO (24-helix bundle (24HB) and 60-helix bundle (60HB)) rendering optically active biohybrids. The assemblies exhibited remarkable resistance to salt-induced aggregation; nevertheless, they could be disassembled upon the addition of a higher ionic concentration.

In Publication **III**, the host-guest molecule such as pillar[5]arene was utilized to form crystalline assemblies with Ft and aFt. The electrostatically self-assembled crystals were then utilized to uptake both organic and inorganic molecules from aqueous media exploiting the innate ability of Ft to leach inorganic molecules and pillararenes for hosting organic molecules due to its hydrophobic cavity, thus proving to be a useful water remediation material.

In Publication **IV**, the protein-protein co-crystals were formed using supercharged cationic FP namely scmGL and aFt. The resultant crystalline assemblies demonstrated robust optical properties. The crystals formed were then studied for their potential activity and stability in a biological light-emitting diode (Bio-LED).

2. Background

2.1 Self-assembly

Self-assembly (SA) of materials has emerged as a critical tactic in the creation and production of nanostructured systems, representing a fundamental methodology for manufacturing advanced materials with widespread applications in biotechnology and the realm of nanomaterials.[3] SA is commonly linked to achieving thermodynamic equilibrium, where the organized structures exhibit a minimum in the free energy of the system.[3] However, this broad definition falls short. A crucial aspect of SA is the organization of building blocks into ordered, macroscopic structures. This form of organization can manifest either through direct engagements, such as inter-particle forces, or indirectly by employing a template or an external field.[19] Non-equilibrium SA is another important facet of SA that operates under different principles. In this form of SA, external forces or energy inputs disrupt the system's equilibrium state.[20] This disruption creates favorable conditions for the spontaneous organization of components into ordered structures, even in systems far from equilibrium. In the realm of living systems, non-equilibrium SA is a critical process for creating organized nanostructures that remain in non-equilibrium states to perform complex functions.[21] Microtubules, vital for cell division, exemplify this concept.[22] They dynamically self-assemble and disassemble through GTP hydrolysis, enabling essential biological functions within non-equilibrium environments. This underscores the central role of non-equilibrium self-assembly in biology. SA can be initiated by covalent bonds[23,24] although it commonly relies on non-covalent interactions like hydrogen bonds, ionic interactions, metal chelation, and various other molecular connections. These interactions are often less strong compared to covalent bonds and can be attenuated, leading to a resultant structure that attains thermodynamic equilibrium with its constituents.[25] The final assembly's shape, size, and function are determined by the delicate balance among these forces. This constant interplay among the assembling particles seeks to attain the system's lowest energy state and imparts durability to the assemblies by allowing corrective measures for unfavorable interactions once they have occurred.[20] Typically, the SA of molecules takes place either in a solution or at an interface, allowing the components to undergo the required assembly pathway. It is important to note that the interaction between the components and their surrounding environment can significantly influence the trajectory and outcome of the SA process.[26] This phenomenon extends to

biomacromolecules as well, presenting new opportunities for their utilization in material sciences and delivery applications.

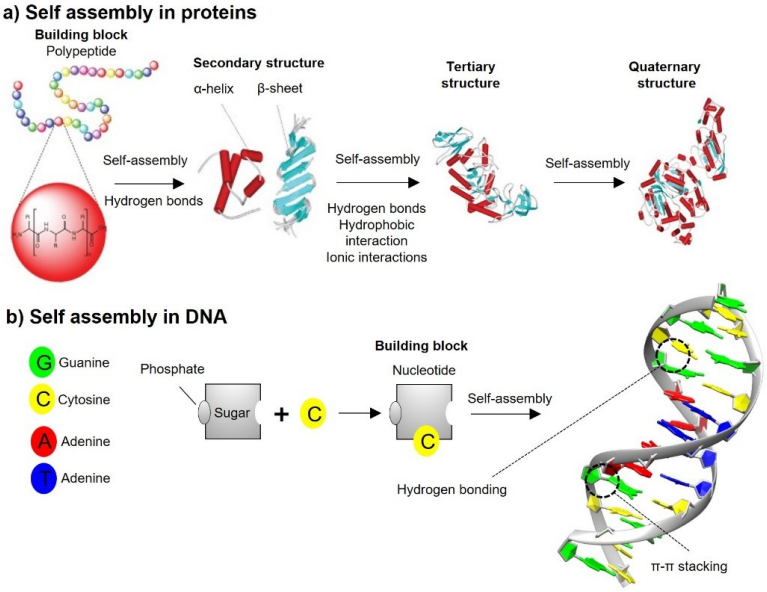

Figure 2: Examples of self-assembled biomolecules such as a) protein and b) DNA molecules with their respective building blocks. Adapted with permission from Ref[25]. © John Wiley & Sons.

In the domain of living materials, SA plays a pivotal role, showcasing its profound importance. This phenomenon is particularly evident in the formation of intricate structures such as lipidic biomembranes, protein macrostructures like photosynthetic antennas, and molecular machines. These entities exhibit a natural propensity for SA, highlighting their significance in this field.[27] Protein folding serves as a prominent illustration of the pivotal role played by non-covalent interactions in SA within aqueous solutions (Figure 2a). The process of attaining the tertiary structure of proteins involves the bending and packing of α-helices and β-sheets, leading to the formation of protein subunits. The conformation of the tertiary structure is governed by diverse interactions, including hydrogen bonds, hydrophobic interactions, and ionic interactions, which facilitate the assembly of functional regions within the protein. Additionally, the quaternary structure of proteins arises from the interaction between these subunits. Another noteworthy instance of SA manifests in double-stranded DNA (Figure 2b). Nucleotides, which consist of a sugar, a nitrogenous base, and a phosphate group, constitute the fundamental building blocks of DNA. Through hydrogen bonding and π-π stacking interactions, complementary pairs of nucleobases from two antiparallel strands intertwine to form a double helix structure. This stable configuration allows DNA to efficiently replicate, transcribe, and translate genetic information. Viruses, supramolecular structures consisting of proteins and nucleic acids, also showcase SA. They possess protein outer shells called capsids, composed of multiple copies of coat proteins arranged symmetrically which encapsulate the viral genome. Viruses have the capacity to adopt either icosahedral or rod-shaped configurations, showcasing adept

management of self-assembled structure dimensions. In addition to proteins and nucleic acids, the cytoplasmic membrane plays a crucial role in SA. Comprised of a phospholipid bilayer, the membrane creates a confined cellular space and serves as a barrier while allowing the transport of specific molecules through its fluidity.

Utilizing the innate inclination of biomolecules for SA and harnessing their fundamental properties, it becomes feasible to engineer intricately organized biomaterials spanning zero-dimensional (0D), one-dimensional (1D), two-dimensional (2D), and three-dimensional (3D) structures.[28] Furthermore, biomolecules possess exceptional capabilities to inspire the creation of hybrid bionanomaterials with enhanced functionalities, employing various strategies.[29–32] This process involves the formation of materials through above mentioned supramolecular interactions. The molecular structure of these building components holds the instructions for assembly, specifically through the precise geometric arrangement of functional groups, enabling a multitude of intra- and intermolecular interactions. The ability to manipulate the strength and directionality of these interactions among the building blocks is a defining characteristic of the field of self-assembled and supramolecular materials.[33] The concentration of self-assembling units significantly influences the diffusion and mobility of the components, as higher concentrations facilitate the assembly of larger structures.[25] Multiple pathways are available to initiate and propel SA, involving gradual modifications to environmental conditions such as the concentration of building blocks, pH, temperature, ionic strength, and solvent properties.[34–38] Alternatively, external stimuli like light or enzyme activity can serve as triggers.[39,40] In this dissertation, the SA based on electrostatic interactions has been heavily explored and hence will be discussed in more detail.

2.1.1 Electrostatic self-assembly

Electrostatic interactions, which are essential non-covalent interactions in supramolecular chemistry, have been effectively utilized in Publications **I**-**IV** to create hybrid assemblies. These interactions can be described by Coulomb's law, a fundamental principle in electromagnetism, which describes the interaction between electric charges. Coulomb's law establishes that the force (F) exerted between two charged entities is directly linked to the multiplication of their charges and inversely related to the square of the separation distance between them

$$F = \frac{|q_1 q_2|}{4\pi\varepsilon_0 r^2} \quad (1)$$

where q_1 and q_2 are two point charges separated by a distance r and the ε_0 is the vacuum electric permittivity constant. However, in a solution, the presence of other charged particles, polar molecules, or atoms surrounding the charged objects can give rise to a screening effect. The screening effect is taken into account by the Yukawa potential, also known as the screened Coulomb potential.[41] Unlike Coulomb's law, the Yukawa potential describes the interaction between

charged particles as a decaying exponential function of the distance between them, rather than the inverse square relationship. The Yukawa potential modified for the finite size of the particle,[42] is given by:

$$V_{Yukawa}\,(r) = \left(\frac{e^{ka}}{1+ka}\right)^2 \frac{Z^2e^2}{\varepsilon r} e^{-kr} \tag{2}$$

Here r is the distance between the dispersing particles, a is the radius of the particle, Z is the surface charge of the particle, e is the electronic charge, ε is the relative permittivity of the medium and k is the Debye-Hückel parameter. This exponential decay represents the reduction in the effective interaction strength due to the screening effect. The screening effect occurs because charged particles in a solution are surrounded by intervening particles that can partially screen the electric field.[43] This shielding weakens the interaction between charges over longer distances, causing a more rapid decrease in strength compared to what Coulomb's law predicts.[41] When considering nanoscale objects, a different potential known as the Lennard-Jones potential also becomes more relevant. The Lennard-Jones potential describes the interaction between neutral atoms or molecules, taking into account both the attractive and repulsive forces.[44] Unlike Coulomb's law, which only considers the electrostatic force between charged objects, the Lennard-Jones potential accounts for van der Waals forces and short-range repulsive interactions. In simple terms, two interacting particles exhibit repulsive forces at extremely short distances, attractive forces at intermediate distances, and negligible interaction at infinitely large separations.

In the realm of electrolyte solutions, the Bjerrum and Debye lengths play significant roles in understanding ionic interactions and screening effects. The Bjerrum length quantifies the strength of the electrostatic interaction between elementary charges in a given medium. When the distance between charged particles is on the order of the Bjerrum length or smaller, the electrostatic forces between them dominate over the thermal energy, leading to strong interactions. In contrast, when the distance is much larger than the Bjerrum length, the thermal energy dominates, and the electrostatic forces become negligible. On the other hand, the Debye length characterizes the distance over which the electrostatic potential decays due to screening in an electrolyte solution. It is influenced by the concentration and charge of ions in the solution and represents the range over which charges are effectively screened. This length is determined according to equation (3)

$$k^{-1} = \sqrt{\frac{\varepsilon_0 \varepsilon_r k_B T}{e^2 \sum_i c_i z_i^2}} \tag{3}$$

where ε_0 is vacuum permittivity, ε_r is the dielectric constant of the solvent, k_B is the Boltzmann constant, T is the absolute temperature (in Kelvin), e is the elementary charge, and c_i and z_i are the densities and valencies of the electrolyte ions.[45] By optimizing the screening, the strength of electrostatic interactions can be controlled, particularly in solutions below 1 M concentration.[46–48] It can be

seen from the equation that the potency of electrostatic interactions can also be modified by manipulating various factors, such as the choice of solvent (dielectric constant) and the concentration and chemical properties (number densities and valencies) of ions in the electrolyte. In scenarios where the ionic strength of the surrounding medium is elevated, the value of k^{-1} diminishes, leading to the prevalence of close-range interactions like van der Waals forces, molecular layering, and hydration effects. These factors take precedence over electrostatic double-layer forces across all distances.[49] Consequently, electrostatic interactions exhibit greater effectiveness over longer distances in dilute ionic solutions compared to concentrated solutions, making them significantly more crucial. Although there are limitations to the theories of electrostatic interactions, screening is crucial for achieving highly ordered structures.

The electrostatic SA of nanoparticles involves the significant influence of both entropy and enthalpy, although, in the case of highly charged colloidal particles, the electrostatic forces are more dominant in particle interactions. This is advantageous since the balance between attractive and repulsive electrostatic forces within charged colloids can be modified by changing the ionic strength of the surrounding solution. Excessive attractive interactions or higher k^{-1} result in fast assembly and result in gel-like aggregates whereas weak interactions or low k^{-1} fail to induce assembly. Interactions that are weakened due to screening allow particles to move freely relative to each other, enabling them to assume the thermodynamically most favorable orientations (Figure 3).[50,51] Once these structures are formed, increasing the ionic strength of the media leads to a decrease in k^{-1} and hence this strategy could be utilized to disassemble the structure.[52]

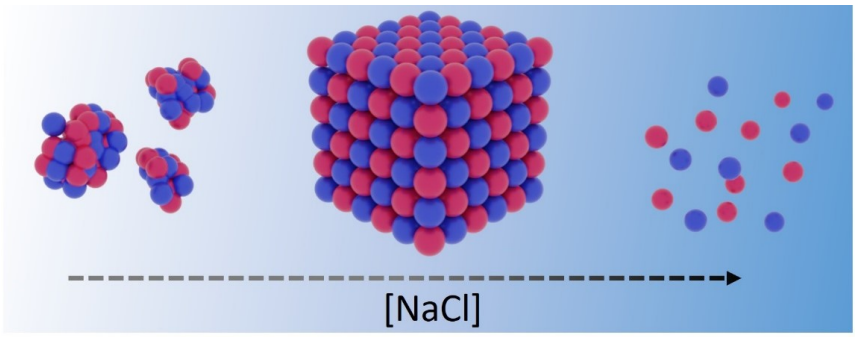

Figure 3: Schematics of typical electrostatic self-assemblies formed at varying ionic strength. (left) Strong interaction leads to aggregates. (center) Partial screening leads to crystalization. (right) Complete screening of electrostatic interaction results in individual building blocks where particle-solvent interaction dominates.

While extensive research has been conducted on synthetic particles, including metallic,[53] inorganic,[54] and polymeric[55] nanoparticles, the utilization of biomolecules in electrostatic SA is particularly appealing due to their multifunctional nature.[51] The utilization of charged biomolecules, such as proteins and DNA, which are rich in oxyanionic groups like carboxylate ions in proteins and phosphate ions in nucleic acids and phospholipids, has greatly facilitated the process of electrostatic SA. Proteins possess a high level of complexity and can be perceived as polyelectrolytes due to their polyampholytic nature, which means their

surface charge distribution depends on pH. The protein's isoelectric point (pI) is the pH where the net electrical charge becomes zero. Below the pI, proteins carry a net positive charge caused by the protonation of basic groups, while above the pI, they exhibit a net negative charge. As a result, the charge magnitude and polarity of these biological building blocks are strongly influenced by pH. By adjusting the pH, the electrostatic SA of these biological nanoparticles can be either facilitated or hindered, providing a means to control their formation.[45] The presence of surface charge patchiness is a significant factor to consider in the study of complexation. It has been observed that an increase in patchiness significantly enhances the probability of complexation with a polyelectrolyte.[56] Proteins with a variety of shapes and sizes have therefore been utilized to make higher-order structures by optimizing all the above-mentioned parameters.[12,45,57–68] Similarly, other biomolecules such as nucleic acids and particularly DNA-based nanostructures *e.g.*, DO, which contains sugar-phosphate backbone that carries a net negative charge and renders them ideal building blocks for electrostatic SA. By exploiting this property, various cationic moieties have been complexed with DO to form self-assembled structures including peptides or proteins,[69–72] capsid proteins,[73,74] dendrons,[75] fluorophores,[76] chitosan,[77] polymers[78–85] and lipids[86].

2.2 Building blocks used in the electrostatic self-assembly

2.2.1 DNA origami

The field of DNA nanotechnology has revolutionized the bottom-up fabrication of structures through SA.[87] This field takes the DNA out of its biological use *i.e.*, transferring genetic information and uses it as a construction material to assemble sophisticated motifs and join them together to create 2D or 3D structures. Utilizing DNA as a building block offers numerous advantages. Firstly, DNA is mostly present in its well-defined B-form structure, forming a right-handed double helix with two complementary single strands. This helix consists of around 10.5 base pairs per turn and has a diameter of approximately 2 nm. Secondly, DNA strands demonstrate predictable interactions through Watson-Crick base pairing, enabling ssDNA to hybridize into a double helix, with adenine (A) pairing with thymine (T) and guanine (G) pairing with cytosine (C). Thirdly, the concerted efforts of oligonucleotide chemists over decades have made synthetic DNA readily accessible through solid-phase synthesis, and its exceptional chemical stability opens up a multitude of diverse practical applications. Moreover, DNA can be easily modified and functionalized with different chemical and biological moieties which subsequently provide chemical, magnetic, electrical, or optical properties. The process of DNA SA ensures exceptional accuracy and precision at the nanoscale level. Additionally, dynamic DNA structures exhibit responses to external stimuli, both spatially and temporally, taking advantage of DNA's inherent sequence specificity, programmability, and addressability.[88]

Initially, the concept of immobile holiday junctions to construct DNA motifs was explored by Nadrian Seeman[89,90] which was followed by making a 3D cube using three-arm junction[91] and later on, double-crossover (DX) molecules which consisted of two DNA double helices connected by two strand crossover, as opposed to the single crossover found in the Holliday junction[92]. Following this, there were numerous notable advancements in the rational design of both 2D and 3D discrete and extended DNA nanostructures, specifically in the development of DNA tiles.[93] These DX provided the necessary geometric rigidity and stability to initiate the construction of extended DNA nanostructures with precise control over their geometry, connectivity, and topology. However, this technique suffers from certain limitations that affect its overall efficiency and applicability. Firstly, the yield of the process is reduced, which can impact its practicality in certain applications. Additionally, the method is limited in its ability to create complex geometric structures. This limitation arises due to the requirement for exact stoichiometric control of nucleotides. Achieving such precision can be challenging due to experimental errors, further adding to the difficulty of the process.

The DO technology, introduced by Paul Rothemund, revolutionized the field of DNA nanotechnology (Figure 4).[94] Rothemund's method involved using a long ssDNA strand (typically a viral DNA approximately 7000 nucleotide long) as a scaffold and folding it into a specific shape using hundreds of short complementary ssDNA strands called staples. The staple strands comprise multiple binding domains, each serving to unite and draw together distant sections of the scaffold employing crossover base pairing. As a result, the scaffold is folded in a way that resembles the technique of knitting. By employing this method, researchers were able to fabricate intricate 2D and 3D structures with an unparalleled degree of accuracy and control.[95,96] Subsequently, they have delved into the possibilities of applying DNA nanotechnology in a range of interdisciplinary fields, thereby forging connections between various fields of study. When contrasted with methods based on tile-based DNA assembly, DO synthesis provides numerous advantages, including enhanced production yield, durability, and the capability to fabricate intricate non-periodic forms. These benefits stem from the high level of cooperativity achieved through multiple interactions between the scaffold and staple molecules during the origami folding process.

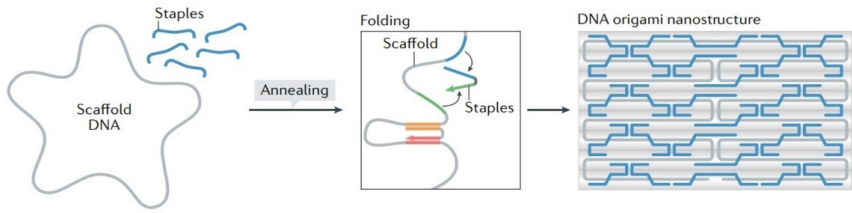

Figure 4: DNA origami technology. A long scaffold of DNA together with multiple short staple strands is folded into a pre-designed shape. Adapted with permission from Ref[96]. © Springer Nature

Due to the aforementioned benefits of utilizing DNA as a fundamental component, its potential can be further harnessed and adapted by leveraging the inherent characteristics of DNA. There are primarily two approaches to enable

its functionalization. The first involves functionalizing it before the SA of the nanostructure, while the second entails functionalizing the complete nanostructure after its SA. In the process of pre-assembly functionalization, desired conjugates are covalently attached to staple strands. These modified strands are then incorporated into the DNA nanostructure during the SA process. This technique has been employed to attach various entities such as fluorophores,[97–99] lipids,[100–102] small molecules,[103–105] aptamers,[106–108] peptides,[109–111] and polymers[112] to DO structures. Pre-assembly functionalization has its advantages but also comes with two main drawbacks. Firstly, conjugates that are sensitive to the elevated temperatures and high salt concentrations necessary for DNA nanostructure SA are not suitable. This applies to proteins that may undergo denaturation and aggregation under such conditions. Secondly, the synthesis, purification, and characterization of individually functionalized staples introduce complexity and time to the process. In contrast, the second approach allows the attachment of desired conjugates to the nanostructure after its SA using non-covalent or covalent methods. By employing non-covalent interactions, this technique allows for the successful post-attachment of proteins,[113–115] peptides,[116–118] lipids,[119–121] fluorophores,[122–124] aptamers,[125–127] small interfering RNA,[128–130] quantum dots,[79] polymers,[112] metals[131–138] and branched oligonucleotides[139] to DNA nanostructures.

Nanocarriers developed for drug delivery *in vitro* and *in vivo* must possess the crucial characteristic of maintaining their structural integrity when exposed to cellular and bodily fluids. And hence DNA nanostructure-based drug delivery systems often require alterations to counter, bypass, or extend the impacts of inherent defense mechanisms.[140] It has been known that the enzymatic breakdown of DO is generally influenced by its superstructure.[141,142] Extensive *in vitro* investigations focusing on the stability of DO have consistently demonstrated its superior stability compared to native DNA structures of similar size.[143–145] The inherent capability of naked DO has been examined in cellular environments, revealing a stability of 12 hours in cell lysates,[146] while live cells gradually digest the DO over a 72-hour incubation period[76]. To this end, a diverse array of strategies has been developed to further enhance the stability and optimize the performance of DNA nanostructure-based drug delivery systems against nucleases (Figure 5). These approaches can be broadly classified into three main categories: 1) Refining the design of nanostructures, which involves optimizing factors such as helix packing density and the incorporation of paranemic crossover (PX) DNA, which outperforms double crossover (DX) DNA[141,143,147–149] (Figure 5a), 2) Chemical modification of the constituent strands of the nanostructure, such as employing click chemistry to crosslink component strands or inducing crosslinking through the formation of a thymidine dimer under ultravoilet (UV) irradiation,[150–152] (Figure 5b) and 3) applying coatings composed of polymers,[77,79,139,153] proteins[70,72,75,154,155] or peptides[83,85]/peptoids,[156] or lipid bilayers[86,157] onto DNA structures (Figure 5c). Thorough exploration and implementation of these strategies offer researchers and practitioners how to maximize the stability, performance, and reliability of DNA nanostructures across a wide range of biological contexts.[158]

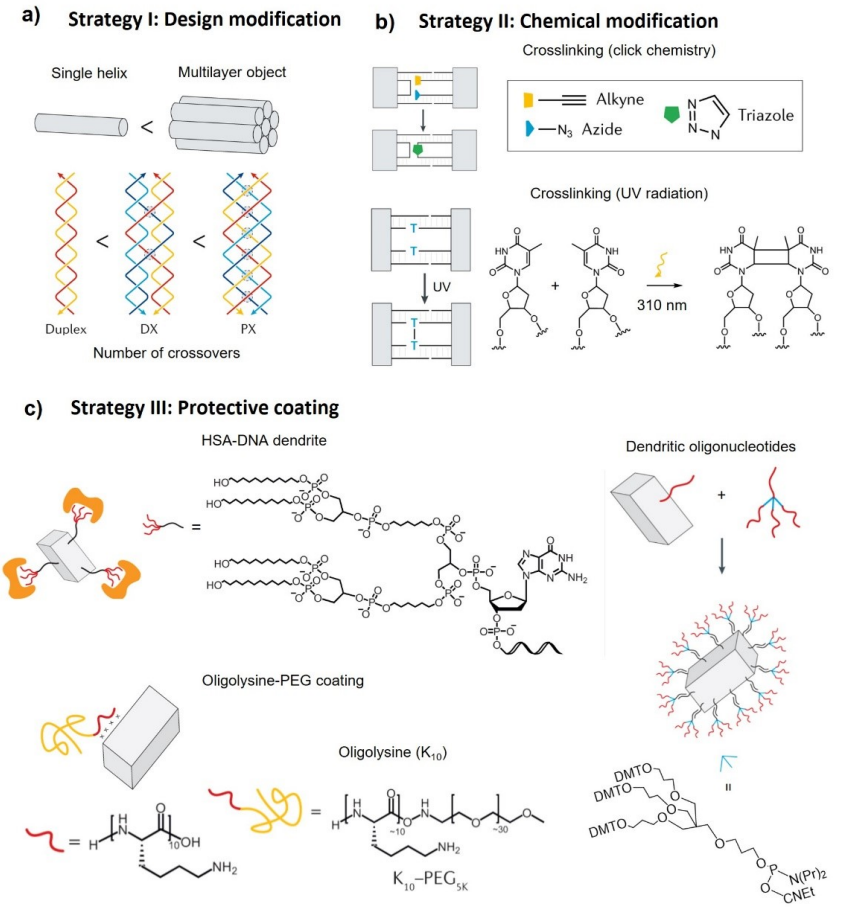

Figure 5: Strategies to protect DNA-based nanostructures from nuclease digestion. a) The utilization of strategies that involve designing DNA nanostructures, such as (top) incorporating closed-packed helices, results in enhanced resistance to nucleases when compared to linear duplexes or plasmid DNA. (bottom) Moreover, DNA motifs with a higher count of crossovers exhibit enhanced resistance to nucleases. b) Various chemical modifications have been demonstrated to augment the resistance of DNA structures against nucleases. These modifications encompass the crosslinking of component strands using click chemistry (top) and the crosslinking of strands through the formation of a thymidine dimer under UV irradiation (bottom). c) Numerous methodologies improve the nuclease resistance of DNA nanostructures by implementing protective coatings. These techniques involve the formation of coatings through the complexation of DNA dendrites with human serum albumin (HSA) (top), employing an oligolysine-PEG coating (bottom), and coating nanostructures with dendritic DNA *via* hybridization to DNA handles (right). Adapted with permission from Ref[140]. © Springer Nature

2.2.2 Protein cages

Proteins are an excellent platform for self-assembling higher-order structures due to their inherent versatility.[11] Their diverse chemical compositions offer the potential to create a wide range of structures, while their chemical and genetic modifications enable the development of precise compositions and functionalities. This flexibility makes proteins a highly adaptable and effective foundation for nanoengineering hierarchical structures.[11] Although lipid bilayers are the most common biological nanocompartments, protein cages stand out in providing uniformity in size and shape with a high tendency for customization and

versatility in their design.[159] They could be divided into viral and non-viral cages. Cowpea chlorotic mottle virus (CCMV) and brome mosaic virus (BMV) are prime examples of viral nanocompartments that protect RNA from the external environment. On the other hand, non-viral protein cages, exemplified by Ft and small heat shock proteins, play integral roles within biological systems, orchestrating a diverse range of vital processes. For instance, Ft is involved in regulating iron levels, while small heat shock proteins contribute to the maintenance of cellular homeostasis through the meticulous refolding of misfolded proteins. Nanocompartments of this nature have been extensively used as carrier entities for molecular delivery.[160,161] These carrier units excel in their functionality due to the unique capability of utilizing the void space created when the existing internal cargo *e.g.*, viral genome is removed. These cargo molecules can be encapsulated within the cages through disassembly and reassembly processes.[162] The cargo becomes trapped during this reassembly process. Both viral and non-viral cages, exemplified by virus-like particles (VLPs) and aFt, feature a charged luminal surface that frequently demonstrates remarkable efficiency in encapsulating polyelectrolyte materials through electrostatic interactions.[163,164] This remarkable capability stems from the intrinsic presence of anionic nucleic acids or charged metal ions within the respective cavities, making these cavities highly receptive to molecules bearing similar charges and properties.[165] Due to their uniform size and shape control, they are widely exploited for precise encapsulation of target molecules, such as drugs, enzymes, or nanoparticles, within the protein cage and have therefore been used for applications like bioimaging agents, delivery vehicles, reaction vessels, and constrained material synthesis for polymeric materials.[58,162,166–169]

The complete protein cages are formed through the SA of multiple subunits symmetrically.[58] The process typically involves the oligomerization of subunits to form intermediate structures, nucleation and assembly of subunits around oligomers, stabilization of the growing protein cage through non-covalent interactions, and fine-tuning and maturation steps. The SA of nanocompartments is driven by the intrinsic properties of the protein subunits and their interactions with each other, resulting in the formation of complex and functional protein cages with precise architectures.[170] Additionally, the interfaces between the subunits also serve as functional sites that can be modified to tune the properties of the cage. Regulating the process by which the subunits come together to form cages is the most straightforward way to control their properties in this manner. In addition, these interactions can be intentionally modified through chemical or genetic methods to alter the subunit interfaces. By doing so, it is possible to control the assembly-disassembly processes in a manner that can be triggered by external stimuli, *i.e.*, stimuli that are not naturally occurring within the cage.[61,62,171–173] The protein cage's outer layer, typically ranging from 2 to 5 nanometers in thickness, acts as a barrier between the interior and exterior spaces. It frequently includes pores that can be selective or non-selective in nature. Furthermore, the external surfaces of protein cages exhibit diverse functionalities, as the exposed peptide components can interact with the surrounding environment. Due to the symmetrical structure of protein cages derived from their

subunit arrangement, these external modifications are evenly distributed on the surface, maintaining a specific distance from one another.

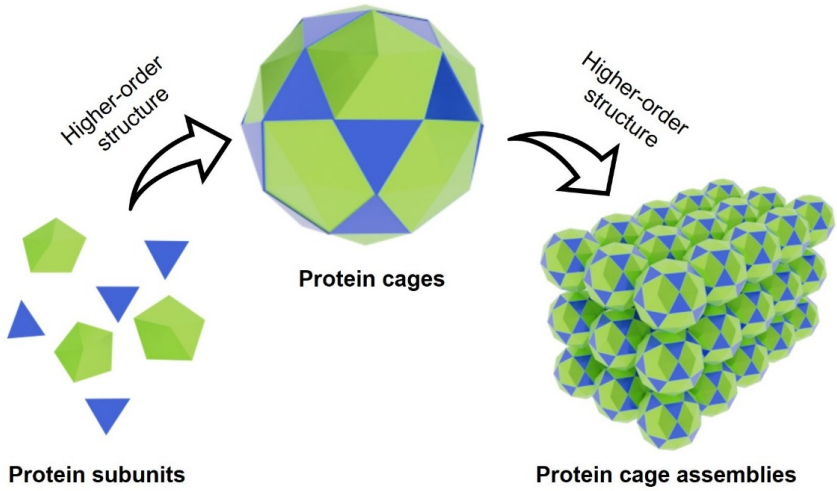

Figure 6: Formation of higher-order protein structures. Small protein subunits can assemble into robust protein cages, which can be further utilized to form higher-order structures.

For making such higher-order structure, the uniform size and shape of the construction material play an important role by promoting close packing, high symmetry, and nucleation (Figure 6). To construct 2D and 3D structures using protein cages as building blocks, two distinct approaches have been established. The first approach capitalizes on the direct physical interactions among protein cages, leveraging factors like electrostatic bonds,[174–180] metal coordination,[62] disulfide bonds,[181,182] or hydrophobic interactions[183–185] on their external surfaces. This can be achieved by careful designing and genetic engineering the amino acid residues at desired sites which promote these interactions. Protein cages typically exhibit an outward appearance that is negatively charged. As a result, it is possible to form protein assemblies by combining them with polycations through electrostatic interactions. The second approach involves the utilization of linker functionalities, which can be either covalent or non-covalent, to connect the protein cages together, enabling the creation of complex architectures.[45,185–189]

Ferritin

Ferritin (Ft) is a globular protein complex consisting of 24 subunits. It was initially isolated from the horse spleen by Victor Laufberger.[190] It is derived from a non-viral container motif, which is found intracellularly in various living organisms and plays a crucial role in iron metabolism.[191] Ft plays an important role in maintaining iron levels within living organisms by efficiently storing the metal in a condensed ferrihydrite mineral form ($5Fe_2O_3 \cdot 9H_2O$). Each subunit of Ft contains an active center that facilitates the conversion of ferrous to ferrihydrite, allowing it to accommodate a substantial amount of up to 4500 iron atoms.[192] aFt, on the other hand, is the protein cage without the iron load and has usually an octahedral shape with an outer diameter of approximately 12 nm with an

overall negative charge on the outer surface and an inner diameter of 7-8 nm (the thickness of the protein layer is ~2 nm).[193] Each subunit consists of four parallel helical peptide chains, providing significant rigidity to the entire cage, and has a molecular weight of around 20 kDa, which varies across aFt obtained from different sources. The vertebrate Ft structure mostly exhibits a symmetrical arrangement, known as 4-3-2 symmetry, where 4-fold and 3-fold symmetry axes intersect the corresponding channels in the shell. Specifically, there are six 4-fold channels and eight 3-fold channels. There is also mini Ft available in bacteria composed of 12 subunits and accommodates a smaller number of iron atoms (<500).[194] The subunits of Ft are classified into two types: H and L, denoting heavy and light chains, or heart and liver types, respectively. The H-type subunit possesses a greater molecular weight compared to the L-type. Additionally, the expression of the H type is predominantly observed in the heart, whereas the L type is primarily found in the liver. The M-type chain, which is absent in mammals, is a third middle chain and is specifically found in amphibians.[195] The 3D structure of the cage is typically consistent across different species, although the primary structure of Ft proteins may differ.

Ft is widely recognized as a favored protein cage for the development of protein-hybrid structures.[196] This preference arises from its renowned structural characteristics, thermal and chemical stability, ability to incorporate drugs and metals into its cage-like structure,[197] and potential for interior modification through genetic engineering[198]. The Ft exhibits a spherical hollow structure, with an overall negative charge present on its outer surface. Due to its charged interior, aFt can encapsulate positively charged small molecules sufficiently. Furthermore, Ft cages have been effectively employed as reaction vessels with restricted dimensions, enabling the synthesis of diverse nanoparticles such as metals, oxides, hydroxides, carbonates, and semiconductors.[199] As a result, numerous approaches have been developed to promote the mineralization process of nanoparticles within Ft. Various strategies involve the manipulation of the interior of the aFt cavity to optimize the formation of nanoparticles (Figure 7, right). The encapsulation of cargo within Ft leads to improved hydrophilicity and biocompatibility of the inorganic materials.[200] Similarly, the exterior surface of Ft can also be modified to exhibit specific functionalities (Figure 7, left). This includes chemically modifying the N-terminal lysine residues on horse-spleen aFt and followed by a series of conjugation reactions.[201] The resultant conjugate was effectively employed as a template for atom transfer radical polymerization (ATRP) to create Ft shells with grafted oligo(ethylene glycol) methacrylate polymers. Notably, this polymer material demonstrates solubility in dichloromethane.

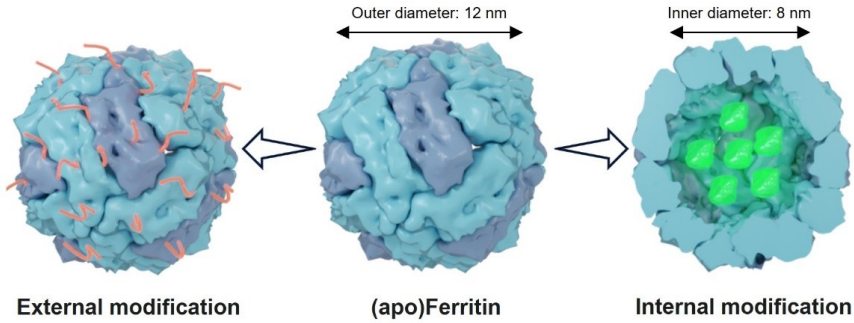

Figure 7: Structure of (a)Ft from horse spleen (PDB ID: 2 WoO). The cage can be modified both externally and internally.

Furthermore, the internal cavity of aFt cages has demonstrated remarkable efficacy in delivering anticancer drugs such as cisplatin[202–204] and doxorubicin[205]. Native heavy-chain-Ft nanocages demonstrate the ability to deliver significant amounts of doxorubicin (DOX) directly to tumor sites, without the need for a targeting ligand.[205] This delivery efficiency is attributed to the higher expression of transferrin receptor 1 in tumor cells, eliminating the requirement for a specific targeting ligand. Additionally, photosensitizers such as zinc phthalocyanine have also been successfully delivered from within the aFt cages, showcasing the versatility and effectiveness of this drug delivery system.[206] On the other hand, genetic engineering allows for the modification of the external surface, enabling its utilization in the creation of more complex structures. A notable example of this is combining a positively supercharged variant of Ft[207] with a native anionic cage.[179] By capitalizing on the inherent functionality of Ft, these crystals can be harnessed as a platform for incorporating inorganic nanoparticles. This is achieved through the process of mineralization within the individual component cages, before their subsequent assembly into a lattice structure. Furthermore, the introduction of metal oxides into the protein framework augments the crystals' oxidase and peroxidase activity, further expanding their potential applications.[174] By introducing specific mutations, aromatic stacking has also been utilized to construct both 2D and 3D superstructures using human heavy-chain Ft. This involved substituting a surface-exposed glutamic acid with phenylalanine or tyrosine, resulting in the desired assemblies.[183] In the case of shrimp Ft, point mutations were introduced by replacing a surface threonine or glutamine with arginine.[208] The resulting three-dimensional lattices were formed through interactions between arginine residues, effectively holding the structures together.

2.2.3 Phthalocyanines

Photosensitizers (PS) play a vital role in various photochemical reactions by absorbing light and transferring energy to neighboring molecules. Biomedical light management using PS offers diverse potential uses, each at different developmental stages. They find wide-ranging applications in photodynamic therapy (PDT),[209] a treatment method that utilizes light-activated photosensitizers to generate reactive oxygen species (ROS) with the ability to eradicate

abnormal cells. PDT has been widely used for treating various conditions including actinic keratoses, cancers like esophageal and lung cancer, warts, acne, and extramammary Paget's disease. In PDT, PS are used to render targeted malignant and diseased cells toxic by generating singlet oxygen ($^1O_2$) and other ROS[210] upon exposure to light. The generation of $^1O_2$ can be explained *via* the Jablonski diagram (Figure 8a), which is a graphical representation of the energy levels and electronic transitions involved in photochemical processes. It shows the different pathways a molecule can follow after absorbing light, including non-radiative relaxation, fluorescence, intersystem crossing, and the formation of $^1O_2$. Singlet oxygen can be formed through the process of intersystem crossing, where a molecule transitions from an excited singlet state to a lower-lying triplet state.[211] The excited triplet state has the capacity to interact with molecular oxygen (O_2), leading to the generation of $^1O_2$ and ROS. These exceedingly reactive and cytotoxic species are widely utilized in the field of PDT with the ultimate aim of killing cancer cells.[212]

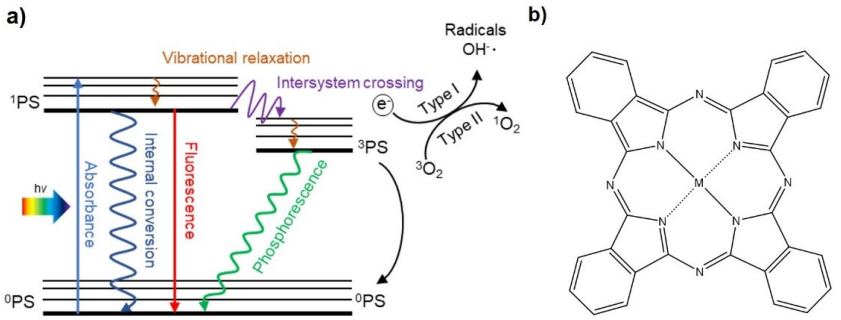

Figure 8: a) Jablonski Energy Diagram. PS in the ground state (^{0}PS) absorbs energy and transitions into an excited state(^{1}PS). The absorbed energy can be released in a non-radiative pathway through internal conversion or a radiative pathway such as fluorescence. PS can undergo a non-radiative intersystem crossing process from the ^{1}PS state to the triplet state (^{3}PS). The relaxation from the ^{3}PS state to the ground state (phosphorescence) is characterized by significantly longer lifetimes compared to fluorescence. This triplet state can also undergo other photoactive reactions such as Type I reactions involving the generation of free radicals or superoxide ions through hydrogen or electron transfer processes. On the other hand, Type II reactions occur when oxygen interacts with the triplet state of a sensitizer, leading to the production of $^1O_2$. b) Chemical structure of a metal-complexed phthalocyanine.

Phthalocyanines (Pc) are a type of synthetic macrocycle composed of four isoindole units linked together by nitrogen atoms, forming a large, planar structure that can host a wide variety of central metal ions. Figure 8b depicts the structure of the Pc macrocycle complexed with a metal atom, showcasing the coordination capabilities of Pc. Furthermore, Pcs offer synthetic variability, allowing for the fine-tuning of their physicochemical properties such as solubility, (photo)stability, and photophysical characteristics. The extensive conjugation in the structure of Pc enables its strong absorption of energy in the near-infrared (NIR) region, particularly within the so-called Q-band centered in the range of 650 to 700 nm.[213–215] This arises from transitions between the highest occupied and lowest unoccupied molecular orbitals (HOMO and LUMO) in the Pc macrocycle. This attribute makes them suitable for PDT applications since NIR light can penetrate deeper into tissues, enabling the treatment of tumors located at greater depths. Additionally, Pcs exhibit another distinct photoelectronic transition namely the Soret band. Traditionally centered in the UV-Vis range, it

emerges from transitions between Pc's ground state and its second excited state. This involves $\pi \rightarrow \pi^*$ interactions, causing pronounced absorption peaks at shorter wavelengths. The positions and intensities of these bands offer valuable insights into the electronic structure and coordination environment of Pc. These factors play a significant role in shaping its absorption and emission properties, allowing for customization to specific applications. Such properties can be finely adjusted through chemical modifications and the choice of metal hosts. This versatility finds practical use across diverse domains, encompassing optoelectronics, diagnostics, biomedicine, and catalysis.[214,216–225] Notably, Pc possesses the ability to generate highly reactive $^1O_2$, which has attracted considerable interest in fields like PDT and water treatment. The majority of present-day PS including Pcs are characterized by their high degree of conjugation, resulting in limited solubility in water or a tendency to aggregate strongly in aqueous solutions. These characteristics diminish their ability to be absorbed effectively and undermine their effectiveness in biomedical applications, particularly in terms of their low photodynamic activities. There are a few strategies by which this problem can be tackled. One method for improving the solubility involves the incorporation of large or elongated molecular groups, such as alkyl or alkoxy, at the outer locations of the Pc structure.[226–229] While covalent methods can indeed be effective for achieving this, it is important to note that the synthesis process itself can be quite intricate and demanding in practice. An alternative approach is to address these crucial concerns by emulating nature and utilizing biologically inspired hybrid materials.[230] These materials aim to preserve or even enhance the optical properties of the photosensitizers in physiological environments. Photoactive biohybrids can be created by associating Pc with biomolecules, either through covalent or non-covalent methods. Covalent approaches offer advantages such as stability and precise localization of the Pc within the biomolecule structure, thanks to advanced biorthogonal and site-specific reactions. However, covalent methods often require complex designs and synthetic routes due to the need for compatible functional groups in both the Pc and biomolecule. On the other hand, supramolecular strategies provide greater flexibility in choosing the conjugation partner and simplify the design and synthesis process.[59,66]

2.2.4 Pillararenes

Macrocycles, including cyclophanes, belong to a versatile class of organic compounds that find wide applications in the field of host-guest chemistry. Cyclophanes, in particular, are defined by their unique composition of one or more aromatic rings, where at least two atoms form a distinct ring system separate from the initial aromatic ring.[231–233] These compounds exhibit an intriguing cage-like structure, characterized by two or more interconnected aromatic rings connected by a bridge. This arrangement allows for the formation of an enclosed space within the macrocycle, enabling interactions with guest molecules. Due to their tailored structural properties, cyclophanes have garnered significant interest as functional building blocks for various supramolecular assemblies and molecular recognition processes. Among the various types of cyclophanes,

pillar[n]arenes have emerged as a prominent class due to their unique host-guest properties.[234–239]

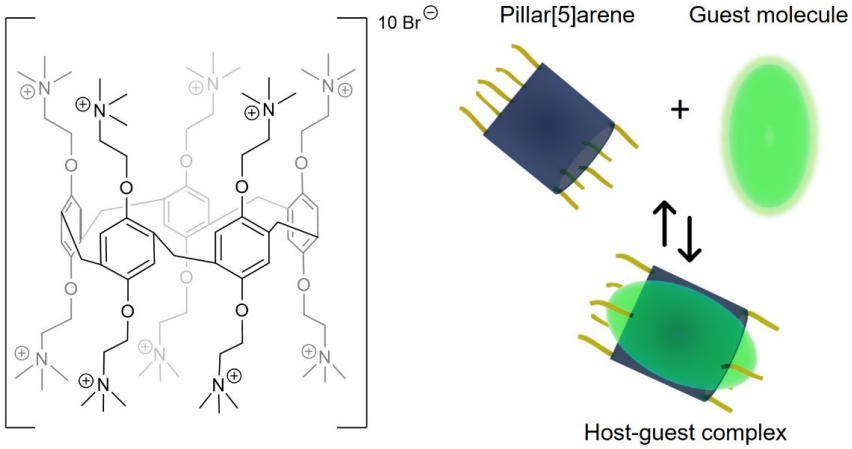

Figure 9: a) Molecular structures of the pillar[5]arenes utilized in this dissertation and b) the formation of a host-guest complex with pillar[5]arene (cylinder-shaped)

Pillar[n]arenes possess a distinct composition where two or more aromatic rings are connected at the para-position through methylene bridges (Figure 9a). This unique arrangement generates a pillar-like structure, conferring symmetrical cylindrical shapes to the molecules. As a result, these structures exhibit conformational stability and equal accessibility from both sides.[240] The number of hydroquinone units within these pillar[n]arenes determines the size and adjustability of the cavity formed, giving rise to varying cavity dimensions. Pillar[n]arenes possess the ability to undergo versatile functionalization, resulting in a wide array of modified derivatives. Functional derivatives of these molecules can be designed to interact with intricate biomolecules, such as proteins while maintaining solubility in aqueous solvents. The presence of multiple aromatic rings in the structures often imparts high hydrophobicity. To enhance aqueous solubility, a viable approach involves introducing charged groups onto each ring, particularly when they are positioned on both sides of the ring structures.[241] These derivatives exhibit anticipated chemical or physical properties, making them valuable for a multitude of applications in the field of supramolecular chemistry.[242–244] These molecules have a hydrophobic cavity that can encapsulate guest molecules, similar to cyclodextrins.[245]

One of the primary applications of pillar[n]arenes is in the field of drug delivery and sensors.[246] Pillararene-based drug delivery systems have been developed for the encapsulation and controlled release of drugs, enhancing their solubility, stability, and therapeutic efficacy.[247] Pillar[n]arenes can also be used as molecular recognition motifs in sensors, where they can selectively bind to specific guest molecules and trigger a signal response.[248] Moreover, they have recently displayed non-bactericidal effects by targeting vital virulence factors in Gram-negative pathogens, effectively suppressing toxins, biofilms, and antibiotic resistance. This discovery holds promise as an innovative approach for addressing a wide range of infections.[239] Furthermore, pillararenes have been utilized in the formation of higher-order structures, such as supramolecular

assemblies and nanoparticles.[57] By self-assembling with other molecules or nanoparticles, pillararenes can form complex architectures with tailored functionalities, offering opportunities for advanced materials and nanotechnology applications.

2.2.5 Fluorescent proteins

The discovery of genetically-encodable FPs has made a significant contribution to the existing library of fluorescent probes. These FPs are particularly valuable as they possess all the necessary information for fluorescence within their primary amino acid sequence. Consequently, FPs have been extensively exploited for live cell imaging.[249] FPs, specifically referring to proteins similar to green fluorescent protein (GFP),[250,251] are intricate 3D polypeptide structures with a size of approximately 25–30 kDa and emit bright green light upon stimulation with UV or blue light[252]. The tertiary configuration of GFP is vital for both the creation of the chromophore and its photophysical characteristics. These arrangements include an organic chromophore that is accountable for their luminous attributes and situated within a rigid β-barrel structure consisting of 11 β-sheets encircling an α-helix. In GFP, the chromophore demonstrates a fundamental structural motif known as 4-(p-hydroxybenzylidene)-5-imidazolinone.[253–256] The chromophore is effectively protected from the surrounding solvent by a comprehensive network of hydrogen bonds that intertwines the surface of the β-barrel. Additionally, the scaffold serves as a protective shell, encapsulating the chromophore and impeding the access of external molecules. It accomplishes this through a combination of structural and electrostatic interactions, including hydrogen bonds, steric interactions with neighboring residues, and the electrostatic field generated by the protein matrix. The chromophore can exist in both anionic and neutral forms, with their relative concentrations dependent on environmental factors such as ionic strength, pH, and temperature.[257] Moreover, the rigid β-barrel structure of FPs not only imparts stability against moderate environmental changes but also plays a crucial role in modulating the spectroscopic properties of the chromophore.[258–261] The protein scaffold provides a suitable environment that facilitates the autocatalytic formation of the chromophore and the reactive processes responsible for generating emissive species. Over the past decade, there has been a growing interest in the utilization of these biological materials and structures for photonic purposes such as lasers[262–264] and LEDs[265–267]. This is due to their favorable spectral characteristics, which have the potential to rival those of synthetic fluorophores.

There is a relentless pursuit of exploring increasingly brighter and improved FPs that can cover a wide range of the electromagnetic spectrum. In addition to brightness, several key enhancements are sought after, such as high quantum yield, significant Stokes shift, insensitivity to pH fluctuations, rapid maturation, reduced tendency to form oligomers, and enhanced photostability.[268] By performing rapid modifications and mutagenesis on the wild-type GFP (wtGFP), the excitation and emission maxima of GFP were altered, leading to the development of FPs capable of emitting light in the blue (BFP), cyan (CFP), and

yellow (YFP) spectral ranges. An additional avenue of enhancement involves the development of techniques to prevent aggregation induced by both thermal and chemical factors, which includes the creation of a supercharged variant of the protein. For example, the supercharged version of GFP maintained nearly identical excitation and emission spectra as the original GFP.[269] These supercharged FPs have been employed to construct hierarchical structures, presenting extensive possibilities for the generation of innovative architectures.[270,271]

3. Material and Methods

Extensive information regarding the materials and methods employed can be found in Publications **I**-**IV**, whereas only a condensed overview will be presented here.

3.1 DNA origami

In Publications **I** and **II**, the 6HB and 60HB DO structures were folded using ssDNA isolated from the M13mp18 plasmid (Tilibit Nanosystems), consisting of 7249 nucleotides (nt). The 24HB structure, on the other hand, was folded using a scaffold of 7560 nt derived from the same plasmid. To facilitate the folding process, a specific number of staple strands (obtained from Integrated DNA Technologies) were utilized: 170 for 6HB, 202 for 24HB, and 141 for 60HB DO. After the folding, the DO structures were purified using PEG purification, and their concentration was estimated through measurements based on the Beer-Lambert relationship and UV-Vis spectroscopy using a Biotek Eon Microplate Spectrophotometer. The design and sequence of the staple strands used for the folding, as well as thermal ramp were adapted from previously published studies (6HB from Bui *et al.*,[272] 24HB from Ijäs *et al.*,[273] and 60HB from Linko *et al.*[274]).

3.2 Agarose Gel Electrophoretic Mobility Shift Assay

In Publications **I** and **II**, agarose gel electrophoresis mobility shift assay (EMSA) was employed to assess the purity of DO structures (6HB, 24HB, 60HB) and explore the optimal co-assembly ratio of DO with ZnPcs. A gel with 2% (w/v) agarose content was prepared by dissolving 2 g of agarose in 90 mL of 1× TAE buffer, heating the mixture until it became clear, and then adding 10 mL of 110 mM MgCl2. For gel visualization, 80 µL of ethidium bromide (EtBr) solution (0.58 mg mL^{-1}) was used to stain the gel before it was poured into the casting tray. The samples were combined with Gel Loading Dye Blue (6×). Electrophoresis was conducted at a constant voltage of 90 V for 45 minutes using a BioRad horizontal-wide Mini-Sub GT electrophoresis system and a BioRad PowerPac™ Basic power supply. The electrophoresis run employed a running buffer of 1× TAE containing 11 mM $MgCl_2$, and the gel chamber was situated on an ice bath throughout the process. Gel visualization was achieved using either a BioRad Gel Doc™ XR+ Documentation system or a BioRad ChemiDoc™ MP Imaging

system, employing excitation wavelengths of 532 nm (Alexa 546) and 633 nm (Alexa 647).

3.3 Microscopy

3.3.1 Optical Microscopy

Publications **I**, **III**, and **IV** utilized optical microscopy to capture images. The images were acquired using either a Leica DM4500 microscope with cross-polarizers or a Zeiss Axio Vert A1 inverted microscope. After the complex formation, the samples were incubated at room temperature for 20 minutes and then refrigerated overnight before imaging on the following day. To prepare the samples, a 5 µL droplet was placed on a glass slide, and a cover slip was applied using double-sided tape on the corners to create a chamber that preserved the structural characteristics of the sample.

3.3.2 Transmission Electron Microscopy

In Publications **I**, transmission electron microscopy (TEM) images were captured using either an FEI Tecnai 12 Bio-Twin instrument or a JEOL JEM-2800 analytical HR-TEM. The FEI Tecnai 12 Bio-Twin operated at an acceleration voltage of 120 kV, while the JEOL JEM-2800 operated at 200 kV. Square mesh copper grids were used to support the samples. For staining, the samples in Publications **I** were negatively stained with uranyl formate.

In Publications **III** and **IV**, cryogenic TEM (cryo-TEM) images were obtained using a JEOL JEM 3200FSC field emission microscope. The microscope was operated at 300 kV in bright field mode, equipped with an Omega-type zero-loss energy filter. Gatan Digital Micrograph software was used to capture the images while maintaining the specimen temperature at -187 °C. To prepare the cryo-TEM samples, a 3 µL aqueous dispersion of the model was placed on a 200-mesh Lacey carbon film on Copper TEM Grids from agar scientific. The grids were then plunge-frozen into liquid ethane using a Leica grid plunger, with a blotting time of 3 seconds under 100% humidity. The grids with vitrified sample solution were stored at liquid nitrogen temperature and cryo-transferred to the microscope.

Before using the TEM grids for all samples, they underwent plasma cleaning using the NanoClean 1070 system from Fischione Instruments. Additionally, ImageJ software was employed for further processing of the acquired images.

3.4 Small Angle X-ray Scattering

In Publications **III** and **IV**, small angle X-ray scattering (SAXS) patterns were recorded using the Xenocs Xeuss 3.0 C instrument, which was equipped with a GeniX 3D Cu microfocus source with a wavelength (λ) of 1.542 Å. The measurements were conducted at a sample-to-detector distance of 0.6 m, utilizing an EIGER2 R 1M hybrid pixel detector. For all measurements, the scattering vector

q was calibrated using a silver behenate standard, and the 2D scattering data were converted into SAXS curves through azimuthal averaging, and the magnitude of the scattering vector (q) was determined by the equation $q = 4\pi \sin\theta/\lambda$, where 2θ represents the scattering angle.

To prepare the samples, gentle mixing was performed using a pipette, resulting in the formation of precipitates immediately after mixing for lower ionic strength, however, higher ionic strength sample remained without visible aggregates. The samples were then incubated in a refrigerator for 1 hour to allow the precipitates to settle. Subsequently, the sedimented samples were then analyzed by SAXS. The samples were sealed in glass capillaries with a diameter of either 1 or 1.5 mm, ensuring that no X-rays were scattered in the measured q range.

3.5 Dynamic light scattering

In Publications **III** and **IV**, the hydrodynamic diameters of self-assembling protein cages (aFt, Ft) combined with cationic pillararenes and scmGL, respectively, were assessed using dynamic light scattering (DLS). Both publications involved dissolving the protein cages in a buffer solution (20 mM Tris, pH 7.5) and then titrating them either with P10+ (structure shown in Figure 9) or scmGL. The Zetasizer Nano ZS Series equipment from Malvern Instruments was employed to monitor the increase in particle count rate and the sizes of secondary assemblies. The measurements and titrations were conducted at a temperature of 25 °C using PMMA cuvettes.

3.6 UV-Vis spectroscopy

In Publications **I-IV**, UV-Vis spectroscopy was performed using a Cytation 3 plate reader from BioTek. In Publications **I** and **II**, the focus was on examining the changes in the absorbance spectra of ZnPc in the presence of DO and NaCl. To prepare the samples, 100 μL PCR tubes were utilized, and then the contents were transferred to a transparent flat-bottom 96-well plate. In Publications **III** and **IV**, crystal preparation followed the respective protocols mentioned in the publications. After overnight incubation in the refrigerator, the supernatant liquid was replaced with fresh buffer (20 mM Tris, pH 7.5) and measurements were carried out.

4. Results and Discussion

Within this section, the outcomes of the publications are examined sequentially based on their numerical arrangement. The publications encompass all the acquired results, while this discussion specifically highlights the most pertinent findings concerning the characterization and application of self-assembled DO and protein cage structures.

4.1 Self-assembly of DNA origami with zinc phthalocyanines

In both Publication **I** and **II**, negatively charged DO was combined with tetra- or octa-cationic ZnPc to create electrostatic self-assembled structures. The research was done to improve the photoactivity of ZnPcs in elevated ionic strength media, and in return, the coating strategy can also protect against the enzymatic digestion of DO. In Publication **I**, cylindrical-shaped, negatively charged 6HB was combined with octa-cationic ZnPc (ZnPc(+8)). To determine the ratio at which the 6HB is completely grafted by the ZnPc(+8), an agarose EMSA was employed. EtBr was used to stain the agarose gels to observe the location of 6HB following the run. Subsequently, the gels were illuminated at 532 nm and 633 nm to visualize EtBr and ZnPc respectively. A fixed concentration of 6HB was subjected to titration with ZnPc(+8). As the ratio of ZnPc(+8) increased, the intensity of the free 6HB band in the gel diminished until it reached a saturation point, indicating full coverage of 6HB (Figure 10a). Moreover, to demonstrate that the assembly is governed by electrostatic forces, NaCl was introduced before complex formation to elevate the ionic strength of the medium. It was observed that higher ionic strength, specifically above 200 mM NaCl, impeded the formation of the complex. As a result, when samples with higher ionic strength were employed, the 6HB band reappeared in the EMSA gel (Figure 10b).

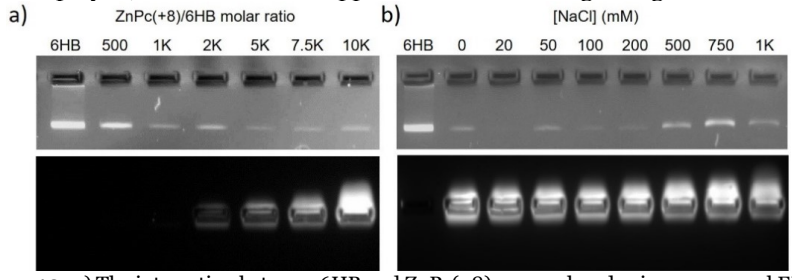

Figure 10: a) The interaction between 6HB and ZnPc(+8) was analyzed using agarose gel EMSA with increasing molar equivalents of ZnPc(+8). (b) Agarose gel EMSA was conducted to examine the ZnPc(+8)–6HB complex under varying NaCl concentrations. The gel exhibited two emission channels: EtBr (532 nm) (top) and ZnPc (633 nm) (bottom). Paper I, © 2020 The authors, reproduced from Royal Society of Chemistry under CC BY 3.0.

To acquire more understanding of the correlation between the properties of the created complexes and the ionic strength of the media, additional information was obtained using UV-Vis absorption spectroscopy and TEM imaging. At various NaCl concentrations, the absorption spectrum of ZnPc(+8) was measured under constant concentration, while ZnPc was present in an amount equivalent to 500 times the concentration of 6HB (Figure 11a). It has been previously known that the ZnPc exhibits a shift in the wavelength of its Q-band absorption when it undergoes aggregation. In its monomeric state, it displays a strong absorption band at 676 nm, whereas in the aggregated state, the absorption becomes broader and less intense, occurring at 632 nm.[215] The efficacy of the studied combination can be assessed by quantifying the ratio of deaggregated and aggregated ZnPc (Figure 11b). In the absence of 6HB, the rise in ionic strength resulted in the anticipated aggregation of ZnPc(+8). However, the introduction of varying amounts of 6HB resulted in two distinct observations. In the initial range of 0 to 200 mM NaCl (referred to as regime A), there was a decrease in the aggregation of ZnPc(+8). However, in the subsequent range of 200 to 1000 mM NaCl (referred to as regime C), an increase in aggregation was observed. Notably, the most significant disruption of aggregation was observed at a NaCl concentration of 200 mM (referred to as regime B), and this effect was only evident at ZnPc(+8)/6HB ratios below saturation (specifically, when the ratio of ZnPc(+8)/6HB was 2000 eq.). Therefore, the prevention of aggregation can be attributed to the formation of a complex between ZnPc(+8) and 6HB, resulting in a disaggregation effect.

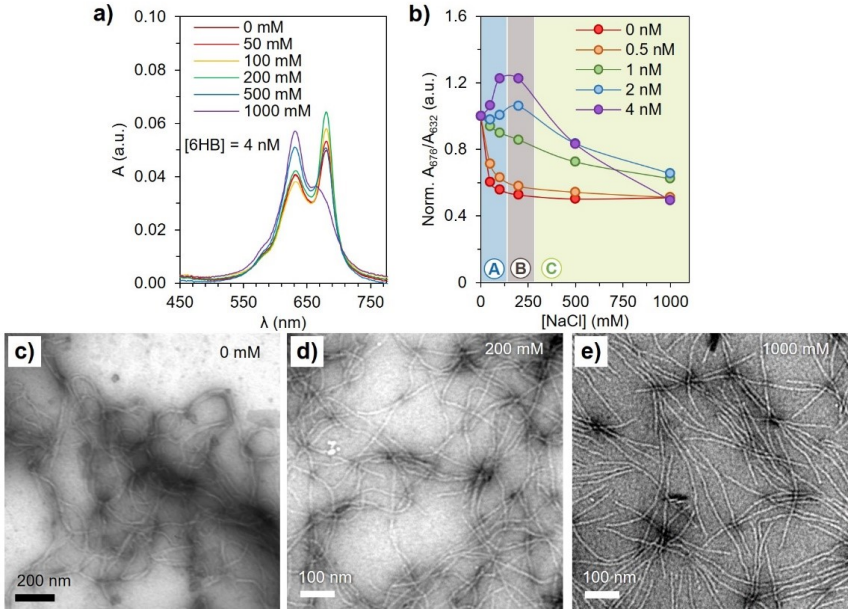

Figure 11: (a) The absorption spectra of ZnPc(+8) were recorded while varying NaCl concentrations, in the presence of 6HB (ZnPc(+8)/6HB = 500). (b) The ratio between the absorption at 676 nm and 632 nm of ZnPc(+8) was determined at different NaCl and 6HB concentrations, with normalization to the value at 0 mM NaCl (c-e) TEM images of the ZnPc(+8)–6HB complexes were captured under three conditions: 0 mM NaCl, 200 mM NaCl, and 1000 mM NaCl. Before imaging, the samples were stained with uranyl formate staining. Paper I, © 2020 The authors, reproduced from Royal Society of Chemistry under CC BY 3.0.

TEM images (Figure 11c–e) confirm the morphological changes that occur in the complexes when the ionic strength is increased. At low levels of ionic strength, noticeable clusters of 6HB are present. This clustering is facilitated by the charged ZnPc acting as a supramolecular adhesive, crosslinking the 6HB. However, as NaCl is gradually added, these larger clusters begin to disintegrate, and individual 6HB structures become visible at a NaCl concentration of 200 mM. Further addition of NaCl (final conc. = 1000 mM) leads to the dissociation of ZnPc(+8) and 6HB, causing the unbound ZnPc to form aggregates in the high ionic strength environment. Therefore, the optimal condition for achieving individual 6HB loaded with a substantial amount of non-aggregated ZnPc is the formulation of the complexes at 200 mM NaCl. This ensures that the ideal optical properties of the complex are maintained.

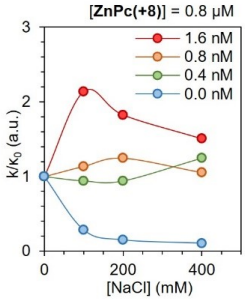

Figure 12: The normalized photooxidative activity (k/k_0) of ZnPc(+8)–6HB complexes was assessed at various 6HB ratios and NaCl concentrations. Paper I, © 2020 The authors, reproduced from Royal Society of Chemistry under CC BY 3.0.

The evaluation of the complex's resistance to photo-oxidative changes caused by aggregation under physiological conditions was conducted using a comparative approach.[275] The effectiveness of this approach is based on the direct correlation between the decomposition of the chemical scavenger 1,3-diphenylisobenzofuran (DPBF) and the production of $^1O_2$ resulting from photoreactions. Different equivalent ratios of ZnPc(+8)/6HB were exposed to varying durations of irradiation at constant fluence rates, in the presence of varying amounts of NaCl and aqueous DPBF (more details in Publication **I**). By studying the slope ratio (k/k_0), where k_0 is the slope of the relativity of absorbance before and after each irradiation step ($\ln(A_0/A_t)$) against the irradiation time (t), in the absence of salt and k represents the same slope but in the presence of salt, it is observed that the photoactivity of complex ZnPc(+8) is significantly suppressed at higher NaCl concentrations (Figure 12). In contrast, the ZnPc(+8)-6HB complex exhibits optimal photoactivity between 100 and 200 mM NaCl. These results are consistent with the previously observed patterns of aggregation and deaggregation, highlighting the ability of these complexes to effectively produce $^1O_2$ in environments that closely resemble physiological conditions.

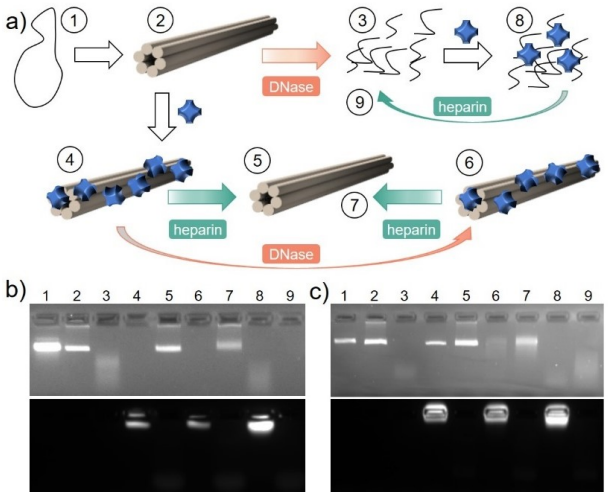

Figure 13: a) Scheme of the digestion experiment. (1) M13mp18 scaffold, (2) 6HB, (3) digested 6HB (d6HB), (4) ZnPc(+8)–6HB, (5) deprotected 6HB, (6) ZnPc(+8)–6HB after digestion, (7) deprotected 6HB after digestion, (8) ZnPc(+8)–d6HB, (9) deprotected d6HB. The numbers in the figure correspond to the agarose gel EMSA lanes at b) 0 mM and c) 200 mM of NaCl. Paper I, © 2020 The authors, reproduced from Royal Society of Chemistry under CC BY 3.0.

The susceptibility of DNA-based drug delivery systems to enzymatic degradation is a significant factor influencing their circulation duration and bioavailability. Deoxyribonuclease (DNase I), as an endonuclease enzyme, cleaves the phosphodiester bonds found within a polynucleotide chain, resulting in the production of smaller oligonucleotide fragments. In EMSA, the degraded DO has higher mobility due to its smaller size. The fetal bovine serum (FBS) contains 0.256–1.024 Kunitz U mL^{-1} of endonuclease activity[145] and when utilizing therapeutic approaches based on DNA, these treatments must be resilient against this enzymatic degradation. Ensuring stability and effective delivery of the therapeutic payload relies on overcoming the activity present in such biological media. In order to assess the protective effect of the combined approach involving ZnPc(+8) and 6HBs against DNase I degradation, the following experiment was devised and examined through EMSA (Figure 13b). As a control, naked 6HB was digested, resulting in the vanishing of the DO band and the emergence of fragments exhibiting greater electrophoretic mobility. The ZnPc(+8)–6HB complex was then subjected to digestion, followed by the disassembly using heparin to assess the integrity of the DO. Heparin, a highly anionic biopolymer, strongly binds to ZnPc(+8), releasing the intact 6HB. Upon recovering the 6HB from the formed complex, it exhibited intact recovery (lane 7), indicating protection against the nuclease. To demonstrate that the DO protection is solely attained through the interaction with ZnPc(+8) and not because of macroscopic complexation or aggregation, the identical experiment was conducted while introducing 200 mM NaCl (Figure 13c), resulting in an identical outcome.

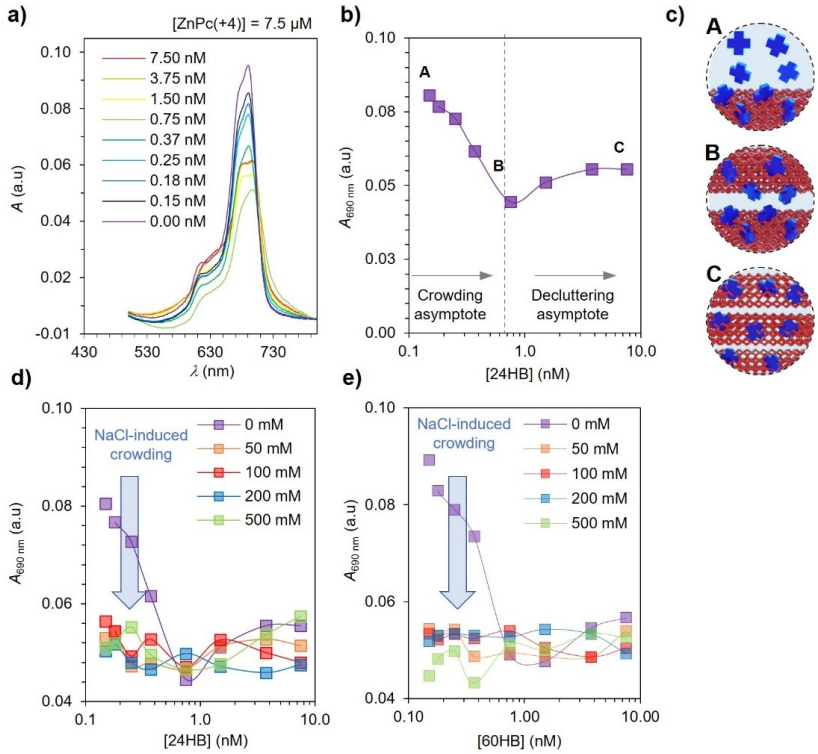

Figure 14: (a) Absorption spectra of ZnPc(+4) in the presence of various concentrations of 24HB. (b) Absorbance of ZnPc(+4) at 690 nm in the presence of different 24HB concentrations. (c) Top to bottom: schematic representation of the ZnPc(+4)–24HB hybrids at (A) 40 000, (B) 10 000, and (C) 2000 equivalents of ZnPc(+4) per 24HB. (d) Absorbance of ZnPc(+4) at increasing amounts of d) 24HB with NaCl and e) 60HB with NaCl. Paper II, © 2022 The authors, reproduced from American Chemical Society under CC BY 4.0.

In Publication **II**, the interaction between a Janus-type ZnPc and two different types of DO *i.e.*, 24HB and 60HB was studied. The term "Janus-type" refers to the unique molecular structure of ZnPc, which exhibits two distinct surfaces within the same molecule. Among the four isoindole rings of this Janus-type ZnPc molecule, one of them carries a total of four positive charges, while on the opposite side, there are six triethylene glycol chains distributed across the remaining three isoindole units. The presence of triethylene glycol chains in the ZnPc molecule confers inert properties and enhances water solubility. Simultaneously, the bulky charged substitution not only shields against the usual aggregation tendencies of ZnPc but also enables interactions with negatively charged biomolecules like DNA. This duality in charge and chemical composition is what makes the ZnPc molecule Janus-type. The tetra-cationic ZnPc (ZnPc(+4)) and DO interaction was studied using UV-Vis spectroscopy. The absorption of ZnPc(+4) at a constant concentration was recorded while increasing the concentrations of 24HB, which demonstrated no significant band shift (Figure 14a). Nevertheless, when plotting the absorbance of ZnPc(+4) at 690 nm against the concentration of 24HB, it becomes evident that two patterns emerge (Figure 14b). Initially, the inclusion of 24HB up to 1.5 nM led to a reduction in the apparent extinction coefficient (ε) (Figure 14c, A). This behavior, known as the binding asymptote, occurs due to an excess of stepwise binding of ZnPc(+4) to

the DO. The saturation point represents the complex with densely packed ZnPc, exhibiting a minimum apparent ε (Figure 14c, B). Further increases in 24HB concentration led to an apparent increase in ε (decluttering asymptote) (Figure 14c, C). In this range, the available surface area of DO increases, causing reduced molecular packing of ZnPc(+4). To delve deeper into this, the previously mentioned experiments were replicated for both DO (*i.e.*, 24HB and 60HB) while introducing increasing concentrations of NaCl. The binding saturation point was essentially absent beyond 50 mM of NaCl, owing to the aggregation of unbound ZnPc(+4) caused by the presence of salt (Figure 14d–e). However, the decluttering asymptote remained, indicating robust binding resilience in high ionic strength media. This phenomenon can be attributed to the establishment of a resilient, kinetically trapped state enabled by the development of a core–shell-like structure. Within this configuration, the charged interface connecting ZnPc(+4) and DO remains shielded from the influence of the media's ionic strength by the hydrophilic yet neutral ethylene glycol corona.

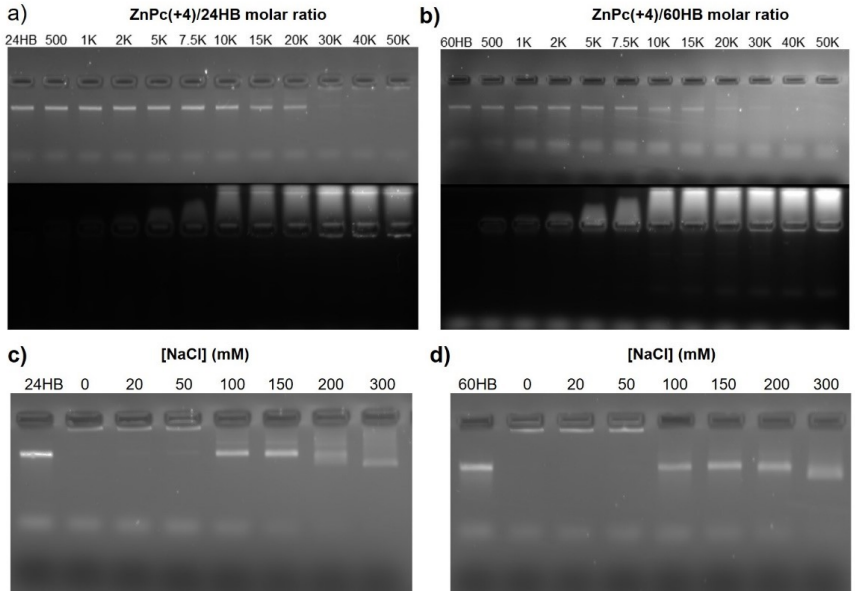

Figure 15: Agarose gel EMSA of a) 24HB and b) 60HB titrated with increasing molar equivalents of ZnPc(+4). EMSA of (c) ZnPc(+4)–24HB complex and ZnPc(+4)–60HB complex in the presence of increasing NaCl concentrations. Paper II, © 2022 The authors, reproduced from American Chemical Society under CC BY 4.0.

The stoichiometric ratio necessary for the formation of the complex was determined using EMSA. ZnPc(+4) was titrated with a constant concentration of 24HB and 60HB to ascertain the maximum binding capacity, referred to as the saturation ratio, which aligns with the methodology described in Publication **I**. With increasing quantities of ZnPc(+4), the intensity of the unbound DO band gradually diminished until reaching an excess at a ZnPc(+4)/DO molar ratio of approximately 40,000 for both 24HB (Figure 15a) and 60HB (Figure 15b). This ratio is considerably higher compared to the amount of ZnPc(+8) required to coat the 6HB, which can be attributed to the lower number of charges present in ZnPc(+4). To confirm the electrostatic nature of the complexation process, different concentrations of NaCl were introduced before mixing ZnPc(+4) with

24HB (Figure 15c) or 60HB (Figure 15d). For this experimental setup, a ZnPc(+4)/DO molar ratio of 40,000 was selected to ensure the complete coverage of DO. The ensuing EMSA analysis unveiled that ZnPc(+4) effectively binds to DO up to 50 mM NaCl. However, the increase of NaCl concentration beyond 100 mM hindered the complexation process, as indicated by the resurgence of a distinct DO band. This observation provides further substantiation that the assembly is predominantly driven by electrostatic interactions.

4.2 Electrostatic self-assembly of protein cages

In Publications **III** and **IV**, anionic protein cages, namely aFt and Ft, were co-crystallized with cationic molecular glues, pillararene and green lantern protein, respectively. In Publication **III**, the pillar[5]arene (p10+)(Figure 9) exhibited five cationic charges on each side of its hydrophobic cavity. This cavity provides an opportunity to accommodate different organic pollutants, while the protein cage has a natural ability to host ionic metals. As a result, the resulting crystalline assemblies can be effectively utilized for the simultaneous removal of both organic and inorganic pollutants from aqueous environments. The progression of the SA procedure was initially monitored by DLS, encompassing the tracking of the elevation in particle count rate and the hydrodynamic diameter (D_h). A constant concentration of aFt or Ft (0.1 mg mL^{-1}) was incrementally mixed with increasing quantities of P10+. Initially, Ft demonstrates a rapid increase in intensity, indicating the presence of aggregates (Figure 16a, left). This occurs at a [P10+] concentration of 10 mg L^{-1}, while for aFt, it occurs at 17.5 mg L^{-1}. The minor variation in the aggregation threshold can be explained by the notably reduced overall molecular weight of aFt, stemming from the absence of the iron oxide core. This decreased weight allows for a higher quantity of cages to exist within a specific volume. Consequently, a higher concentration of P10+ is required to promote the formation of complexes.

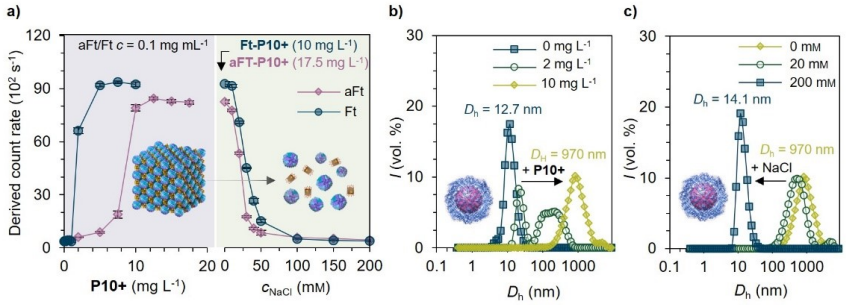

Figure 16: SA of protein cage-P10+ complexes was examined through DLS. a) (left) DLS measurements were conducted on solutions of Ft and aFt, which were titrated with increasing concentrations of P10+. This demonstrates the formation of complexes involving both protein cages. (right) the complexes were disassembled by raising the ionic strength of the medium through the addition of NaCl. b) DLS data illustrates the volume-averaged size distribution of free Ft when titrated with increasing amounts of P10+. c) the resulting complexes are shown to disassemble upon the introduction of NaCl. Paper III, © 2022 The authors, reproduced from Wiley-VCH GmbH under CC BY 4.0.

To demonstrate that electrostatic interactions play a crucial role in the recognition process, the complexes formed between the protein cages were disassembled by increasing the ionic strength. This disassembly was observed for both protein cages at similar levels of NaCl concentration (above 50 mM), as depicted in Figure 16a (right). This phenomenon correlates with the observed changes in the D_h of Ft. With increasing P10+ concentration, the peak representing the native size of Ft decreases, as shown in Figure 16b. Nonetheless, elevating the ionic strength of the surrounding medium leads to the D_h reverting to its initial dimensions. This observation suggests that the system can be effectively disassembled to its original state by merely augmenting the electrolyte concentration, as depicted in Figure 16c.

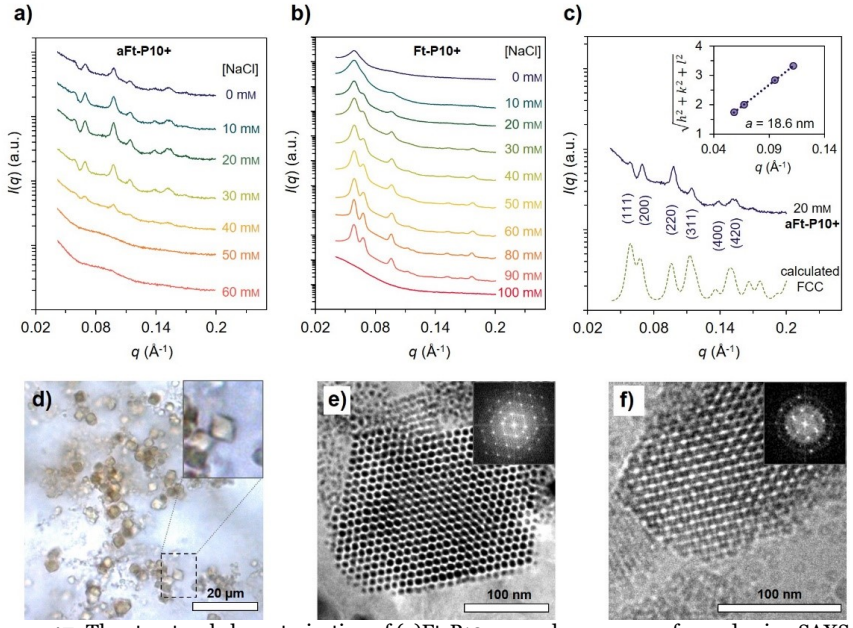

Figure 17: The structural characterization of (a)Ft-P10+ complexes was performed using SAXS diffractograms. Measurements were taken for both a) aFt-P10+ and b) Ft-P10+ complexes at various NaCl concentrations. In c), the SAXS data for the aFt-P10+ complex at 20 mM NaCl is compared to the fitted FCC model, with the inset showing the square root of the sum of the square of the Miller indexes of the assigned reflections for the FCC structure versus the measured q-vector positions. Additionally, d) presents an optical microscopy image of Ft-P10+ crystals exhibiting an octahedral habit. Furthermore, e) and f) shows a cryo-TEM image of vitrified aqueous solutions containing Ft-P10+ with 80 mM NaCl and aFt-P10+ with 20 mM NaCl respectively. Insets in both images show the corresponding fast Fourier transforms (FFT). Paper III, © 2022 The authors, reproduced from Wiley-VCH GmbH under CC BY 4.0.

SAXS was utilized to investigate the morphology of aFt and Ft CPFs. The experimental setup involved mixing a constant concentration of aFt or Ft under various NaCl concentrations. The SAXS analysis revealed distinct Bragg reflections. For the aFt–P10+ complex, well-defined diffraction peaks were observed at low NaCl concentrations (0–40 mm) (Figure 17a). Nevertheless, with the increase in electrolyte concentration, the strength of attractive interactions weakened, impeding the formation of assemblies. In contrast, the Ft-P10+ complexes exhibited Bragg reflections even at elevated ionic strengths, reaching up to 90 mM (Figure 17b). In both cases, the relative positions of the peaks corresponded to the first allowed reflections of a face-centered cubic (FCC) lattice. By fitting

the FCC system, a lattice parameter of a_{SAXS}=18.6 nm was determined (Figure 17c). The calculated nearest-neighbor distance for aFt was found to be 13.2 nm, which agrees well with the reported diameter of aFt (d_{aFt} ~12 nm) and the observed DLS dimensions. Using the hanging drop method, large macroscopic Ft-P10+ crystals were observed with an octahedral shape and an approximate size of 5 µm (Figure 17d). To gain insights into the formed lattices in solution, cryo-TEM was employed. Figure 17e–f displays typical small crystallites with a well-organized arrangement of individual Ft or aFt particles, providing a visual representation of the structures formed.

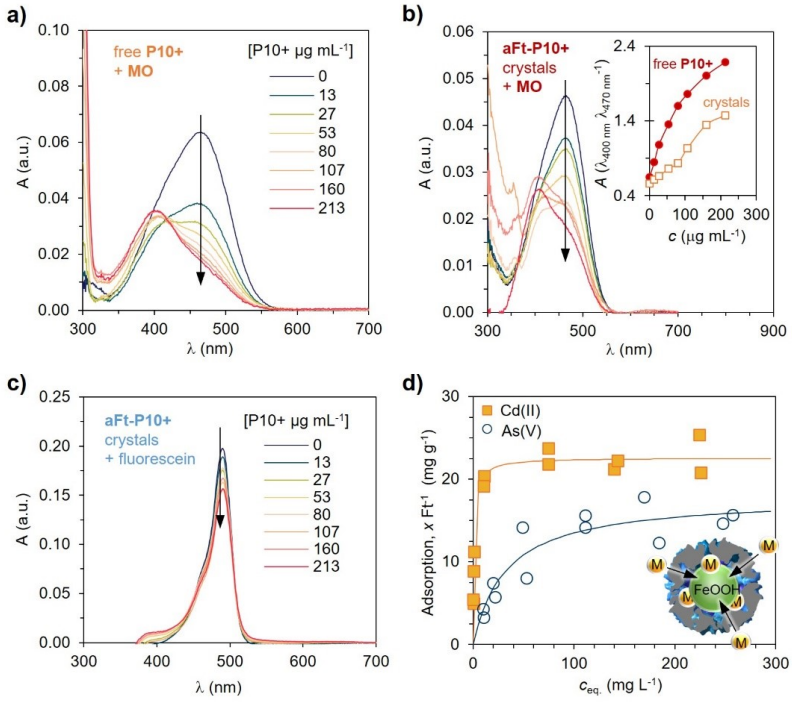

Figure 18: Host-guest binding of organic and inorganic materials. UV-Vis titration of MO with a) P10+ and b) aFt–P10+ shows clear binding. Inset: shows the absorbance ratio at 400/470 nm for P10+ and aFt-P10+ crystals indicating clear binding interactions. c) As a control, fluorescein, which is too large to efficiently bind inside the P10+ cavity, exhibited minimal changes in the spectrum during titration. d) The adsorption of Cd(II) and As(V) on Ft-P10+ complexes was analyzed using inductive coupled plasma-optical emission spectrometry (ICP-OES). Inset: a schematic representation of Cd(II) and As(V) (generalized as M) adsorption on the mineral core of Ft. Paper III, © 2022 The authors, reproduced from Wiley-VCH GmbH under CC BY 4.0.

The (a)Ft-P10+ complexes exhibit partially occupied voids between the protein cages, with P10+ acting as bridges, creating available binding sites for small-molecular guests. To verify this, the selective binding of organic guest molecules was investigated by examining changes in the absorption spectra of methyl orange (MO) and fluorescein. MO, which can fit inside the hydrophobic cavity of cationic pillararenes, produces a solvatochromic effect. In contrast, fluorescein can only partially fit into the cavity. Titration of MO with free P10+ results in a noticeable decrease in the UV-Vis absorption spectrum at 470 nm and an increase at 400 nm, indicating the binding of MO within the host cavity. (Figure 18a). The aFt–P10+ crystals also yield comparable changes in the absorption spectra (Figure 18b). The plot of absorbance ratios against the

concentration of the host reveals that the crystals exhibit slightly lower binding efficiency compared to freely soluble hosts when considering P10+ concentration (Figure 18b - inset). This can be attributed to the potential influence of aFt binding on the host's ability to accommodate guest molecules. However, despite this effect, binding still occurs within the crystals. The UV-Vis titration data demonstrate minimal changes in fluorescein absorption when it binds to P10+.

The porous Ft–P10+ complexes were investigated for their ability to capture both organic and inorganic materials. For the simultaneous binding of these guest species, the aFt-P10+ crystals were initially loaded with MO. Subsequently, batch sorption isotherms for As(V) and Cd(II) were evaluated using inductive coupled plasma-optical emission spectrometry (ICP-OES). The procedure encompassed establishing equilibrium between a known concentration of the pollutants and a fixed amount of the Ft-P10+ crystal (Figure 18d). By fitting the measured adsorption data, a maximum adsorption capacity of 24.5 mg g^{-1} for Cd(II) and 17.8 mg g^{-1} for As(V) was determined (more details can be found in Publication **III**). This indicates that these protein co-assemblies have the potential to effectively remove both organic and inorganic pollutants from water, making them suitable for water remediation applications.

In Publication **IV**, a unique FP called scmGL was employed for the investigation. This protein was designed to have 22 positive charges strategically placed around its structure to facilitate long-range electrostatic interactions. To examine the interaction between scmGL and aFt, we initially employed DLS. A fixed concentration of aFt (0.1 mg mL^{-1}) in Tris buffer was gradually titrated with increasing concentrations of scmGL. The DLS analysis revealed a rapid increase in the particle count rate as scmGL concentration increased. The complete complexation of aFt was achieved with a minimum scmGL concentration of 0.045 mg mL^{-1}. (Figure 19a, left). Based on the molecular weight of scmGL and aFt, there are ~8 scmGL proteins surrounding each aFt protein cage. To establish that the primary binding driving force is electrostatic interactions, the complexes were disassembled by gradually raising the ionic strength of the media, increasing the NaCl concentration (Figure 19a, right), and reaching a total disassembly at 150 mM NaCl. Similar changes are observed when analyzing D_h with an increase in scmGL concentration and ionic strength. Upon increasing the scmGL concentration, the peak at 15.4 nm (native size of aFt) decreases, and a new peak at ~2 μm evolves at 0.045 mg mL^{-1} (Figure 19b, left). At this point, the ionic strength was increased (Figure 19b, right), showing a decrease of D_h down to a similar size of free aFt (*i.e.*, 13.4 nm).

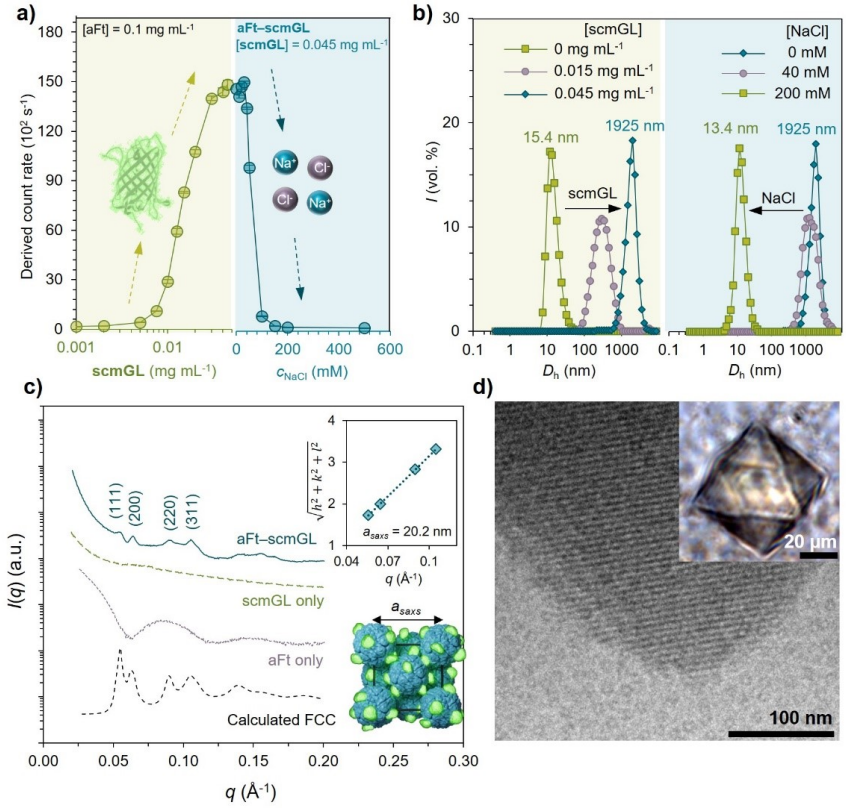

Figure 19: SA and structural analysis of aFt-scmGL complexes were performed. a) DLS was used to monitor the changes in aFt solution as scmGL concentration increased (left). The aFt-scmGL complexes were then disassembled by elevating the ionic strength of the medium using NaCl (right). b) presents DLS data, illustrating the size distribution of free aFt titrated with increasing scmGL concentration (left), and the disassembly of aFt-scmGL complexes with NaCl (right). c) SAXS diffractograms were obtained for the aFt-scmGL complex in the presence of 50 mM NaCl. These patterns were compared to the FCC model, as well as the individual components, free aFt and scmGL (offset in the y-direction for clarity). Inset: square root of the sum of the square of the Miller indexes of the assigned reflections for the FCC structure, compared to the measured *q*-vector positions. d) cryo-TEM was used to capture images of vitrified aqueous solutions containing aFt-scmGL complexes in the presence of 50 mM NaCl. Inset: an optical microscopy image of the aFt-scmGL complex at the same NaCl concentration.

The crystalline structure of aFt-scmGL was examined using SAXS. The SAXS patterns displayed distinct Bragg reflections with clearly resolved diffraction peaks (Figure 19c). The relative positions of the peaks corresponded to the first allowed reflections of a FCC lattice, similar to the aFt-P10+ complexes discussed earlier in Publication **III**. The lattice parameter determined for the FCC system was found to be a_{SAXS} = 20.2 nm, which closely matched the calculated nearest-neighbor distance between the centers of aFt particles (14.3 nm). This agreement aligns well with the known diameter of aFt particles (approximately 12 nm). Additionally, the Bravais lattice space group Fm3m (no. 225) was supported by comparing the SAXS pattern to a simulated curve generated from a finite FCC structure. Notably, the aFt-scmGL crystals exhibited the same octahedral crystal habit observed in aFt-P10+ crystals (Figure 19d - inset), indicating that the [111] direction was thermodynamically favored for crystal growth. To further confirm the arrangement of aFt particles, cryo-TEM was employed,

revealing a well-structured arrangement of individual aFt particles within the aFt-scmGL sample (Figure 19d).

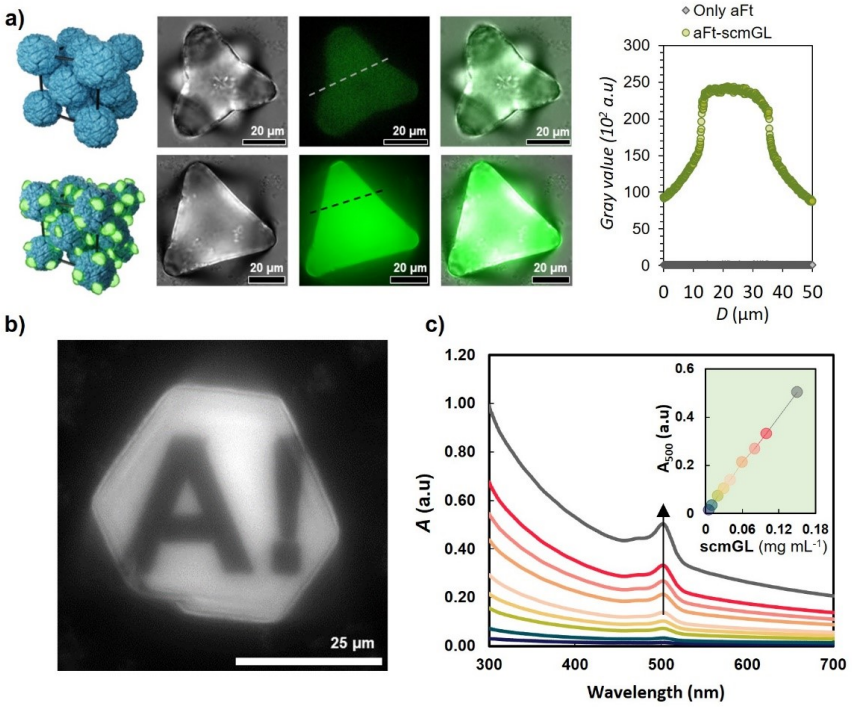

Figure 20: a) Comparison of aFt crystals and aFt-scmGL crystals. Top lane: bright-field, fluorescence, and composite images of the aFt crystals formed using $CdSO_4$. Bottom line: bright-field, fluorescence, and composite images of aFt-scmGL crystals. Right: Fluorescence intensity profiles (raw pixel values) correspond to the cross-sectional lines in the fluorescence images (center) of both aFt and aFt-scmGL crystals. b) Fluorescence microscopy image of a selected area photobleached (Aalto University logo) on the aFt-scmGL crystal. (c) UV-Vis spectra of different concentrations of aFt-scmGL cocrystals. Inset: linear increase in 500 nm wavelength.

Fluorescence microscopy was employed to compare the signal strength between aFt and aFt-scmGL crystals. The fluorescence signal emitted by aFt-scmGL crystals was found to be 1000 times stronger than that of aFt crystals, as depicted in Figure 20a. Additionally, a specific region within the crystal was subjected to photobleaching using a high-intensity laser beam. No recovery of the fluorescence signal was observed over time, indicating that the surplus scmGL proteins in the surrounding environment did not diffuse and replace the photobleached scmGL proteins within the crystal lattice. This observation confirms that the aFt-scmGL crystal structure is static and stable (Figure 20b). The optical properties of the aFt-scmGL cocrystals were further investigated using UV-Vis absorption spectroscopy. The absorption spectra displayed a linear increase in absorption intensity at 500 nm with the addition of more protein cocrystals (Figure 20c).

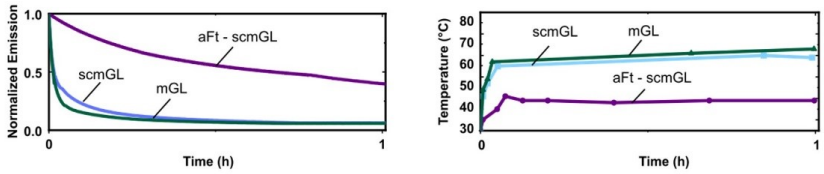

Figure 21: Device stability (left) and temperature (right) operating at high power conditions

To assess the performance of the crystals, a BioLED device was created using a silicone-processed mould that incorporated aFt–scmGL crystals. When subjected to high-power driving conditions, the device demonstrated remarkable stability, with an approximate 50% reduction in the initial intensity of the conversion band occurring after approximately 40 minutes. Throughout this period, the working temperature of the device remained around 40 °C, as depicted in Figure 21 (left). This outcome is particularly noteworthy when compared to control devices containing the same quantities of scmGL and uncharged mGL, which exhibited stabilities of less than 1 minute and reached working temperatures of 65 °C, as illustrated in Figure 21 (right). The enhanced stability of the device can be attributed to the crystal structure, which restricts the movement of the FP and hinders heat transfer, effectively minimizing heat generation resulting from light exposure.

5. Conclusion and outlook

The research conducted in this dissertation highlights the efficacy of electrostatic interactions in driving the SA of two biomolecules-based materials, namely DO and protein cages. Notably, the assembly processes were achieved without the need for modifying the protein cages and DO themselves, underscoring the simplicity of the assembly process despite the inherent complexity of these molecular structures. In essence, the results presented in this study shed light on the remarkable potential of DO and protein cages in creating versatile and functional biohybrid materials. Furthermore, this research offers valuable insights into the influence of electrolyte concentration on the structure and functionality of self-assembling complexes and crystals. We have observed that varying the electrolyte concentration has a significant impact on the assembly process, leading to distinct structural arrangements and functional properties. By systematically investigating these effects, we gained a deeper understanding of how electrolyte concentration can be precisely controlled to modulate the characteristics of the resulting assemblies. This knowledge is crucial for the rational design and optimization of self-assembled systems, including materials science, nanotechnology, and biomedicine.

In Publication **I**, the combination of electrostatic complexation between ZnPc(+8) and 6HB presents a promising and synergistic approach for the development of photosensitizing systems based on DNA. Under optimal conditions, the ZnPc bound to DO remains in a non-aggregated state, preserving its ability to generate $^1O_2$ as a photosensitizer. Moreover, this complexation offers protection to the DO nanocarrier against enzymatic degradation, potentially enhancing its bioavailability. Furthermore, precise control over the optical and morphological properties is attainable through modulation of the ionic strength within a biologically relevant range that aligns with DO compatibility. The generation of $^1O_2$ and other ROS holds significance in numerous applications within biological systems, including diagnostic arrays, PDT, and oxidative photocatalysis. This study introduces novel prospects for investigating materials that amalgamate programmable DNA nanostructures with functional dyes such as Pc, thereby paving the way for unexplored avenues in future research within this domain.

Publication **II** showcased the successful demonstration of efficient and reversible electrostatic binding between ZnPc(+4) and DO structures. This binding capability is crucial for the development of DO complexes that hold relevance in PDT. Notably, the resulting biohybrids exhibit impressive resistance to disassembly triggered by changes in the ionic strength of the surrounding

media. This work represents an initial advancement towards using Janus-type Pc materials with robust optical properties and targeted binding abilities towards biomolecules. However, it should be noted that the binding occurs only under specific conditions, limiting their applicability in biological environments. Therefore, there is a need to refine the structures, including the introduction of DNA-interacting functional groups such as amino groups and intercalating groups. This refinement aims to enhance the binding affinity to biomolecules, particularly DNA, and explores alternative interactions beyond electrostatics, thereby achieving improved selectivity.

In Publication **III**, the electrostatic SA of aFt and Ft protein cages with the molecular host P10+ results in the formation of porous crystals. The characterization methods provided compelling evidence of the formation of well-defined crystalline protein frameworks with an FCC packing arrangement. Moreover, through host-guest studies, it was demonstrated that these composite crystals possess efficient binding capabilities for both organic pollutants, such as MO, and inorganic pollutants, including Cd(II) and As(V). This binding ability is facilitated by the porous protein-molecular host network, allowing for the effective sequestration of pollutants within the crystals. Importantly, these findings highlight the multifunctionality of the system and open avenues for designing protein assemblies with controlled and synergistic chemical environments. This work not only demonstrates the versatility of the system but also provides a foundation for the future design of protein assemblies with confined chemical environments, enabling various applications in the field of materials science and environmental remediation.

Publication **IV** introduces a novel approach to enhance the performance of protein-based lighting devices. This approach involves the utilization of cocrystals formed by combining aFt and the highly positively charged mGL as color down-converting materials. Furthermore, the cationic-charged variant scmGL facilitates efficient long-range electrostatic interactions, enabling the formation of the cocrystal between aFt and FPs. These cocrystals exhibit a strong and stable assembly while maintaining the same emission efficiency (Φ) and emission band shape. By incorporating these protein cocrystals, silicone-based color filters were created and applied to high-power on-chip devices. These filters surpassed the performance of the reference filters, demonstrating a remarkable 40-fold improvement in stability.

When considering practical applications, it is crucial to evaluate the feasibility of biological building blocks, such as DO and protein cages, from a broader perspective. Both DO and protein cages offer unique advantages, including unparalleled selectivity and robustness. However, they both face limitations that hinder their widespread adoption in real-world scenarios. One common challenge is the cost associated with these nanosystems. Both DO and protein cages are currently not the most cost-effective options available, which limits their applicability in practical settings. Efforts should be made to optimize production processes and find ways to reduce costs to enhance their affordability. To make cost-effective anti-cancer therapy based on DO, it would be desirable to reduce the production cost of DNA nanostructures to £0.15/mg.[276] This target cost has

already been achieved by biotechnological mass production of DO.[277] Furthermore, in the context of therapeutic applications, ensuring impeccable purity and the complete absence of contaminants stemming from the production process is imperative. Achieving these exacting purity standards frequently entails downstream processing, demanding the development of tailored methodologies for each material to meet stringent purity criteria. The harmonious resolution of both cost and purity challenges will play a pivotal role in unlocking the full potential of these biological building blocks within practical applications. Living organisms encounter various factors that vary across different locations, including pH, electrolyte composition, and temperature. Consequently, the development of resilient systems becomes essential to maintain functionality in dynamic environments. An example of a challenge faced by these systems is the suboptimal performance of electrostatic interactions in high electrolyte concentration environments, such as *in vivo* conditions or being prepared in precise electrolyte concentration. Therefore, future studies should prioritize the development of building blocks that demonstrate tolerance and stability to variations in solution conditions. Further investigations should also delve deeper into the use of advanced coatings or modifications to enhance the stability and adaptability of DO and protein cages in diverse environments. Additionally, exploring methods such as crosslinking protein cage higher-order structures[65] or incorporating them into a polymer matrix can not only enhance their mechanical properties at a macroscopic level but also introduce stimuli responsiveness or self-healing capabilities.[278–280] Addressing these common challenges faced by DO and protein cages, such as cost, performance under a variety of conditions, material quantities, and robustness, is crucial for advancing their real-world applications and realizing their full potential.

In conclusion, the comprehensive study of biohybrid materials involving DO and protein cages has only recently begun, offering insights that can pave the way for the development of innovative nanotechnologies. The biocompatibility and the ability to modify both the inner and outer surfaces of DO and protein cages make them particularly promising for applications in the fields of biomedicine, drug delivery, and material science.

6. References

(1) Gong, C.; Sun, S.; Zhang, Y.; Sun, L.; Su, Z.; Wu, A.; Wei, G. Hierarchical Nanomaterials via Biomolecular Self-Assembly and Bioinspiration for Energy and Environmental Applications. *Nanoscale* **2019**, *11* (10), 4147–4182.

(2) Wang, J.; Li, Y.; Nie, G. Multifunctional Biomolecule Nanostructures for Cancer Therapy. *Nat. Rev. Mater.* **2021**, *6* (9), 766–783

(3) Whitesides, G. M.; Grzybowski, B. Self-Assembly at All Scales. *Science* **2002**, *295* (5564), 2418–2421.

(4) Zhang, S. Fabrication of Novel Biomaterials through Molecular Self-Assembly. *Nat. Biotechnol.* **2003**, *21* (10), 1171–1178.

(5) Busseron, E.; Ruff, Y.; Moulin, E.; Giuseppone, N. Supramolecular Self-Assemblies as Functional Nanomaterials. *Nanoscale* **2013**, *5* (16), 7098–7140.

(6) Wang, J.; Wang, D. X.; Liu, B.; Jing, X.; Chen, D. Y.; Tang, A. N.; Cui, Y. X.; Kong, D. M. Recent Advances in Constructing Higher-Order DNA Structures. *Chem. Asian. J.* **2022**, *17* (5), e202101315.

(7) Knappe, G. A.; Wamhoff, E. C.; Bathe, M. Functionalizing DNA Origami to Investigate and Interact with Biological Systems. *Nat. Rev. Mater.* **2023**, *8* (2), 123–138.

(8) Saccà, B.; Niemeyer, C. M. Functionalization of DNA Nanostructures with Proteins. *Chem. Soc. Rev.* **2011**, *40* (12), 5910–5921.

(9) Lu, S.; Shen, J.; Fan, C.; Li, Q.; Yang, X. DNA Assembly-Based Stimuli-Responsive Systems. *Adv. Sci.* **2021**, *8* (13), 2100328.

(10) Hannewald, N.; Winterwerber, P.; Zechel, S.; Ng, D. Y. W.; Hager, M. D.; Weil, T.; Schubert, U. S. DNA Origami Meets Polymers: A Powerful Tool for the Design of Defined Nanostructures. *Angew. Chem. Int. Ed.* **2021**, *60* (12), 6218–6229.

(11) Zhu, J.; Avakyan, N.; Kakkis, A.; Hoffnagle, A. M.; Han, K.; Li, Y.; Zhang, Z.; Choi, T. S.; Na, Y.; Yu, C. J.; Tezcan, F. A. Protein Assembly by Design. *Chem. Rev*. **2021**, *121* (22), 13701–13796.

(12) Korpi, A.; Anaya-Plaza, E.; Välimäki, S.; Kostiainen, M. Highly Ordered Protein Cage Assemblies: A Toolkit for New Materials. *WIREs Nanomed. Nanobiotechnol.* **2020**, *12* (1), e1578.

(13) Sun, H.; Luo, Q.; Hou, C.; Liu, J. Nanostructures Based on Protein Self-Assembly: From Hierarchical Construction to Bioinspired Materials. *Nano Today* **2017**, *14*, 16–41.

(14) Niemeyer, C. M. Nanoparticles, Proteins, and Nucleic Acids: Biotechnology Meets Materials Science. *Angew. Chem. Int. Ed.* **2001**, *40* (22), 4128–4158.

(15) Yang, D.; Campolongo, M. J.; Nhi Tran, T. N.; Ruiz, R. C. H.; Kahn, J. S.; Luo, D. Novel DNA Materials and Their Applications. *WIREs Nanomed. Nanobiotechnol.* **2010**, *2* (6), 648–669.

(16) Seeman, N. C. DNA in a Material World. *Nature* **2003**, *421* (6921), 427–431.

(17) Pitchiaya, S.; Krishnan, Y. First Blueprint, Now Bricks: DNA as Construction Material on the Nanoscale. *Chem. Soc. Rev.* **2006**, *35* (11), 1111–1121.

(18) Datta, L. P.; Manchineella, S.; Govindaraju, T. Biomolecules-Derived Biomaterials. *Biomaterials* **2020**, *230*, 119633.

(19) Grzelczak, M.; Vermant, J.; Furst, E. M.; Liz-Marzán, L. M. Directed Self-Assembly of Nanoparticles. *ACS Nano* **2010**, *4* (7), 3591–3605.

(20) Grzybowski, B. A.; Wilmer, C. E.; Kim, J.; Browne, K. P.; Bishop, K. J. M. Self-Assembly: From Crystals to Cells. *Soft Matter* **2009**, *5* (6), 1110–1128.

(21) Wang, Q.; Qi, Z.; Chen, M.; Qu, D. Out-of-Equilibrium Supramolecular Self-Assembling Systems Driven by Chemical Fuel. *Aggregate* **2021**, *2* (5), e110.

(22) Hess, H.; Ross, J. L. Non-Equilibrium Assembly of Microtubules: From Molecules to Autonomous Chemical Robots. *Chem. Soc. Rev.* **2017**, *46* (18), 5570–5587.

(23) Björk, J.; Hanke, F.; Stafström, S. Mechanisms of Halogen-Based Covalent Self-Assembly on Metal Surfaces. *J. Am. Chem. Soc.* **2013**, *135* (15), 5768–5775.

(24) Fu, S.; An, G.; Sun, H.; Luo, Q.; Hou, C.; Xu, J.; Dong, Z.; Liu, J. Laterally Functionalized Pillar[5]Arene: A New Building Block for Covalent Self-Assembly. *Chem. Comm.* **2017**, *53* (64), 9024–9027.

(25) Mendes, A. C.; Baran, E. T.; Reis, R. L.; Azevedo, H. S. Self-Assembly in Nature: Using the Principles of Nature to Create Complex Nanobiomaterials. *WIREs Nanomed. Nanobiotechnol.* **2013**, *5* (6), 582–612.

(26) Whitesides, G. M.; Boncheva, M. Beyond Molecules: Self-Assembly of Mesoscopic and Macroscopic Components. *Proc. Natl. Acad. Sci. U.S.A* **2002**, *99* (8), 4769–4774.

(27) Whitesides, G. M.; Mathias, J. P.; Seto, C. T. Molecular Self-Assembly and Nanochemistry: A Chemical Strategy for the Synthesis of Nanostructures. *Science* **1991**, *254* (5036), 1312–1319.

(28) Gong, C.; Sun, S.; Zhang, Y.; Sun, L.; Su, Z.; Wu, A.; Wei, G. Hierarchical Nanomaterials via Biomolecular Self-Assembly and Bioinspiration for Energy and Environmental Applications. *Nanoscale* **2019**, *11* (10), 4147–4182.

(29) Samsoninkova, V.; Seidt, B.; Hanßke, F.; Wagermaier, W.; Börner, H. G. Peptide–Polymer Conjugates for Bioinspired Compatibilization of Internal Composite Interfaces: Via Specific Interactions toward Stiffer and Tougher Materials. *Adv. Mater. Interfaces* **2017**, *4* (1), 1600501.

(30) Cheng, Y.; Koh, L. D.; Li, D.; Ji, B.; Zhang, Y.; Yeo, J.; Guan, G.; Han, M. Y.; Zhang, Y. W. Peptide-Graphene Interactions Enhance the Mechanical Properties of Silk Fibroin. *ACS Appl. Mater. Inter.* **2015**, *7* (39), 21787–21796.

(31) Zhang, W.; Lin, D.; Wang, H.; Li, J.; Nienhaus, G. U.; Su, Z.; Wei, G.; Shang, L. Supramolecular Self-Assembly Bioinspired Synthesis of Luminescent Gold Nanocluster-Embedded Peptide Nanofibers for Temperature Sensing and Cellular Imaging. *Bioconjugate Chem.* **2017**, *28* (9), 2224–2229.

(32) Yang, M.; Zhou, G.; Shuai, Y.; Wang, J.; Zhu, L.; Mao, C. Ca2+-Induced Self-Assembly of Bombyx Mori Silk Sericin into a Nanofibrous Network-like Protein Matrix for Directing Controlled Nucleation of Hydroxylapatite Nano-Needles. *J. Mater. Chem. B* **2015**, *3* (12), 2455–2462.

(33) Aida, T.; Meijer, E. W.; Stupp, S. I. Functional Supramolecular Polymers. *Science* **2012**, *335* (6070), 813–817.

(34) Hartgerink, J. D.; Beniash, E.; Stupp, S. I. Peptide-Amphiphile Nanofibers: A Versatile Scaffold for the Preparation of Self-Assembling Materials. *Proc. Natl. Acad. Sci. U.S.A* **2002**, *99* (8), 5133–5138.

(35) Rajangam, K.; Behanna, H. A.; Hui, M. J.; Han, X.; Hulvat, J. F.; Lomasney, J. W.; Stupp, S. I. Heparin Binding Nanostructures to Promote Growth of Blood Vessels. *Nano Lett.* **2006**, *6* (9), 2086–2090.

(36) Chen, L.; Pont, G.; Morris, K.; Lotze, G.; Squires, A.; Serpell, L. C.; Adams, D. J. Salt-Induced Hydrogelation of Functionalised-Dipeptides at High pH. *Chem. Comm.* **2011**, *47* (44), 12071–12073.

(37) Chen, L.; McDonald, T. O.; Adams, D. J. Salt-Induced Hydrogels from Functionalised-Dipeptides. *RSC Adv.* **2013**, *3* (23), 8714–8720.

(38) Mahler, A.; Reches, M.; Rechter, M.; Cohen, S.; Gazit, E. Rigid, Self-Assembled Hydrogel Composed of a Modified Aromatic Dipeptide. *Adv. Mater.* **2006**, *18* (11), 1365–1370.

(39) Williams, R. J.; Smith, A. M.; Collins, R.; Hodson, N.; Das, A. K.; Ulijn, R. V. Enzyme-Assisted Self-Assembly under Thermodynamic Control. *Nat. Nanotechnol.* **2008**, *4* (1), 19–24.

(40) Yagai, S.; Karatsu, T.; Kitamura, A. Photocontrollable Self-Assembly. *Chem. Eur. J.* **2005**, *11* (14), 4054–4063.

(41) Yukawa, H. On the Interaction of Elementary Particles. I. *Proceedings of the Physico-Mathematical Society of Japan. 3rd Series* **1935**, *17*, 48–57.

(42) Matsumoto, T.; Inoue, H. Application of the Yukawa Potential to the Auto-Controlled Mechanism of the Ovalbumin Molecule in Aqueous Systems. *Chem. Phys.* **1992**, *166* (1–2), 299–302.

(43) Blanco, M. A.; Sahin, E.; Robinson, A. S.; Roberts, C. J. Coarse-Grained Model for Colloidal Protein Interactions, B22, and Protein Cluster Formation. *J. Phys. Chem. B* **2013**, *117* (50), 16013–16028.

(44) Lennard-Jones, J. E. Cohesion. *Proc. Phys. Soc.* **1931**, *43* (5), 461.

(45) Kostiainen, M. A.; Hiekkataipale, P.; Laiho, A.; Lemieux, V.; Seitsonen, J.; Ruokolainen, J.; Ceci, P. Electrostatic Assembly of Binary Nanoparticle Superlattices Using Protein Cages. *Nat. Nanotechnol.* **2013**, *8* (1), 52–56.

(46) Ducker, W. A.; Senden, T. J.; Pashley, R. M. Measurement of Forces in Liquids Using a Force Microscope. *Langmuir* **1992**, *8*, 1831–1836.

(47) Pashley, R. M. DLVO and Hydration Forces between Mica Surfaces in Li+, Na+, K+, and Cs+ Electrolyte Solutions: A Correlation of Double-Layer and Hydration Forces with Surface Cation Exchange Properties. *J. Colloid Interf. Sci.* **1981**, *83* (2), 531–546.

(48) Israelachvili, J. N.; Adams, G. E. Measurement of Forces between Two Mica Surfaces in Aqueous Electrolyte Solutions in the Range 0–100 Nm. *J. Chem. Soc., Faraday Trans*. 1, **1978**, 74, 975-1001.

(49) Gaddam, P.; Ducker, W. Electrostatic Screening Length in Concentrated Salt Solutions. *Langmuir* **2019**, *35* (17), 5719–5727.

(50) Kalsin, A. M.; Fialkowski, M.; Paszewski, M.; Smoukov, S. K.; Bishop, K. J. M.; Grzybowski, B. A. Electrostatic Self-Assembly of Binary Nanoparticle Crystals with a Diamond-like Lattice. *Science* **2006**, *312* (5772), 420–424.

(51) Velev, O. D. Self-Assembly of Unusual Nanoparticle Crystals. *Science* **2006**, *312* (5772), 376–377.

(52) Liljeström, V.; Mikkilä, J.; Kostiainen, M. A. Self-Assembly and Modular Functionalization of Three-Dimensional Crystals from Oppositely Charged Proteins. *Nat. Commun.,* **2014**, *5* (1), 1–9.

(53) Bian, T.; Gardin, A.; Gemen, J.; Houben, L.; Perego, C.; Lee, B.; Elad, N.; Chu, Z.; Pavan, G. M.; Klajn, R. Electrostatic Co-Assembly of Nanoparticles with Oppositely Charged Small Molecules into Static and Dynamic Superstructures. *Nat. Chem.* **2021**, *13* (10), 940–949.

(54) Hueckel, T.; Hocky, G. M.; Palacci, J.; Sacanna, S. Ionic Solids from Common Colloids. *Nature* **2020**, *580* (7804), 487–490.

(55) Spruijt, E.; Bakker, H. E.; Kodger, T. E.; Sprakel, J.; Cohen Stuart, M. A.; Van Der Gucht, J. Reversible Assembly of Oppositely Charged Hairy Colloids in Water. *Soft Matter* **2011**, *7* (18), 8281–8290.

(56) Kim, S.; Sureka, H. V.; Kayitmazer, A. B.; Wang, G.; Swan, J. W.; Olsen, B. D. Effect of Protein Surface Charge Distribution on Protein-Polyelectrolyte Complexation. *Biomacromolecules* **2020**, *21* (8), 3026–3037.

(57) Beyeh, N. K.; Nonappa; Liljeström, V.; Mikkilä, J.; Korpi, A.; Bochicchio, D.; Pavan, G. M.; Ikkala, O.; Ras, R. H. A.; Kostiainen, M. A. Crystalline Cyclophane-Protein Cage Frameworks. *ACS Nano* **2018**, *12* (8), 8029–8036.

(58) Aumiller, W. M.; Uchida, M.; Douglas, T. Protein Cage Assembly across Multiple Length Scales. *Chem. Soc. Rev.* **2018**, *47* (10), 3433–3469.

(59) Mikkilä, J.; Anaya-Plaza, E.; Liljeström, V.; Caston, J. R.; Torres, T.; De La Escosura, A. A.; Kostiainen, M. A. Hierarchical Organization of Organic Dyes and Protein Cages into Photoactive Crystals. *ACS Nano* **2016**, *10* (1), 1565–1571.

(60) Korpi, A.; Ma, C.; Liu, K.; Nonappa; Herrmann, A.; Ikkala, O.; Kostiainen, M. A. Self-Assembly of Electrostatic Cocrystals from Supercharged Fusion Peptides and Protein Cages. *ACS Macro Lett.* **2018**, *7* (3), 318–323.

(61) Uchida, M.; McCoy, K.; Fukuto, M.; Yang, L.; Yoshimura, H.; Miettinen, H. M.; LaFrance, B.; Patterson, D. P.; Schwarz, B.; Karty, J. A.; Prevelige, P. E.; Lee, B.; Douglas, T. Modular Self-Assembly of Protein Cage Lattices for Multistep Catalysis. *ACS Nano* **2018**, *12* (2), 942–953.

(62) Huard, D. J. E.; Kane, K. M.; Akif Tezcan, F. Re-Engineering Protein Interfaces Yields Copper-Inducible Ferritin Cage Assembly. *Nat. Chem. Bio.* **2013**, *9* (3), 169–176.

(63) Chakraborti, S.; Korpi, A.; Kumar, M.; Stępień, P. S.; Kostiainen, M. A.; Heddle, J. G. Three-Dimensional Protein Cage Array Capable of Active Enzyme Capture and Artificial Chaperone Activity. *Nano Lett.* **2019**, *19* (6).

(64) Abe, S.; Maity, B.; Ueno, T. Design of a Confined Environment Using Protein Cages and Crystals for the Development of Biohybrid Materials. *Chem. Comm.* **2016**, *52* (39), 6496–6512.

(65) Maity, B.; Abe, S.; Ueno, T. Observation of Gold Sub-Nanocluster Nucleation within a Crystalline Protein Cage. *Nat. Commun.* **2017**, *8* (1), 14820.

(66) Anaya-Plaza, E.; Aljarilla, A.; Beaune, G.; Nonappa; Timonen, J. V. I.; de la Escosura, A.; Torres, T.; Kostiainen, M. A. Phthalocyanine–Virus Nanofibers as Heterogeneous Catalysts for Continuous-Flow Photo-Oxidation Processes. *Adv. Mater.* **2019**, *31* (39), 1902582.

(67) Liu, Q.; Zhou, Y.; Shaukat, A.; Meng, Z.; Kyllönen, D.; Seitz, I.; Langerreiter, D.; Kuntze, K.; Priimagi, A.; Zheng, L.; Kostiainen, M. A. Optically Controlled Construction of Three-Dimensional Protein Arrays. *Angew. Chem. Int. Ed.* **2023**, e202303880.

(68) Liljeström, V.; Ora, A.; Hassinen, J.; Rekola, H. T.; Nonappa, N.; Heilala, M.; Hynninen, V.; Joensuu, J. J.; Ras, R. H. A.; Törmä, P.; Ikkala, O.; Kostiainen, M. A. Cooperative Colloidal Self-Assembly of Metal-Protein Superlattice Wires. *Nat. Commun.* **2017**, *8* (1), 1–10.

(69) Jiang, T.; Meyer, T. A.; Modlin, C.; Zuo, X.; Conticello, V. P.; Ke, Y. Structurally Ordered Nanowire Formation from Co-Assembly of DNA Origami and Collagen-Mimetic Peptides. *J. Am. Chem. Soc.* **2017**, *139* (40), 14025–14028.

(70) Xu, X.; Fang, S.; Zhuang, Y.; Wu, S.; Pan, Q.; Li, L.; Wang, X.; Sun, X.; Liu, B.; Wu, Y. Cationic Albumin Encapsulated DNA Origami for Enhanced Cellular Transfection and Stability. *Materials* **2019**, *12* (6), 949.

(71) Smolková, B.; MacCulloch, T.; Rockwood, T. F.; Liu, M.; Henry, S. J. W.; Frtús, A.; Uzhytchak, M.; Lunova, M.; Hof, M.; Jurkiewicz, P.; Dejneka, A.; Stephanopoulos, N.; Lunov, O. Protein Corona Inhibits Endosomal Escape of Functionalized DNA Nanostructures in Living Cells. *ACS Appl. Mater. Inter.* **2021**, *13* (39), 46375–46390.

(72) Estrich, N. A.; Hernandez-Garcia, A.; De Vries, R.; LaBean, T. H. Engineered Diblock Polypeptides Improve DNA and Gold Solubility during Molecular Assembly. *ACS Nano* **2017**, *11* (1), 831–842.

(73) Mikkilä, J.; Eskelinen, A. P.; Niemelä, E. H.; Linko, V.; Frilander, M. J.; Törmä, P.; Kostiainen, M. A. Virus-Encapsulated DNA Origami Nanostructures for Cellular Delivery. *Nano Lett.* **2014**, *14* (4), 2196–2200.

(74) Kopatz, I.; Zalk, R.; Levi-Kalisman, Y.; Zlotkin-Rivkin, E.; Frank, G. A.; Kler, S. Packaging of DNA Origami in Viral Capsids. *Nanoscale* **2019**, *11* (21), 10160–10166.

(75) Auvinen, H.; Zhang, H.; Nonappa; Kopilow, A.; Niemelä, E. H.; Nummelin, S.; Correia, A.; Santos, H. A.; Linko, V.; Kostiainen, M. A. Protein Coating of DNA Nanostructures for Enhanced Stability and Immunocompatibility. *Adv. Healthc. Mater.* **2017**, *6* (18), 1700692.

(76) Shen, X.; Jiang, Q.; Wang, J.; Dai, L.; Zou, G.; Wang, Z. G.; Chen, W. Q.; Jiang, W.; Ding, B. Visualization of the Intracellular Location and Stability of DNA Origami with a Label-Free Fluorescent Probe. *Chem. Comm.* **2012**, *48* (92), 11301–11303.

(77) Ahmadi, Y.; De Llano, E.; Barišić, I. (Poly)Cation-Induced Protection of Conventional and Wireframe DNA Origami Nanostructures. *Nanoscale* **2018**, *10* (16), 7494–7504.

(78) Kiviaho, J. K.; Linko, V.; Ora, A.; Tiainen, T.; Järvihaavisto, E.; Mikkilä, J.; Tenhu, H.; Nonappa; Kostiainen, M. A. Cationic Polymers for DNA Origami Coating – Examining Their Binding Efficiency and Tuning the Enzymatic Reaction Rates. *Nanoscale* **2016**, *8* (22), 11674–11680.

(79) Agarwal, N. P.; Matthies, M.; Gür, F. N.; Osada, K.; Schmidt, T. L. Block Copolymer Micellization as a Protection Strategy for DNA Origami. *Angew. Chem. Int. Ed.* **2017**, *56* (20), 5460–5464.

(80) Eklund, A. S.; Comberlato, A.; Parish, I. A.; Jungmann, R.; Bastings, M. M. C. Quantification of Strand Accessibility in Biostable DNA Origami with Single-Staple Resolution. *ACS Nano* **2021**, *15* (11), 17668–17677.

(81) Sigl, C.; Willner, E. M.; Engelen, W.; Kretzmann, J. A.; Sachenbacher, K.; Liedl, A.; Kolbe, F.; Wilsch, F.; Aghvami, S. A.; Protzer, U.; Hagan, M. F.; Fraden, S.; Dietz, H. Programmable Icosahedral Shell System for Virus Trapping. *Nat. Mater.* **2021**, *20* (9), 1281–1289.

(82) Fragasso, A.; De Franceschi, N.; Stömmer, P.; Van Der Sluis, E. O.; Dietz, H.; Dekker, C. Reconstitution of Ultrawide DNA Origami Pores in Liposomes for Transmembrane Transport of Macromolecules. *ACS Nano* **2021**, *15* (8), 12768–12779.

(83) Anastassacos, F. M.; Zhao, Z.; Zeng, Y.; Shih, W. M. Glutaraldehyde Cross-Linking of Oligolysines Coating DNA Origami Greatly Reduces Susceptibility to Nuclease Degradation. *J. Am. Chem. Soc.* **2020**, *142* (7), 3311–3315.

(84) Ahmadi, Y.; Barisic, I. Gene-Therapy Inspired Polycation Coating for Protection of DNA Origami Nanostructures. *J. Vis. Exp.* **2019**, *2019* (143), e58771.

(85) Ponnuswamy, N.; Bastings, M. M. C.; Nathwani, B.; Ryu, J. H.; Chou, L. Y. T.; Vinther, M.; Li, W. A.; Anastassacos, F. M.; Mooney, D. J.; Shih, W. M. Oligolysine-Based Coating Protects DNA Nanostructures from Low-Salt Denaturation and Nuclease Degradation. *Nat. Commun.* **2017**, *8* (1), 1–9.

(86) Julin, S.; Nonappa; Shen, B.; Linko, V.; Kostiainen, M. A. DNA-Origami-Templated Growth of Multilamellar Lipid Assemblies. *Angew. Chem. Int. Ed.* **2021**, *133* (2), 840–846.

(87) Nummelin, S.; Kommeri, J.; Kostiainen, M. A.; Linko, V. Evolution of Structural DNA Nanotechnology. *Adv. Mater.* **2018**, *30* (24), 1703721.

(88) Zhan, P.; Peil, A.; Jiang, Q.; Wang, D.; Mousavi, S.; Xiong, Q.; Shen, Q.; Shang, Y.; Ding, B.; Lin, C.; Ke, Y.; Liu, N. Recent Advances in DNA Origami-Engineered Nanomaterials and Applications. *Chem. Rev.* **2023**, *123* (7), 3976–4050.

(89) Seeman, N. C. Nucleic Acid Junctions and Lattices. *J. Theor. Biol.* **1982**, *99* (2), 237–247.

(90) Kallenbach, N. R.; Ma, R. I.; Seeman, N. C. An Immobile Nucleic Acid Junction Constructed from Oligonucleotides. *Nature* **1983**, *305* (5937), 829–831.

(91) Chen, J.; Seeman, N. C. Synthesis from DNA of a Molecule with the Connectivity of a Cube. *Nature* **1991**, *350* (6319), 631–633.

(92) Tsu-Ju, F.; Seeman, N. C. DNA Double-Crossover Molecules. *Biochemistry* **1993**, *32* (13), 3211–3220.

(93) Lin, C.; Liu, Y.; Rinker, S.; Yan, H. DNA Tile Based Self-Assembly: Building Complex Nanoarchitectures. *ChemPhysChem* **2006**, *7* (8), 1641–1647.

(84) Rothemund, P. W. K. Folding DNA to Create Nanoscale Shapes and Patterns. *Nature* **2006**, *440*, 297–302.

(95) Ramezani, H.; Dietz, H. Building Machines with DNA Molecules. *Nat. Rev. Genet.* **2019**, *21* (1), 5–26.

(96) Dey, S.; Fan, C.; Gothelf, K. V.; Li, J.; Lin, C.; Liu, L.; Liu, N.; Nijenhuis, M. A. D. D.; Saccà, B.; Simmel, F. C.; Yan, H.; Zhan, P. DNA Origami. *Nat. Rev. Methods Primers* **2021**, *1* (1), 13.

(97) Burns, J. R.; Lamarre, B.; Pyne, A. L. B.; Noble, J. E.; Ryadnov, M. G. DNA Origami Inside-Out Viruses. *ACS Synth. Biol.* **2018**, *7* (3), 767–773.

(98) Angelin, A.; Weigel, S.; Garrecht, R.; Meyer, R.; Bauer, J.; Kumar, R. K.; Hirtz, M.; Niemeyer, C. M. Multiscale Origami Structures as Interface for Cells. *Angew. Chem. Int. Ed.* **2015**, *54* (52), 15813–15817.

(99) Kern, N.; Dong, R.; Douglas, S. M.; Vale, R. D.; Morrissey, M. A. Tight Nanoscale Clustering of Fcγ Receptors Using DNA Origami Promotes Phagocytosis. *Elife* **2021**, *10*.

(100) Czogalla, A.; Kauert, D. J.; Franquelim, H. G.; Uzunova, V.; Zhang, Y.; Seidel, R.; Schwille, P. Amphipathic DNA Origami Nanoparticles to Scaffold and Deform Lipid Membrane Vesicles. *Angew. Chem. Int. Ed.* **2015**, *54* (22), 6501–6505.

(101) Journot, C. M. A.; Ramakrishna, V.; Wallace, M. I.; Turberfield, A. J. Modifying Membrane Morphology and Interactions with DNA Origami Clathrin-Mimic Networks. *ACS Nano* **2019**, *13* (9), 9973–9979.

(102) Jorge, A. F.; Aviñó, A.; Pais, A. A. C. C.; Eritja, R.; Fàbrega, C. DNA-Based Nanoscaffolds as Vehicles for 5-Fluoro-2'-Deoxyuridine Oligomers in Colorectal Cancer Therapy. *Nanoscale* **2018**, *10* (15), 7238–7249.

(103) Shaw, A.; Hoffecker, I. T.; Smyrlaki, I.; Rosa, J.; Grevys, A.; Bratlie, D.; Sandlie, I.; Michaelsen, T. E.; Andersen, J. T.; Högberg, B. Binding to Nanopatterned Antigens Is Dominated by the Spatial Tolerance of Antibodies. *Nat. Nanotechnol.* **2019**, *14* (2), 184–190.

(104) Bell, N. A. W.; Keyser, U. F. Digitally Encoded DNA Nanostructures for Multiplexed, Single-Molecule Protein Sensing with Nanopores. *Nat. Nanotechnol.* **2016**, *11* (7), 645–651.

(105) Wijesekara, P.; Liu, Y.; Wang, W.; Johnston, E. K.; Sullivan, M. L. G.; Taylor, R. E.; Ren, X. Accessing and Assessing the Cell-Surface Glycocalyx Using DNA Origami. *Nano Lett.* **2021**, *21* (11), 4765–4773.

(106) Liu, K.; Xu, C.; Liu, J. Regulation of Cell Binding and Entry by DNA Origami Mediated Spatial Distribution of Aptamers. *J. Mater. Chem. B* **2020**, *8* (31), 6802–6809.

(107) Lu, Z.; Wang, Y.; Xu, D.; Pang, L. Aptamer-Tagged DNA Origami for Spatially Addressable Detection of Aflatoxin B1. *Chem. Comm.* **2017**, *53* (5), 941–944.

(108) Wu, X.; Liu, Q.; Liu, F.; Wu, T.; Shang, Y.; Liu, J.; Ding, B. An RNA/DNA Hybrid Origami-Based Nanoplatform for Efficient Gene Therapy. *Nanoscale* **2021**, *13* (30), 12848–12853.

(109) Udomprasert, A.; Bongiovanni, M. N.; Sha, R.; Sherman, W. B.; Wang, T.; Arora, P. S.; Canary, J. W.; Gras, S. L.; Seeman, N. C. Amyloid Fibrils Nucleated and Organized by DNA Origami Constructions. *Nat. Nanotechnol.* **2014**, *9* (7), 537–541.

(110) Numajiri, K.; Yamazaki, T.; Kimura, M.; Kuzuya, A.; Komiyama, M. Discrete and Active Enzyme Nanoarrays on DNA Origami Scaffolds Purified by Affinity Tag Separation. *J. Am. Chem. Soc.* **2010**, *132* (29), 9937–9939.

(111) Grome, M. W.; Zhang, Z.; Pincet, F.; Lin, C. Vesicle Tubulation with Self-Assembling DNA Nanosprings. *Angew. Chem. Int. Ed.* **2018**, *57* (19), 5330–5334.

(112) Sørensen, R. S.; Okholm, A. H.; Schaffert, D.; Kodal, A. L. B.; Gothelf, K. V.; Kjems, J. Enzymatic Ligation of Large Biomolecules to DNA. *ACS Nano* **2013**, *7* (9), 8098–8104.

(113) Wang, D.; Zhang, G.; Zhang, Y.; Xin, L.; Dong, Y.; Liu, Y.; Liu, D. An Addressable 2D Heterogeneous Nanoreactor to Study the Enzyme-Catalyzed Reaction at the Interface. *Small* **2017**, *13* (43), 1700594.

(114) Rosier, B. J. H. M.; Markvoort, A. J.; Gumí Audenis, B.; Roodhuizen, J. A. L.; den Hamer, A.; Brunsveld, L.; de Greef, T. F. A. Proximity-Induced Caspase-9 Activation on a DNA Origami-Based Synthetic Apoptosome. *Nat. Catal.* **2020**, *3* (3), 295–306.

(115) Teixeira, A. I.; Fang, T.; Alvelid, J.; Spratt, J.; Ambrosetti, E.; Testa, I. Spatial Regulation of T-Cell Signaling by Programmed Death-Ligand 1 on Wireframe DNA Origami Flat Sheets. *ACS Nano* **2021**, *15* (2), 3441–3452.

(116) Sprengel, A.; Lill, P.; Stegemann, P.; Bravo-Rodriguez, K.; Schöneweiß, E. C.; Merdanovic, M.; Gudnason, D.; Aznauryan, M.; Gamrad, L.; Barcikowski, S.; Sanchez-Garcia, E.; Birkedal, V.; Gatsogiannis, C.; Ehrmann, M.; Saccà, B. Tailored Protein Encapsulation into a DNA Host Using Geometrically Organized Supramolecular Interactions. *Nat. Commun.* **2017**, *8* (1), 1–12.

(117) Liu, S.; Jiang, Q.; Zhao, X.; Zhao, R.; Wang, Y.; Wang, Y.; Liu, J.; Shang, Y.; Zhao, S.; Wu, T.; Zhang, Y.; Nie, G.; Ding, B. A DNA Nanodevice-Based Vaccine for Cancer Immunotherapy. *Nat. Mater.* **2020**, *20* (3), 421–430.

(118) Veneziano, R.; Moyer, T. J.; Stone, M. B.; Wamhoff, E. C.; Read, B. J.; Mukherjee, S.; Shepherd, T. R.; Das, J.; Schief, W. R.; Irvine, D. J.; Bathe, M. Role of Nanoscale Antigen Organization on B-Cell Activation Probed Using DNA Origami. *Nat. Nanotechnol.* **2020**, *15* (8), 716–723.

(119) Johnson-Buck, A.; Jiang, S.; Yan, H.; Walter, N. G. DNA-Cholesterol Barges as Programmable Membrane-Exploring Agents. *ACS Nano* **2014**, *8* (6), 5641–5649.

(120) Xu, W.; Nathwani, B.; Lin, C.; Wang, J.; Karatekin, E.; Pincet, F.; Shih, W.; Rothman, J. E. A Programmable DNA Origami Platform to Organize SNAREs for Membrane Fusion. *J. Am. Chem. Soc.* **2016**, *138* (13), 4439–4447.

(121) Khmelinskaia, A.; Mücksch, J.; Petrov, E. P.; Franquelim, H. G.; Schwille, P. Control of Membrane Binding and Diffusion of Cholesteryl-Modified DNA Origami Nanostructures by DNA Spacers. *Langmuir* **2018**, *34* (49), 14921–14931.

(122) Franquelim, H. G.; Dietz, H.; Schwille, P. Reversible Membrane Deformations by Straight DNA Origami Filaments. *Soft Matter* **2021**, *17* (2), 276–287.

(123) Liu, J.; Li, M.; Li, F.; Ge, Z.; Li, Q.; Liu, M.; Shi, J.; Wang, L.; Zuo, X.; Fan, C.; Mao, X. Reconstructing Soma-Soma Synapse-like Vesicular Exocytosis with DNA Origami. *ACS Cent. Sci.* **2021**, *7* (8), 1400–1407.

(124) Li, S.; Jiang, Q.; Liu, S.; Zhang, Y.; Tian, Y.; Song, C.; Wang, J.; Zou, Y.; Anderson, G. J.; Han, J. Y.; Chang, Y.; Liu, Y.; Zhang, C.; Chen, L.; Zhou, G.; Nie, G.; Yan, H.; Ding, B.; Zhao, Y. A DNA Nanorobot Functions as a Cancer Therapeutic in Response to a Molecular Trigger In Vivo. *Nat. Biotechnol.* **2018**, *36* (3), 258–264.

(125) Silvester, E.; Vollmer, B.; Pražák, V.; Vasishtan, D.; Machala, E. A.; Whittle, C.; Black, S.; Bath, J.; Turberfield, A. J.; Grünewald, K.; Baker, L. A. DNA Origami Signposts for Identifying Proteins on Cell Membranes by Electron Cryotomography. *Cell* **2021**, *184* (4), 1110-1121.e16.

(126) Daems, D.; Rutten, I.; Bath, J.; Decrop, D.; Van Gorp, H.; Ruiz, E. P.; De Feyter, S.; Turberfield, A. J.; Lammertyn, J. Controlling the Bioreceptor Spatial Distribution at the Nanoscale for Single Molecule Counting in Microwell Arrays. *ACS Sens.* **2019**, *4* (9), 2327–2335.

(127) Raveendran, M.; Lee, A. J.; Sharma, R.; Wälti, C.; Actis, P. Rational Design of DNA Nanostructures for Single Molecule Biosensing. *Nat. Commun.* **2020**, *11* (1), 1–9.

(128) Zhang, H.; Demirer, G. S.; Zhang, H.; Ye, T.; Goh, N. S.; Aditham, A. J.; Cunningham, F. J.; Fan, C.; Landry, M. P. DNA Nanostructures Coordinate Gene Silencing in Mature Plants. *Proc. Natl. Acad. Sci U.S.A* **2019**, *116* (15), 7543–7548.

(129) Rahman, M. A.; Wang, P.; Zhao, Z.; Wang, D.; Nannapaneni, S.; Zhang, C.; Chen, Z.; Griffith, C. C.; Hurwitz, S. J.; Chen, Z. G.; Ke, Y.; Shin, D. M. Systemic Delivery of Bc12-Targeting SiRNA by DNA Nanoparticles Suppresses Cancer Cell Growth. *Angew. Chem. Int. Ed.* **2017**, *56* (50), 16023–16027.

(130) Wang, Z.; Song, L.; Liu, Q.; Tian, R.; Shang, Y.; Liu, F.; Liu, S.; Zhao, S.; Han, Z.; Sun, J.; Jiang, Q.; Ding, B. A Tubular DNA Nanodevice as a SiRNA/Chemo-Drug Co-Delivery Vehicle for Combined Cancer Therapy. *Angew. Chem. Int. Ed.* **2021**, *60* (5), 2594–2598.

(131) Takenaka, T.; Endo, M.; Suzuki, Y.; Yang, Y.; Emura, T.; Hidaka, K.; Kato, T.; Miyata, T.; Namba, K.; Sugiyama, H. Photoresponsive DNA Nanocapsule Having an Open/Close System for Capture and Release of Nanomaterials. *Chem. Eur. J.* **2014**, *20* (46), 14951–14954.

(132) Ijäs, H.; Hakaste, I.; Shen, B.; Kostiainen, M. A.; Linko, V. Reconfigurable DNA Origami Nanocapsule for pH-Controlled Encapsulation and Display of Cargo. *ACS Nano* **2019**, *13* (5), 5959–5967.

(133) Xing, C.; Huang, Y.; Dai, J.; Zhong, L.; Wang, H.; Lin, Y.; Li, J.; Lu, C. H.; Yang, H. H. Spatial Regulation of Biomolecular Interactions with a Switchable Trident-Shaped DNA Nanoactuator. *ACS Appl. Mater. Inter.* **2018**, *10* (38), 32579–32587.

(134) Grossi, G.; Dalgaard Ebbesen Jepsen, M.; Kjems, J.; Andersen, E. S. Control of Enzyme Reactions by a Reconfigurable DNA Nanovault. *Nat. Commun.* **2017**, *8* (1), 1–8.

(135) Meyer, T. A.; Zhang, C.; Bao, G.; Ke, Y. Programmable Assembly of Iron Oxide Nanoparticles Using DNA Origami. *Nano Lett.* **2020**, *20* (4), 2799–2805.

(136) Jiang, Q.; Shi, Y.; Zhang, Q.; Li, N.; Zhan, P.; Song, L.; Dai, L.; Tian, J.; Du, Y.; Cheng, Z.; Ding, B. A Self-Assembled DNA Origami-Gold Nanorod Complex for Cancer Theranostics. *Small* **2015**, *11* (38), 5134–5141.

(137) Jiang, D.; Ge, Z.; Im, H. J.; England, C. G.; Ni, D.; Hou, J.; Zhang, L.; Kutyreff, C. J.; Yan, Y.; Liu, Y.; Cho, S. Y.; Engle, J. W.; Shi, J.; Huang, P.; Fan, C.; Yan, H.; Cai, W. DNA Origami Nanostructures Can Exhibit Preferential Renal Uptake and Alleviate Acute Kidney Injury. *Nat. Biomed. Eng.* **2018**, *2* (11), 865–877.

(138) Douglas, S. M.; Bachelet, I.; Church, G. M. A Logic-Gated Nanorobot for Targeted Transport of Molecular Payloads. *Science* **2012**, *335* (6070), 831–834.

(139) Kim, Y.; Yin, P. Enhancing Biocompatible Stability of DNA Nanostructures Using Dendritic Oligonucleotides and Brick Motifs. *Angew. Chem. Int. Ed.* **2020**, *59* (2), 700–703.

(140) Chandrasekaran, A. R. Nuclease Resistance of DNA Nanostructures. *Nat. Rev. Chem.* **2021**, *5* (4), 225–239.

(141) Xin, Y.; Piskunen, P.; Suma, A.; Li, C.; Ijäs, H.; Ojasalo, S.; Seitz, I.; Kostiainen, M. A.; Grundmeier, G.; Linko, V.; Keller. Environment-Dependent Stability and Mechanical Properties of DNA Origami Six-Helix Bundles with Different Crossover Spacings. *Small* **2022**, *18* (18), 2107393.

(142) Ramakrishnan, S.; Shen, B.; Kostiainen, M. A.; Grundmeier, G; Keller, A.; Linko, V. Real-Time Observation of Superstructure-Dependent DNA Origami Digestion by DNase I Using High-Speed Atomic Force Microscopy. *ChemBioChem* **2019**, *20* (22), 2818–2823.

(143) Keum, J. W.; Bermudez, H. Enhanced Resistance of DNA nanostructures to Enzymatic Digestion. *Chem. Comm.* **2009**, 45, 7036–7038.

(144) Jiang, Q.; Song, C.; Nangreave, J.; Liu, X.; Lin, L.; Qiu, D.; Wang, Z. G.; Zou, G.; Liang, X.; Yan, H.; Ding, B. DNA Origami as a Carrier for Circumvention of Drug Resistance. *J. Am. Chem. Soc.* **2012**, *134* (32), 13396–13403.

(145) Hahn, J.; Wickham, S. F. J.; Shih, W. M.; Perrault, S. D. Addressing the Instability of DNA Nanostructures in Tissue Culture. *ACS Nano* **2014**, *8* (9), 8765–8775.

(146) Mei, Q.; Wei, X.; Su, F.; Liu, Y.; Youngbull, C.; Johnson, R.; Lindsay, S.; Yan, H.; Meldrum, D. Stability of DNA Origami Nanoarrays in Cell Lysate. *Nano Lett.* **2011**, *11* (4), 1477–1482.

(147) Benson, E.; Mohammed, A.; Gardell, J.; Masich, S.; Czeizler, E.; Orponen, P.; Högberg, B. DNA Rendering of Polyhedral Meshes at the Nanoscale. *Nature* **2015**, *523* (7561), 441–444.

(148) Chandrasekaran, A. R.; Vilcapoma, J.; Dey, P.; Wong-Deyrup, S. W.; Dey, B. K.; Halvorsen, K. Exceptional Nuclease Resistance of Paranemic Crossover (PX) DNA and Crossover-Dependent Biostability of DNA Motifs. *J. Am. Chem. Soc.* **2020**, *142* (14), 6814–6821.

(149) Castro, C. E.; Kilchherr, F.; Kim, D. N.; Shiao, E. L.; Wauer, T.; Wortmann, P.; Bathe, M.; Dietz, H. A Primer to Scaffolded DNA Origami. *Nat. Methods* **2011**, *8* (3), 221–229.

(150) Cassinelli, V.; Oberleitner, B.; Sobotta, J.; Nickels, P.; Grossi, G.; Kempter, S.; Frischmuth, T.; Liedl, T.; Manetto, A. One-Step Formation of “Chain-Armor”-Stabilized DNA Nanostructures. *Angew. Chem. Int. Ed.* **2015**, *54* (27), 7795–7798.

(151) Gerling, T.; Kube, M.; Kick, B.; Dietz, H. Sequence-Programmable Covalent Bonding of Designed DNA Assemblies. *Sci. Adv.* **2018**, *4* (8).

(152) Liu, Q.; Liu, G.; Wang, T.; Fu, J.; Li, R.; Song, L.; Wang, Z. G.; Ding, B.; Chen, F. Enhanced Stability of DNA Nanostructures by Incorporation of Unnatural Base Pairs. *ChemPhysChem* **2017**, *18* (21), 2977–2980.

(153) Kiviaho, J. K.; Linko, V.; Ora, A.; Tiainen, T.; Järvihaavisto, E.; Mikkilä, J.; Tenhu, H.; Nonappa; Kostiainen, M. A. Cationic Polymers for DNA Origami Coating-Examining Their Binding Efficiency and Tuning the Enzymatic Reaction Rates. *Nanoscale* **2016**, *8* (22), 11674–11680.

(154) Hernandez-Garcia, A.; Estrich, N. A.; Werten, M. W. T.; Van Der Maarel, J. R. C.; LaBean, T. H.; De Wolf, F. A.; Cohen Stuart, M. A.; De Vries, R. Precise Coating of a Wide Range of DNA Templates by a Protein Polymer with a DNA Binding Domain. *ACS Nano* **2017**, *11* (1), 144–152.

(155) Lacroix, A.; Edwardson, T. G. W.; Hancock, M. A.; Dore, M. D.; Sleiman, H. F. Development of DNA Nanostructures for High-Affinity Binding to Human Serum Albumin. *J. Am. Chem. Soc.* **2017**, *139* (21), 7355–7362.

(156) Wang, S. T.; Gray, M. A.; Xuan, S.; Lin, Y.; Byrnes, J.; Nguyen, A. I.; Todorova, N.; Stevens, M. M.; Bertozzi, C. R.; Zuckermann, R. N.; Gang, O. DNA Origami Protection and Molecular Interfacing through Engineered Sequence-Defined Peptoids. *Proc. Natl. Acad. Sci. U.S.A* **2020**, *117* (12), 6339–6348.

(157) Perrault, S. D.; Shih, W. M. Virus-Inspired Membrane Encapsulation of DNA Nanostructures to Achieve In Vivo Stability. *ACS Nano* **2014**, *8* (5), 5132–5140.

(158) Linko, V.; Ora, A.; Kostiainen, M. A. DNA Nanostructures as Smart Drug-Delivery Vehicles and Molecular Devices. *Trends Biotechnol.* **2015**, *33* (10), 586–594.

(159) Liu, Q.; Shaukat, A.; Kyllönen, D.; Kostiainen, M. A. Polyelectrolyte Encapsulation and Confinement within Protein Cage-Inspired Nanocompartments. *Pharmaceutics* **2021**, *13* (10), 1551.

(160) Uchida, M.; Klem, M. T.; Allen, M.; Suci, P.; Flenniken, M.; Gillitzer, E.; Varpness, Z.; Liepold, L. O.; Young, M.; Douglas, T. Biological Containers: Protein Cages as Multifunctional Nanoplatforms. *Adv. Mater.* **2007**, *19* (8), 1025–1042.

(161) Edwardson, T. G. W.; Levasseur, M. D.; Tetter, S.; Steinauer, A.; Hori, M.; Hilvert, D. Protein Cages: From Fundamentals to Advanced Applications. *Chem. Rev.* **2022**, 122, 9, 9145–9197.

(162) Rother, M.; G. Nussbaumer, M.; Renggli, K.; Bruns, N. Protein Cages and Synthetic Polymers: A Fruitful Symbiosis for Drug Delivery Applications, Bionanotechnology and Materials Science. *Chem. Soc. Rev.* **2016**, *45* (22), 6213–6249.

(163) Ueno, T.; Abe, M.; Hirata, K.; Abe, S.; Suzuki, M.; Shimizu, N.; Yamamoto, M.; Takata, M.; Watanabe, Y. Process of Accumulation of Metal Ions on the Interior Surface of Apo-Ferritin: Crystal Structures of a Series of Apo-Ferritins Containing Variable Quantities of Pd(II) Ions. *J. Am. Chem. Soc.* **2009**, *131* (14), 5094–5100.

(164) Garcea, R. L.; Gissmann, L. Virus-like Particles as Vaccines and Vessels for the Delivery of Small Molecules. *Curr. Opin. Biotechnol.* **2004**, *15* (6), 513–517.

(165) Azuma, Y.; Zschoche, R.; Tinzl, M.; Hilvert, D. Quantitative Packaging of Active Enzymes into a Protein Cage. *Angew. Chem. Int. Ed.* **2016**, *55* (4), 1531–1534.

(166) Strable, E.; Finn, M. G. Chemical Modification of Viruses and Virus-like Particles. *Curr. Top. Microbiol. Immunol.* **2009**, *327*, 1–21.

(167) Khoshnejad, M.; Parhiz, H.; Shuvaev, V. V.; Dmochowski, I. J.; Muzykantov, V. R. Ferritin-Based Drug Delivery Systems: Hybrid Nanocarriers for Vascular Immunotargeting. *J. Control. Release* **2018**, *282*, 13–24.

(168) Ma, Y.; Nolte, R. J. M.; Cornelissen, J. J. L. M. Virus-Based Nanocarriers for Drug Delivery. *Adv. Drug. Deliv. Rev.* **2012**, *64* (9), 811–825.

(169) Wörsdörfer, B.; Woycechowsky, K. J.; Hilvert, D. Directed Evolution of a Protein Container. *Science* **2011**, *331* (6017), 589–592.

(170) Majsterkiewicz, K.; Azuma, Y.; Heddle, J. G. Connectability of Protein Cages. *Nanoscale Adv.* **2020**, *2* (6), 2255–2264.

(171) Naskalska, A.; Borzęcka-Solarz, K.; Różycki, J.; Stupka, I.; Bochenek, M.; Pyza, E.; Heddle, J. G. Artificial Protein Cage Delivers Active Protein Cargos to the Cell Interior. *Biomacromolecules* **2021**, *22* (10), 4146–4154.

(172) Malay, A. D.; Miyazaki, N.; Biela, A.; Chakraborti, S.; Majsterkiewicz, K.; Stupka, I.; Kaplan, C. S.; Kowalczyk, A.; Piette, B. M. A. G.; Hochberg, G. K. A.; Wu, D.; Wrobel, T. P.; Fineberg, A.; Kushwah, M. S.; Kelemen, M.; Vavpetič, P.; Pelicon, P.; Kukura, P.; Benesch, J. L. P.; Iwasaki, K.; Heddle, J. G. An Ultra-Stable Gold-Coordinated Protein Cage Displaying Reversible Assembly. *Nature* **2019**, *569* (7756), 438–442.

(173) Stupka, I.; Azuma, Y.; Biela, A. P.; Imamura, M.; Scheuring, S.; Pyza, E.; Woźnicka, O.; Maskell, D. P.; Heddle, J. G. Chemically Induced Protein Cage Assembly with Programmable Opening and Cargo Release. *Sci. Adv.* **2022**, *8* (1), 9424.

(174) Lach, M.; Künzle, M.; Beck, T. Free-Standing Metal Oxide Nanoparticle Superlattices Constructed with Engineered Protein Containers Show in Crystallo Catalytic Activity. *Chem. Eur. J.* **2017**, *23* (69), 17482–17486.

(175) Böhler, H.; Orth-Alampour, S.; Baaten, C.; Riedner, M.; Jankowski, J.; Beck, T. Assembly of Chemically Modified Protein Nanocages into 3D Materials for the Adsorption of Uremic Toxins. *J. Mater. Chem. B.* **2022**, *11* (1), 55–60.

(176) Lach, M.; Strelow, C.; Meyer, A.; Mews, A.; Beck, T. Encapsulation of Gold Nanoparticles into Redesigned Ferritin Nanocages for the Assembly of Binary Superlattices Composed of Fluorophores and Gold Nanoparticles. *ACS Appl. Mater. Inter.* **2022**, *14* (8), 10656–10668.

(177) Välimäki, S.; Mikkilä, J.; Liljeström, V.; Rosilo, H.; Ora, A.; Kostiainen, M. A. Hierarchically Ordered Supramolecular Protein-Polymer Composites with Thermoresponsive Properties. *Int. J. Mol. Sci.* **2015**, *16* (5), 10201–10213.

(178) Kostiainen, M. A.; Ceci, P.; Fornara, M.; Hiekkataipale, P.; Kasyutich, O.; Nolte, R. J. M.; Cornelissen, J. J. L. M.; Desautels, R. D.; van Lierop, J. Hierarchical Self-Assembly and Optical Disassembly for Controlled Switching of Magnetoferritin Nanoparticle Magnetism. *ACS Nano* **2011**, *5* (8), 6394–6402.

(179) Künzle, M.; Eckert, T.; Beck, T. Binary Protein Crystals for the Assembly of Inorganic Nanoparticle Superlattices. *J. Am. Chem. Soc.* **2016**, *138* (39), 12731–12734.

(180) Kostiainen, M. A.; Kasyutich, O.; Cornelissen, J. J. L. M.; Nolte, R. J. M. Self-Assembly and Optically Triggered Disassembly of Hierarchical Dendron-Virus Complexes. *Nat. Chem.* **2010**, *2* (5), 394–399.

(181) Zhang, J.; Wang, X.; Zhou, K.; Chen, G.; Wang, Q. Self-Assembly of Protein Crystals with Different Crystal Structures Using Tobacco Mosaic Virus Coat Protein as a Building Block. *ACS Nano* **2018**, *12* (2), 1673–1679.

(182) Zhou, K.; Chen, H.; Zhang, S.; Wang, Y.; Zhao, G. Disulfide-Mediated Reversible Two-Dimensional Self-Assembly of Protein Nanocages. *Chem. Comm.* **2019**, *55* (52), 7510–7513.

(183) Zhou, K.; Zang, J.; Chen, H.; Wang, W.; Wang, H.; Zhao, G. On-Axis Alignment of Protein Nanocage Assemblies from 2D to 3D through the Aromatic Stacking Interactions of Amino Acid Residues. *ACS Nano* **2018**, *12* (11), 11323–11332.

(184) Zheng, B.; Zhou, K.; Zhang, T.; Lv, C.; Zhao, G. Designed Two-and Three-Dimensional Protein Nanocage Networks Driven by Hydrophobic Interactions Contributed by Amyloidogenic Motifs. *Nano Lett.* **2019**, *19* (6), 4023–4028.

(185) Bellapadrona, G.; Sinkar, S.; Sabanay, H.; Liljeström, V.; Kostiainen, M.; Elbaum, M. Supramolecular Assembly and Coalescence of Ferritin Cages Driven by Designed Protein–Protein Interactions. *Biomacromolecules* **2015**, *16* (7), 2006–2011

(186) Uchida, M.; LaFrance, B.; Broomell, C. C.; Prevelige, P. E.; Douglas, T. Higher Order Assembly of Virus-like Particles (VLPs) Mediated by Multivalent Protein Linkers. *Small* **2015**, *11* (13), 1562–1570.

(187) Liljeström, V.; Seitsonen, J.; Kostiainen, M. A. Electrostatic Self-Assembly of Soft Matter Nanoparticle Cocrystals with Tunable Lattice Parameters. *ACS Nano* **2015**, *9* (11), 11278–11285.

(188) Sontz, P. A.; Bailey, J. B.; Ahn, S.; Tezcan, F. A. A Metal Organic Framework with Spherical Protein Nodes: Rational Chemical Design of 3D Protein Crystals. *J. Am. Chem. Soc.* **2015**, *137* (36), 11598–11601.

(189) Bailey, J. B.; Zhang, L.; Chiong, J. A.; Ahn, S.; Tezcan, F. A. Synthetic Modularity of Protein–Metal–Organic Frameworks. *J. Am. Chem. Soc.* **2017**, *139* (24), 8160–8166.

(190) Laufberger, V. Sur La Cristallisation de La Ferritine. *Soc. Chim. Biol.* **1937**, *19*, 1575–1582.

(191) Honarmand Ebrahimi, K.; Hagedoorn, P. L.; Hagen, W. R. Unity in the Biochemistry of the Iron-Storage Proteins Ferritin and Bacterioferritin. *Chem. Rev.* **2015**, *115* (1), 295–326.

(192) Harrison, P. M.; Arosio, P. The Ferritins: Molecular Properties, Iron Storage Function and Cellular Regulation. *BBA Bioenergetics* **1996**, *1275* (3), 161–203.

(193) Arosio, P.; Ingrassia, R.; Cavadini, P. Ferritins: A Family of Molecules for Iron Storage, Antioxidation and More. *BBA-Gen. Subjects* **2009**, *1790* (7), 589–599.

(194) Bevers, L. E.; Theil, E. C. Maxi- and Mini-Ferritins: Minerals and Protein Nanocages. *Prog. Mol. Subcell. Biol.* **2011**, *52*, 29.

(195) Mohanty, A.; Parida, A.; Raut, R. K.; Behera, R. K. Ferritin: A Promising Nanoreactor and Nanocarrier for Bionanotechnology. *ACS Bio Med Chem Au* **2022**, *2* (3), 258–281.

(196) Jutz, G.; Van Rijn, P.; Santos Miranda, B.; Böker, A. Ferritin: A Versatile Building Block for Bionanotechnology. *Chem. Rev.* **2015**, *115* (4), 1653–1701

(197) Yamashita, I.; Iwahori, K.; Kumagai, S. Ferritin in the Field of Nanodevices. *BBA-Gen. Subjects* **2010**, *1800* (8), 846–857.

(198) Kramer, R. M.; Li, C.; Carter, D. C.; Stone, M. O.; Naik, R. R. Engineered Protein Cages for Nanomaterial Synthesis. *J. Am. Chem. Soc.* **2004**, *126* (41), 13282–13286.

(199) Uchida, M.; Kang, S.; Reichhardt, C.; Harlen, K.; Douglas, T. The Ferritin Superfamily: Supramolecular Templates for Materials Synthesis. *BBA-Gen. Subjects* **2010**, *1800* (8), 834–845.

(200) Fan, R.; Chew, S. W.; Cheong, V. V.; Orner, B. P. Fabrication of Gold Nanoparticles Inside Unmodified Horse Spleen Apoferritin. *Small* **2010**, *6* (14), 1483–1487.

(201) Zeng, Q.; Li, T.; Cash, B.; Li, S.; Xie, F.; Wang, Q. Chemoselective Derivatization of a Bionanoparticle by Click Reaction and ATRP Reaction. *Chem. Comm.* **2007**, 14, 1453–1455.

(202) Yang, Z.; Wang, X.; Diao, H.; Zhang, J.; Li, H.; Sun, H.; Guo, Z. Encapsulation of Platinum Anticancer Drugs by Apoferritin. *Chem. Comm.* **2007**, 33, 3453–3455.

(203) Xing, R.; Wang, X.; Zhang, C.; Zhang, Y.; Wang, Q.; Yang, Z.; Guo, Z. Characterization and Cellular Uptake of Platinum Anticancer Drugs Encapsulated in Apoferritin. *J. Inorg. Biochem.* **2009**, *103* (7), 1039–1044.

(204) Falvo, E.; Tremante, E.; Fraioli, R.; Leonetti, C.; Zamparelli, C.; Boffi, A.; Morea, V.; Ceci, P.; Giacomini, P. Antibody–Drug Conjugates: Targeting Melanoma with Cisplatin Encapsulated in Protein-Cage Nanoparticles Based on Human Ferritin. *Nanoscale* **2013**, *5* (24), 12278–12285.

(205) Liang, M.; Fan, K.; Zhou, M.; Duan, D.; Zheng, J.; Yang, D.; Feng, J.; Yan, X. H-Ferritin-Nanocaged Doxorubicin Nanoparticles Specifically Target and Kill Tumors with a Single-Dose Injection. *Proc. Natl. Acad. Sci. U.S.A* **2014**, *111* (41), 14900–14905.

(206) Zhen, Z.; Tang, W.; Guo, C.; Chen, H.; Lin, X.; Liu, G.; Fei, B.; Chen, X.; Xu, B.; Xie, J. Ferritin Nanocages to Encapsulate and Deliver Photosensitizers for Efficient Photodynamic Therapy against Cancer. *ACS Nano* **2013**, *7* (8), 6988–6996.

(207) Beck, T.; Tetter, S.; Künzle, M.; Hilvert, D. Construction of Matryoshka-Type Structures from Supercharged Protein Nanocages. *Angew. Chem. Int. Ed.* **2015**, *54* (3), 937–940.

(208) Chen, H.; Zhang, T.; Tan, X.; Wang, Y.; Liu, Y.; Zhao, G. Construction of Thermally Robust and Porous Shrimp Ferritin Crystalline for Molecular Encapsulation through Intermolecular Arginine-Arginine Attractions. *Food Chem.* **2021**, *349*, 129089.

(209) Abdel-Kader, M. H. Photodynamic Therapy: From Theory to Application. *Photodynamic Therapy: From Theory to Application* **2014**, 1–312.

(210) Nonell, S.; Flors, C. *Singlet Oxygen: Applications in Biosciences and Nanosciences,*; Royal Society of Chemistry, **2016,** 1.

(211) Sasikumar, D.; John, A. T.; Sunny, J.; Hariharan, M. Access to the Triplet Excited States of Organic Chromophores. *Chem. Soc. Rev.* **2020**, *49* (17), 6122–6140.

(212) Ochsner, M. Photophysical and Photobiological Processes in the Photodynamic Therapy of Tumours. *J. Photochem. Photobiol. B* **1997**, *39* (1), 1–18.

(213) Wong, R. C. H.; Lo, P. C.; Ng, D. K. P. Stimuli Responsive Phthalocyanine-Based Fluorescent Probes and Photosensitizers. *Coord. Chem. Rev.* **2019**, *379*, 30–46.

(214) Li, X.; De Zheng, B.; Peng, X. H.; Li, S. Z.; Ying, J. W.; Zhao, Y.; Huang, J. D.; Yoon, J. Phthalocyanines as Medicinal Photosensitizers: Developments in the Last Five Years. *Coord. Chem. Rev.* **2019**, *379*, 147–160.

(215) Nyokong, T. Effects of Substituents on the Photochemical and Photophysical Properties of Main Group Metal Phthalocyanines. *Coord. Chem. Rev.* **2007**, *251* (13–14), 1707–1722.

(216) Lo, P. C.; Rodríguez-Morgade, M. S.; Pandey, R. K.; Ng, D. K. P.; Torres, T.; Dumoulin, F. The Unique Features and Promises of Phthalocyanines as Advanced Photosensitisers for Photodynamic Therapy of Cancer. *Chem. Soc. Rev.* **2020**, *49* (4), 1041–1056.

(217) Chinna Ayya Swamy, P.; Sivaraman, G.; Priyanka, R. N.; Raja, S. O.; Ponnuvel, K.; Shanmugpriya, J.; Gulyani, A. Near Infrared (NIR) Absorbing Dyes as Promising Photosensitizer for Photo Dynamic Therapy. *Coord. Chem. Rev.* **2020**, *411*, 213233.

(218) Zheng, B. De; He, Q. X.; Li, X.; Yoon, J.; Huang, J. D. Phthalocyanines as Contrast Agents for Photothermal Therapy. *Coord. Chem. Rev.* **2021**, *426*, 213548.

(219) Galstyan, A. Turning Photons into Drugs: Phthalocyanine-Based Photosensitizers as Efficient Photoantimicrobials. *Chem. Eur. J.* **2021**, *27* (6), 1903–1920.

(220) Wong, R. C. H.; Lo, P. C.; Ng, D. K. P. Stimuli Responsive Phthalocyanine-Based Fluorescent Probes and Photosensitizers. *Coord. Chem. Rev.* **2019**, *379*, 30–46.

(221) Yamazaki, S. Metalloporphyrins and Related Metallomacrocycles as Electrocatalysts for Use in Polymer Electrolyte Fuel Cells and Water Electrolyzers. *Coord. Chem. Rev.* **2018**, *373*, 148–166.

(222) Monteiro, C. J. P.; Faustino, M. A. F.; Neves, M. da G. P. M. S.; Simões, M. M. Q.; Sanjust, E. Metallophthalocyanines as Catalysts in Aerobic Oxidation. *Catalysts* **2021**, *11* (1), 122.

(223) Urbani, M.; Ragoussi, M. E.; Nazeeruddin, M. K.; Torres, T. Phthalocyanines for Dye-Sensitized Solar Cells. *Coord. Chem. Rev*. **2019**, *381*, 1–64.

(224) Bottari, G.; de la Torre, G.; Guldi, D. M.; Torres, T. An Exciting Twenty-Year Journey Exploring Porphyrinoid-Based Photo- and Electro-Active Systems. *Coord. Chem. Rev.* **2021**, *428*, 213605.

(225) Urbani, M.; De La Torre, G.; Nazeeruddin, M. K.; Torres, T. Phthalocyanines and Porphyrinoid Analogues as Hole- and Electron-Transporting Materials for Perovskite Solar Cells. *Chem. Soc. Rev.* **2019**, *48* (10), 2738–2766.

(226) Dumoulin, F.; Durmuş, M.; Ahsen, V.; Nyokong, T. Synthetic Pathways to Water-Soluble Phthalocyanines and Close Analogs. *Coord. Chem. Rev.* **2010**, 254 (23–24), 2792–2847.

(227) Hamuryudan, E.; Merey, S.; Altuntas Bayir, Z. Synthesis of Phthalocyanines with Tridentate Branched Bulky and Alkylthio Groups. *Dyes Pigments* **2003**, *59* (3), 263–268.

(228) Singh, S.; Aggarwal, A.; Bhupathiraju, N. V. S. D. K.; Arianna, G.; Tiwari, K.; Drain, C. M. Glycosylated Porphyrins, Phthalocyanines, and Other Porphyrinoids for Diagnostics and Therapeutics. *Chem. Rev.* **2015**, *115* (18), 10261–10306.

(229) Lourenço, L. M. O.; Neves, M. G. P. M. S.; Cavaleiro, J. A. S.; Tomé, J. P. C. Synthetic Approaches to Glycophthalocyanines. *Tetrahedron* **2014**, *70* (17), 2681–2698.

(230) Almeida-Marrero, V.; Van De Winckel, E.; Anaya-Plaza, E.; Torres, T.; De La Escosura, A. Porphyrinoid Biohybrid Materials as an Emerging Toolbox for Biomedical Light Management. *Chem. Soc. Rev.* **2018**, *47* (19), 7369–7400.

(231) Ramaiah, D.; Neelakandan, P. P.; Nair, A. K.; Avirah, R. R. Functional Cyclophanes: Promising Hosts for Optical Biomolecular Recognition. *Chem. Soc. Rev.* **2010**, *39* (11), 4158–4168.

(232) Guyard, L.; Audebert, P. Synthesis and Electrochemical Polymerization of Bis-Dithienyl Cyclophane. *Electrochem. Commun.* **2001**, *3* (4), 164–167.

(233) Morisaki, Y.; Chujo, Y. Cyclophane-Containing Polymers. *Prog. Polym. Sci.* **2008**, *33* (3), 346–364.

(234) Xue, M.; Yang, Y.; Chi, X.; Zhang, Z.; Huang, F. Pillararenes, a New Class of Macrocycles for Supramolecular Chemistry. *Acc. Chem. Res.* **2012**, *45* (8), 1294–1308.

(235) Hua, B.; Shao, L.; Zhang, Z.; Liu, J.; Huang, F. Cooperative Silver Ion-Pair Recognition by Peralkylated Pillar[5]Arenes. *J. Am. Chem. Soc.* **2019**, *141* (38), 15008–15012.

(236) Ogoshi, T.; Yamagishi, T.; Nakamoto, Y. Pillar-Shaped Macrocyclic Hosts Pillar[n]Arenes: New Key Players for Supramolecular Chemistry. *Chem. Rev.* **2016**, *116* (14), 7937–8002.

(237) Cragg, P.J.; Sharma, K. Pillar[5]Arenes: Fascinating Cyclophanes with a Bright Future. *Chem. Soc. Rev.* **2012**, *41* (2), 597–607.

(238) Xue, M.; Yang, Y.; Chi, X.; Zhang, Z.; Huang, F. Pillararenes, A New Class of Macrocycles for Supramolecular Chemistry. *Acc. Chem. Res.* **2012**, *45* (8), 1294–1308.

(239) Jonkergouw, C.; Beyeh, N. K.; Osmekhina, E.; Leskinen, K.; Taimoory, S. M.; Fedorov, D.; Anaya-Plaza, E.; Kostiainen, M. A.; Trant, J. F.; Ras, R. H. A.; Saavalainen, P.; Linder, M. B. Repurposing Host-Guest Chemistry to Sequester Virulence and Eradicate Biofilms in Multidrug Resistant Pseudomonas Aeruginosa and Acinetobacter Baumannii. *Nat. Commun.* **2023**, *14* (1), 1–18.

(240) Li, C.; Ma, J.; Zhao, L.; Zhang, Y.; Yu, Y.; Shu, X.; Li, J.; Jia, X. Molecular Selective Binding of Basic Amino Acids by a Water-Soluble Pillar[5]Arene. *Chem. Commun.* **2013**, *49* (19), 1924–1926.

(241) Ogoshi, T.; Aoki, T.; Kitajima, K.; Fujinami, S.; Yamagishi, T. A.; Nakamoto, Y. Facile, Rapid, and High-Yield Synthesis of Pillar[5]Arene from Commercially Available Reagents and Its X-Ray Crystal Structure. *J. Org. Chem.* **2011**, *76* (1), 328–331.

(242) Feng, W.; Jin, M.; Yang, K.; Pei, Y.; Pei, Z. Supramolecular Delivery Systems Based on Pillararenes. *Chem. Comm.* **2018**, *54* (97), 13626–13640.

(243) Li, C. Pillararene-Based Supramolecular Polymers: From Molecular Recognition to Polymeric Aggregates. *Chem. Comm.* **2014**, *50* (83), 12420–12433.

(244) Li, Q.; Zhu, H.; Huang, F. Pillararene-Based Supramolecular Functional Materials. *Trends Chem.* **2020**, *2* (9), 850–864.

(245) Hu, X. Y.; Zhang, P.; Wu, X.; Xia, W.; Xiao, T.; Jiang, J.; Lin, C.; Wang, L. Pillar[5]Arene-Based Supramolecular Polypseudorotaxanes Constructed from Quadruple Hydrogen Bonding. *Polym. Chem.* **2012**, *3* (11), 3060–3063.

(246) Zyryanov, G. V.; Kopchuk, D. S.; Kovalev, I. S.; Santra, S.; Majee, A.; Ranu, B. C. Pillararenes as Promising Carriers for Drug Delivery. *Int. J. Mol. Sci.* **2023**, *24* (6), 5167.

(247) Wang, C.; Li, H.; Dong, J.; Chen, Y.; Luan, X.; Li, X.; Du, X. Pillararene-Based Supramolecular Vesicles for Stimuli-Responsive Drug Delivery. *Chem. Eur. J.* **2022**, *28* (71), e202202050.

(248) Chen, J. F.; Lin, Q.; Zhang, Y. M.; Yao, H.; Wei, T. B. Pillararene-Based Fluorescent Chemosensors: Recent Advances and Perspectives. *Chem. Comm.* **2017**, *53* (100), 13296–13311.

(249) Chudakov, D. M.; Lukyanov, S.; Lukyanov, K. A. Fluorescent Proteins as a Toolkit for In Vivo Imaging. *Trends Biotechnol.* **2005**, *23* (12), 605–613.

(250) Shimomura, O.; Johnson, F. H.; Saiga, Y. Extraction, Purification and Properties of Aequorin, a Bioluminescent Protein from the Luminous Hydromedusan, Aequorea. *J. Cell Comp. Physiol.* **1962**, *59* (3), 223–239.

(251) Zimmer, M. Green Fluorescent Protein (GFP): Applications, Structure, and Related Photophysical Behavior. *Chem. Rev.* **2002**, *102* (3), 759–781.

(252) Ward, W. W. Biochemical and Physical Properties of Green Fluorescent Protein. *Methods Biochem. Anal.* **2005**, *47*, 39–65.

(253) Remington, S. J. Green Fluorescent Protein: A Perspective. *Protein Sci.* **2011**, *20* (9), 1509–1519.

(254) Grigorenko, B. L.; Krylov, A. I.; Nemukhin, A. V. Molecular Modeling Clarifies the Mechanism of Chromophore Maturation in the Green Fluorescent Protein. *J. Am. Chem. Soc.* **2017**, *139* (30), 10239–10249.

(255) Wachter, R. M. Chromogenic Cross-Link Formation in Green Fluorescent Protein. *Acc. Chem. Res.* **2007**, *40* (2), 120–127.

(256) Craggs, T. D. Green Fluorescent Protein: Structure, Folding and Chromophore Maturation. *Chem. Soc. Rev.* **2009**, *38* (10), 2865–2875.

(257) Fernández-Luna, V.; Coto, P. B.; Costa, R. D. When Fluorescent Proteins Meet White Light-Emitting Diodes. *Angew. Chem. Int. Ed.* **2018**, *57* (29), 8826–8836.

(258) Tsien, R. Y. Constructing and Exploiting the Fluorescent Protein Paintbox (Nobel Lecture). *Angew. Chem. Int. Ed.* **2009**, *48* (31), 5612–5626.

(259) Day, R. N.; Davidson, M. W. The Fluorescent Protein Palette: Tools for Cellular Imaging. *Chem. Soc. Rev.* **2009**, *38* (10), 2887–2921.

(260) Tsien, R. Y. The Green Fluorescent Protein. *Annu. Rev. Biochem.* **2003**, *67*, 509–544.

(261) Chudakov, D. M.; Matz, M. V.; Lukyanov, S.; Lukyanov, K. A. Fluorescent Proteins and Their Applications in Imaging Living Cells and Tissues. *Physiol. Rev.* **2010**, *90* (3), 1103–1163.

(262) Gather, M. C.; Yun, S. H. Single-Cell Biological Lasers. *Nature* **2011**, *5* (7), 406–410.

(263) Pikas, D. J.; Kirkpatrick, S. M.; Tewksbury, E.; Brott, L. L.; Naik, R. R.; Stone, M. O.; Dennis, W. M. Nonlinear Saturation and Lasing Characteristics of Green Fluorescent Protein. *J. Phys. Chem. B* **2002**, *106* (18), 4831–4837.

(264) Mysliwiec, J.; Cyprych, K.; Sznitko, L.; Miniewicz, A. Biomaterials in Light Amplification. *J. Opt.* **2017**, *19* (3), 033003.

(265) Press, D. A.; Melikov, R.; Conkar, D.; Firat-Karalar, E. N.; Nizamoglu, S. Fluorescent Protein Integrated White LEDs for Displays. *Nanotechnology* **2016**, *27* (45), 45LT01.

(266) Weber, M. D.; Niklaus, L.; Pröschel, M.; Coto, P. B.; Sonnewald, U.; Costa, R. D. Bioinspired Hybrid White Light-Emitting Diodes. *Adv. Mater.* **2015**, *27* (37), 5493–5498.

(267) Niklaus, L.; Tansaz, S.; Dakhil, H.; Weber, K. T.; Pröschel, M.; Lang, M.; Kostrzewa, M.; Coto, P. B.; Detsch, R.; Sonnewald, U.; Wierschem, A.; Boccaccini, A. R.; Costa, R. D. Micropatterned Down-Converting Coating for White Bio-Hybrid Light-Emitting Diodes. *Adv. Funct. Mater.* **2017**, *27* (1), 1601792.

(268) Shaner, N. C.; Patterson, G. H.; Davidson, M. W. Advances in Fluorescent Protein Technology. *J. Cell. Sci.* **2007**, *120* (24), 4247–4260.

(269) Lawrence, M. S.; Phillips, K. J.; Liu, D. R. Supercharging Proteins Can Impart Unusual Resilience. *J. Am. Chem. Soc.* **2007**, *129* (33), 10110.

(270) Simon, A. J.; Zhou, Y.; Ramasubramani, V.; Glaser, J.; Pothukuchy, A.; Gollihar, J.; Gerberich, J. C.; Leggere, J. C.; Morrow, B. R.; Jung, C.; Glotzer, S. C.; Taylor, D. W.; Ellington, A. D. Supercharging Enables Organized Assembly of Synthetic Biomolecules. *Nat. Chem.* **2019**, *11* (3), 204–212.

(271) Jacobs, M. I.; Bansal, P.; Shukla, D.; Schroeder, C. M. Understanding Supramolecular Assembly of Supercharged Proteins. *ACS Cent. Sci.* **2022**, *8* (9), 1350–1361.

(272) Bui, H.; Onodera, C.; Kidwell, C.; Tan, Y.; Graugnard, E.; Kuang, W.; Lee, J.; Knowlton, W. B.; Yurke, B.; Hughes, W. L. Programmable Periodicity of Quantum Dot Arrays with DNA Origami Nanotubes. *Nano Lett.* **2010**, *10* (9), 3367–3372.

(273) Ijäs, H.; Shen, B.; Heuer-Jungemann, A.; Keller, A.; Kostiainen, M. A.; Liedl, T.; Ihalainen, J. A.; Linko, V. Unraveling the Interaction between Doxorubicin and DNA Origami Nanostructures for Customizable Chemotherapeutic Drug Release. *Nucleic Acids Res.* **2021**, *49* (6), 3048–3062.

(274) Linko, V.; Shen, B.; Tapio, K.; Toppari, J. J.; Kostiainen, M. A.; Tuukkanen, S. One-Step Large-Scale Deposition of Salt-Free DNA Origami Nanostructures. *Sci. Rep.* **2015**, *5* (1), 1–8.

(275) Nombona, N.; Maduray, K.; Antunes, E.; Karsten, A.; Nyokong, T. Synthesis of Phthalocyanine Conjugates with Gold Nanoparticles and Liposomes for Photodynamic Therapy. *J. Photochem. Photobiol. B* **2012**, *107* (1), 35–44.

(276) Coleridge, E. L.; Dunn, K. E. Assessing the Cost-Effectiveness of DNA Origami Nanostructures for Targeted Delivery of Anti-Cancer Drugs to Tumours. *Biomed. Phys. Eng. Express* **2020**, *6* (6), 065030.

(277) Praetorius, F.; Kick, B.; Behler, K. L.; Honemann, M. N.; Weuster-Botz, D.; Dietz, H.; Coli, P. E. Biotechnological Mass Production of DNA Origami. *Nature* **2017**, *552* (7683), 84–87.

(278) Zhang, L.; Bailey, J. B.; Subramanian, R. H.; Groisman, A.; Tezcan, F. A. Hyperexpandable, Self-Healing Macromolecular Crystals with Integrated Polymer Networks. *Nature* **2018**, *557* (7703), 86–91.

(279) Han, K.; Na, Y.; Zhang, L.; Tezcan, F. A. Dynamic, Polymer-Integrated Crystals for Efficient, Reversible Protein Encapsulation. *J. Am. Chem. Soc.* **2022**, *144* (23), 10139–10144.

(280) Han, K.; Bailey, J. B.; Zhang, L.; Tezcan, F. A. Anisotropic Dynamics and Mechanics of Macromolecular Crystals Containing Lattice-Patterned Polymer Networks. *J. Am. Chem. Soc.* **2020**, *142* (45), 19402–19410.

Electrostatic self-assembly, a subtle yet powerful force governing non-covalent interactions, orchestrates the precise arrangement of charged constituents at the atomic scale.
Central to this scholarly work is the fusion of DNA origami and protein cages with cationic molecular glues, culminating in a cohort of biohybrid materials showcasing notable functionality. These adaptable materials hold immense promise for transformative breakthroughs in nanomedicine, optoelectronics, and water treatment, marked by exceptional biocompatibility and precise compositional control.

Aalto-DT 186/2023

ISBN 978-952-64-1511-6 (printed)
ISBN 978-952-64-1512-3 (pdf)
ISSN 1799-4934 (printed)
ISSN 1799-4942 (pdf)

Aalto University
School of Chemical Engineering
Department of Bioproducts and Biosystems
www.aalto.fi

BUSINESS + ECONOMY

ART + DESIGN + ARCHITECTURE

SCIENCE + TECHNOLOGY

CROSSOVER

DOCTORAL THESES